2 (mix)

NASA TECHNICAL MEMORANDUM

NASA TM X-62,017

NASA TM X-62,017

LOW–SPEED AERODYNAMIC CHARACTERISTICS OF A LARGE–SCALE STOL TRANSPORT MODEL WITH AN AUGMENTED JET FLAP

Anthony M. Cook and Thomas N. Aiken

Ames Research Center
Moffett Field, Calif. 94035

March 1971

NOTATION

A	net thrust augmentation ratio of the jet augmentor, $\frac{J_A}{J_I}$
b	wing span, m (ft)
BLC	boundary layer control, fuselage, wing center section
c	wing chord, m (ft)
$\bar{c}$	reference wing chord, 1.272 m (5.667 ft)
C_D	drag coefficient, $\frac{\text{drag}}{qS}$
$C_{D_{MJ85}}$	intake momentum drag coefficient, compressor J85
$C_{D_{MV}}$	intake momentum drag coefficient, compressor vipers
$C_{J_{AI}}$	augmentor isentropic jet thrust coefficient, $\frac{\text{isentropic thrust}}{qS}$
C_{J_I}	total isentropic jet thrust coefficient, $C_{J_{AI}} + C_{\mu_a} + C_{\mu_F}$, $\frac{\text{thrust}}{qS}$
C_l	rolling moment coefficient, $\frac{\text{rolling moment}}{qSb}$
C_L	lift coefficient, $\frac{\text{lift}}{qS}$
C_m	pitching moment coefficient, $\frac{\text{pitching moment}}{qS\bar{c}}$
C_n	yawing moment coefficient, $\frac{\text{yawing moment}}{qSb}$
C_T	tail pipe thrust coefficient, $\frac{\text{thrust}}{qS}$
$C_{T_{th}}$	underwing engine thrust coefficient, $\frac{\text{thrust}}{qS}$
C_y	side force coefficient, $\frac{\text{side force}}{qS}$
C_{μ_a}	aileron BLC coefficient, $\frac{\text{BLC thrust}}{qS}$
C_{μ_F}	fuselage BLC coefficient, $\frac{\text{BLC thrust}}{qS}$

d	distance between trailing edges of flap and shroud, m (ft)
i_T	horizontal tail incidence, positive with trailing edge down, deg
J	augmentor static thrust, N (lb)
q	freestream dynamic pressure, N/m^2 (lb/ft^2)
S	wing area, sq m (sq ft)
Z_{JP}	distance between moment center and line of action of jet-pipe residual thrust, m (ft)
α	model angle of attack, deg
β	angle of sideslip of plane of symmetry, deg
δ_a	aileron deflection, (δ_a = 45/60 means port aileron at 45°, starboard aileron at 60°), positive with trailing edge down, deg
δ_e	elevator deflection, positive with trailing edge down, deg
δ_f	augmentor flap deflection, deg
δ_{ID}	intake door angle, deg
δ_{JP}	deflection of jet pipes relative to fuselage datum plane, deg
δ_{sp}	spoiler deflection, positive trailing edge up, deg
δ_{th}	angle of thrust deflection of underwing J85 engines, deg
Δd	reduction in distance between trailing edges of flap and shroud, percent
θ	augmentor jet angle relative to wing chord plane, deg

Subscripts

a	aileron
A	augmentor
F	fuselage
f	flap

I	isentropic
JP	jet-pipe, fuselage, compressor residual exhaust
p	port
s	starboard
th	underwing engine thrust
u	uncorrected

LOW-SPEED AERODYNAMIC CHARACTERISTICS OF A LARGE-SCALE STOL TRANSPORT MODEL WITH AN AUGMENTED JET FLAP

Anthony M. Cook and Thomas N. Aiken

Ames Research Center

SUMMARY

An investigation was made to study the aerodynamic characteristics of a large scale model equipped with an augmented-jet flap and underwing cruise engines with deflectable thrust capability. The augmented-jet flap is a jet flap with the primary jet thrust increased by means of a spanwise ejector system installed in the wing trailing-edge flap. The flap installation was on the inboard part of the wing, with blown ailerons outboard.

Primary configurations tested were those selected previously for landing approach and takeoff, for direct application of the data to a proposed flight research aircraft. Assessment was made of the effects of the underwing engines and nacelles with variations in thrust magnitude and direction. The effects of fuselage BLC were also measured. In addition, several methods of lateral control were investigated to obtain measurements of lateral derivatives and roll control power.

The tests were made with and without the horizontal tail at a wind tunnel dynamic pressure of 383 newtons per square meter (8 pounds per square foot), corresponding to a Reynolds number of 2.9 million. The range of jet momentum coefficients was 0 to 1.07.

INTRODUCTION

This paper presents the results of a recent investigation into the low speed aerodynamics of the augmentor-wing type jet flap. A large-scale model of a typical STOL (short takeoff and landing) transport configuration incorporating this high lift concept was previously tested in the Ames 40- by 80-foot (12.2- by 24.4-meter) wind tunnel and reported in reference 1.

The tests reported herein are the most recent large scale tests in a continuing effort to simplify the augmentor flap geometry for consideration of application to a proposed research aircraft (CV-7A "Buffalo" aircraft). The augmentor flap design was simplified from the design of the flaps tested in reference 1 by removing the blowing BLC nozzle on the trailing edge flaps, removing the flap secondary air inlet, and in general reducing the complexity of mechanism of the various portions of the flap and their relative motions to each other. The model geometrically simulated a CV-7A aircraft with an augmented jet flap extending over 55 percent of the wing span. In addition, underwing cruise engines were mounted on the model. These were provided with deflectable thrust capability for simulation of landing conditions.

Static tests and wind tunnel tests, out of ground effect, were made for flap angles of 50° and 75°, representing takeoff and landing settings respectively, over a range of augmentor jet coefficients. Also investigated were effects of fuselage BLC and methods for lateral control, including blown ailerons, upper wing spoilers, and differential augmentor area throttling.

MODEL AND APPARATUS

Basic Model

The model is shown installed in the wind tunnel in the photographs of figure 1. Reference dimensions are listed in Table I and geometric details are shown in the sketches of figure 2.

Augmentor Flap

The geometry of the augmentor flap cross-section is shown in figure 2(b). The details and operation of the flap components are considerably simplified over the arrangement originally presented in reference 1. The upper surface blowing BLC system has been discarded in favor of an upper surface slot for secondary flow entrainment. A constant gap between the (upper) shroud and (lower) flap surfaces has now been established for all flap settings. Deployment of the flap therefore requires only two motions; one that raises the intake door and shroud from the nested position to the required gap, followed by rotation of the entire augmentor assembly to the desired deflection.

Blowing Systems

The model was equipped with three blowing systems: The augmentor jet, aileron BLC and fuselage BLC. Air supply for the augmentor and aileron blowing system was provided by the compressor unit shown in figure 2(d). Hot gas exhaust from a J85 gas turbine engine powered the turbines of modified Viper engines and exhausted residually out the tail pipes. The Viper compressor output supplied the wing augmentor jet and aileron BLC airflow as shown in figure 2(e). The fuselage BLC air was supplied by the J85 compressor bleed, as shown in figure 2(g).

Augmentor jet.- The augmentor was a spanwise ejector system formed by the component parts shown in figure 2(b). Primary compressor air was delivered through the wing trailing-edge nozzle, and augmented with secondary air entrained from (a) the wing upper surface, (b) the two slots formed by the lower flap and Coandă surface, and (c) the upper slot between the intake door and the shroud. The mixed jet was ejected downward between the (lower) flap and (upper) shroud.

In order to maintain attached flow on the leading edge of the intake for various flap angles, the intake door could be rotated about the pivot point shown in figure 2(b). Optimum intake door angle for takeoff flap setting (50° δ_f) was found to be 30°, and for landing flap setting (75° δ_f), 55° intake door angle was used. The force output of the augmentor was varied during the tests by the adjustment of throttle setting of the gas generator.

Aileron BLC.- As shown in Figure 2(e), the aileron BLC system was fed through the forward air supply duct of the augmentor. Aileron blowing was therefore coupled with augmentor output and was never varied independently. Airflow to the ailerons was approximately 5% of total Viper compressor output.

Fuselage BLC.- A blowing BLC ejector nozzle, located just aft of the wing leading edge in the part of the wing spanning the fuselage, was installed with the intention of entraining sufficient flow along the wing center section to reduce variations in spanwise flow distribution. As shown in figure 2(g), BLC air was provided by J85 compressor bleed, and was controlled by an inline valve.

Underwing Engines

A podded J85 turbojet engine was installed on each wing as shown in the photographs of figure 1. The engines were equipped with a 90° exhaust diverter valve and various downward nozzle angles as shown in figure 2(f). This system simulated a rotating type nozzle as might be designed for a flight article, with the capacity for full aft (0° δ_{th}) exhaust for take-off and cruise flight, and downward vectoring for approach and landing.

Lateral Control Systems

The model was equipped with several methods for lateral control:

Ailerons.- Lift requirements for landing and takeoff resulted in symmetrical drooping of the BLC ailerons to 45°. Lateral control therefore, could be obtained by differentially deflecting the ailerons about the 45° droop position. Aileron chord was 35 percent of wing chord.

Spoilers.- Two types of upper wing spoilers were installed on the left wing for lateral control; panel type and sector type, as shown in figure 2(h). The panel spoilers were 10% chord panels, located either ahead of the outboard half of the augmentor flap, or ahead of the aileron. Spoiler deflections of 25° and 50° were adjustable. The sector-type spoilers had a fully extended height of 7.6 percent wing chord and were located in the same positions as the panel-type spoilers.

Augmentor throttling.- Provision was made to insert wedge-shaped blocks into the outboard sections of the augmentor flap as shown in figure 2(i), to reduce augmentor exit area and effect a local throttling of the augmentor eflux to provide rolling moment. Wedge blocks were provided for testing up to 75% area reduction. The blocks simulated a deflectable aft portion of the lower augmentor flap.

TESTS

Table II is an index to the data acquired in these tests, and lists the effects shown on each data figure.

Test procedure consisted primarily of varying angle of attack at constant augmentor duct pressure and at a wind tunnel dynamic pressure of 383 N/sq m (8 lb/sq ft). Reynolds number, based upon the reference chord, was 2.9 million. The angle of attack range was from -12° to 30°. Sideslip range was from -10° to 6°.

Two augmentor flap deflections were used; 50° representing a take-off flap setting, and 75° representing a landing flap setting. These deflections were selected from previous wind tunnel tests as those providing the calculated performance requirements for the proposed flight research aircraft.

Among the power variables tested were: (1) augmentor jet coefficient, (2) effect of fuselage (wing center section) blowing BLC, and (3) underwing jet engine thrust and thrust deflection. Control power variables included: (1) effect of horizontal tail and elevator, (2) ailerons, (3) spoilers, both sector and panel type, and (4) asymmetric augmentor throttling.

DATA REDUCTION

Correction to Data

For all force and moment data presented, the effects of compressor residual jet thrust, and the intake momentum drag of the fuselage mounted J85 and Viper engines, have been subtracted from the measured values. No corrections have been made for the underwing J85's. Forces and moments are referred to the stability axes. The corrections made for thrust and ram drag are as follows:

$$C_L = C_{L_u} - C_T \sin(\alpha_u - \delta_{JP})$$

$$C_{D_{net}} = C_{D_u} + C_T \cos(\alpha_u - \delta_{JP}) - C_{D_{MJ85}} - C_{D_{M_V}}$$

$$C_{M_{net}} = C_{M_u} - C_T \frac{Z_{JP}}{\bar{c}}$$

Wind tunnel boundary corrections were based upon the "aerodynamic C_L", computed as follows:

$$C_{L_{AERO}} = C_L - C_{J_{AI}} (A) \sin (\theta + \alpha_u) \quad \text{(Augmentor)}$$

$$- C_{\mu_{ap}} \sin (\delta_{a_p} + \alpha_u) \quad \text{(Aileron BLC, port)}$$

$$- C_{\mu_{as}} \sin (\delta_{a_s} + \alpha_u) \quad \text{(Aileron BLC, starboard)}$$

$$- C_{\mu_f} \sin \alpha_u \quad \text{(Fuselage BLC)}$$

$$- C_{T_{th_p}} \sin (\delta_p + \alpha_u) \quad \text{(U/wing engine, port)}$$

$$- C_{T_{th_s}} \sin (\delta_s + \alpha_u) \quad \text{(U/wing engine, starboard)}$$

Thus, the following boundary corrections were made:

$$\alpha = \alpha_u + 0.458\, C_{L_{AERO}}$$

$$C_D = C_{D_{net}} + 0.00799\, C_{L_{AERO}}^2$$

$$C_m = C_{m_{net}} + 0.0299\, C_{L_{AERO}} \quad \text{(Tail on only)}$$

The moment center used for data computation was located at 0.25 $\bar{c}$ and 0.20 $\bar{c}$ below the wing chord datum.

Augmentor Jet Thrust Coefficient

Augmentor power settings were based upon augmentor duct pressures in inches of mercury, gauge. These measured values are related to the total isentropic thrust coefficient (C_{J_I}) as indicated on the data figures. This coefficient is the sum of the isentropic thrust coefficients of the augmentor alone ($C_{J_{AI}}$), the aileron BLC (C_{μ_a}) and the

fuselage BLC ($C_{\mu F}$). The table below shows typical values of these quantities for each of the four augmentor duct pressures used during testing. Wind tunnel dynamic pressure of q = 383 N/sq m (8 lb/sq ft).

Nominal Augmentor Duct Pressure Cm Hg (In Hg)	Aug. $C_{J_{AI}}$	Aileron BLC C_{μ_a}		Fuselage BLC	Total C_{J_I}	
		Port	Stbd.		Fus. BLC On	Fus. BLC Off
20.3 (8)	0.28	.008	.008	.030	0.33	0.30
40.7 (16)	0.54	.015	.017	.047	0.62	0.57
61.0 (24)	0.76	.023	.024	.059	0.87	0.81
76.2 (30)	0.95	.028	.029	.065	1.07	1.01

Note that thrust forces and intake momentum drag forces of the underwing J85 engines are included in the plotted force data. The approximate augmentation ratios for 50 and 75 degrees flap deflection are 1.16 and 1.11 respectively.

Ames Research Center
National Aeronautics and Space Administration
Moffett Field, Calif. 94035, March 17, 1971

REFERENCES

1. Koenig, D. G., Corsiglia, V. R., Morelli, J. P.: Aerodynamic Characteristics of a Large Scale Model with an Unswept Wing and Augmented Jet Flap. NASA TN D-4610, June 1968.

2. Pope, Alan, and Harper, John J.: Low Speed Wind Tunnel Testing. John Wiley and Sons Inc. 1966.

TABLE I - MODEL GEOMETRY

Wing

Gross area, sq m (sq ft)	21.40	(230.4)
Net area, sq m (sq ft)	18.62	(200.4)
Span, m (ft)	13.45	(44.15)
Aspect ratio	8.45	
Area spanned by one augmentor, sq m (sq ft)	6.59	(70.9)
Aera spanned by one aileron, sq m (sq ft)	2.72	(29.3)
Thickness/chor ratio	0.16	
Reference chord length, m (ft)	1.727	(5.667)

Section, 16% NACA 747A forward of 40% c,
NACA 0016-34 aft of 40% c,
camber 2.23%, $C_{L_{design}} = 0.3$

Tailplane

Area, sq m (sq ft)	5.82	(63.7)
Span, m (ft)	5.27	(17.28)
Aspect ratio	4.68	
Volume coefficient	1.16	
Height above wing datum, m (ft)	2.42	(7.94)
Elevator chord ratio	0.41	

Vertical tail

Area, sq m (sq ft)	3.89	(41.9)
Height, above fuselage surface, m (ft)	2.30	(7.56)
Aspect ratio	1.365	
Volume coefficient	0.0845	

Section, NACA 63-015 mod.

TABLE II - INDEX TO DATA

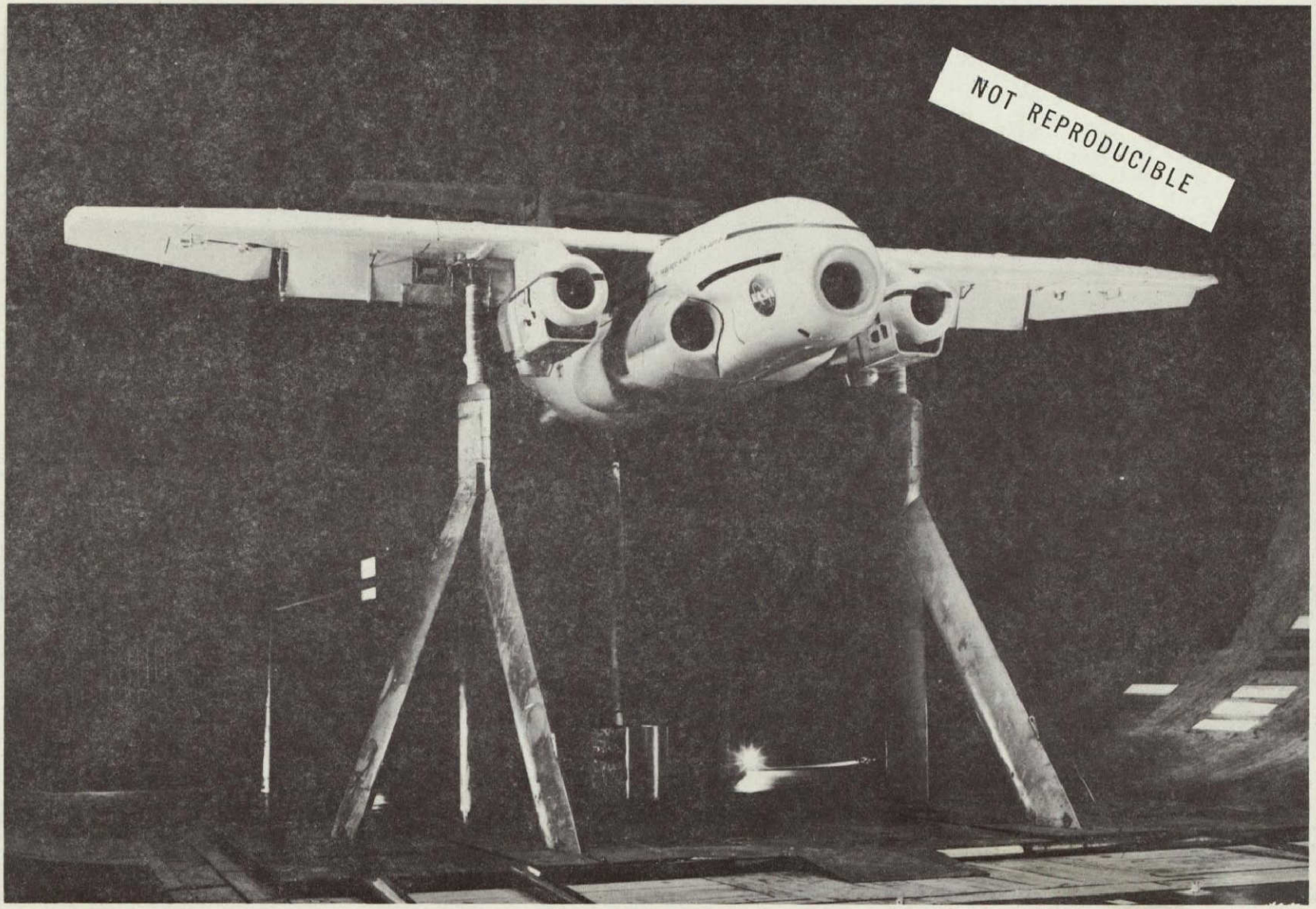

(a) Front view of model.

Figure 1.- Views of the model installed in the Ames 40- by 80-Foot Wind Tunnel

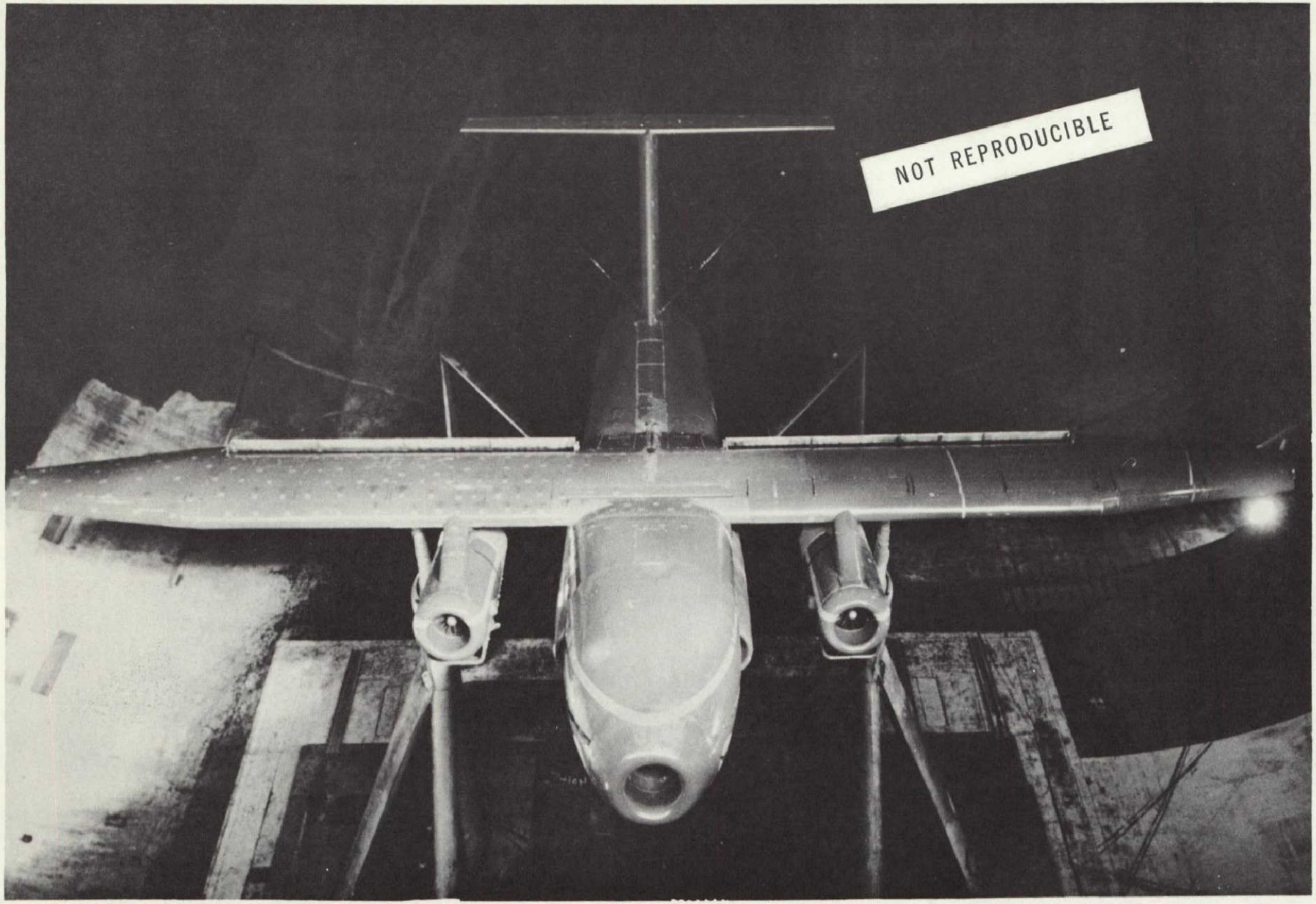

(b) Upper view of model, showing spanwise augmentor intake door.

Figure 1.- Continued.

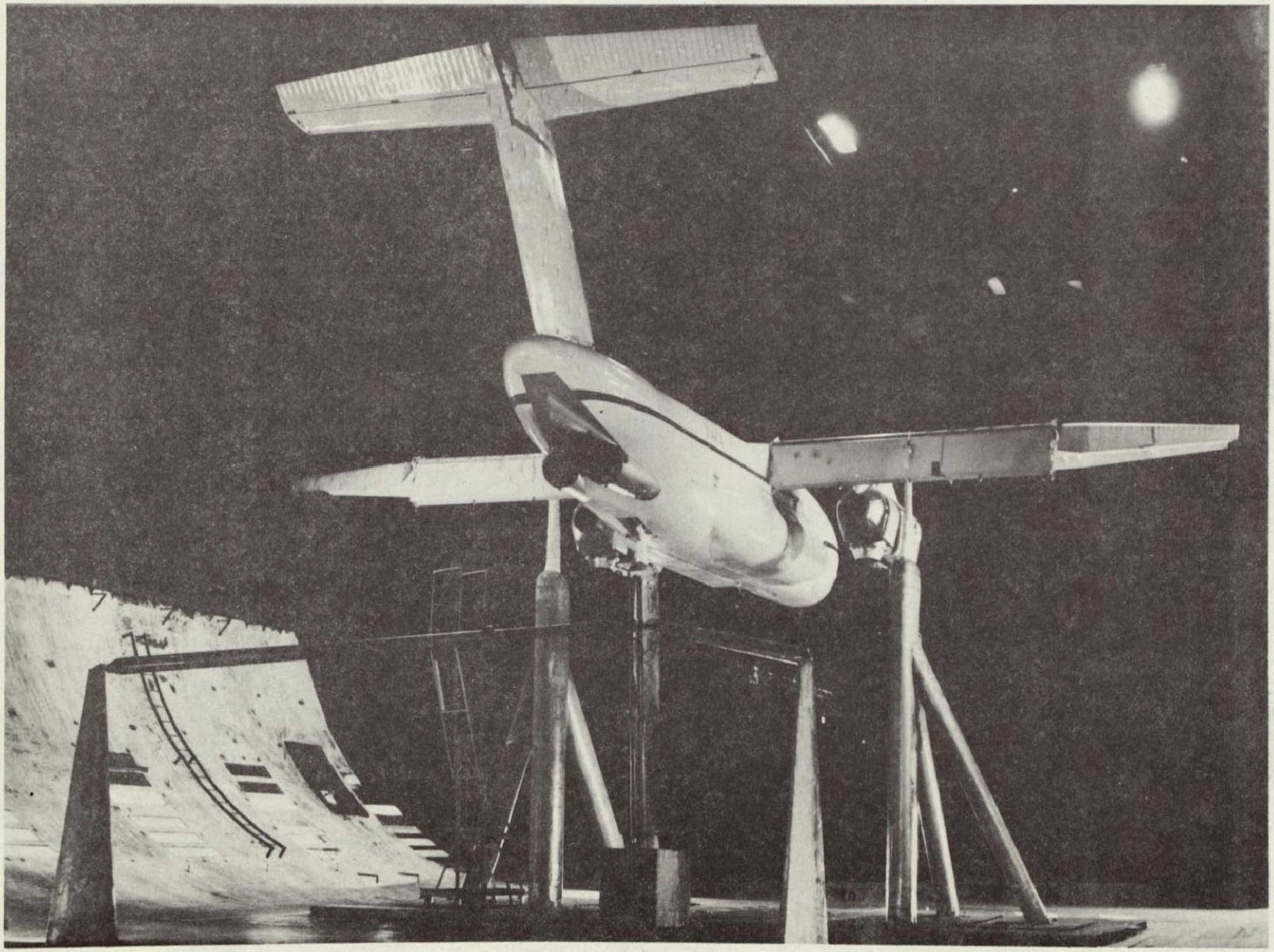

(c) Rear view of model.

Figure 1.- Concluded.

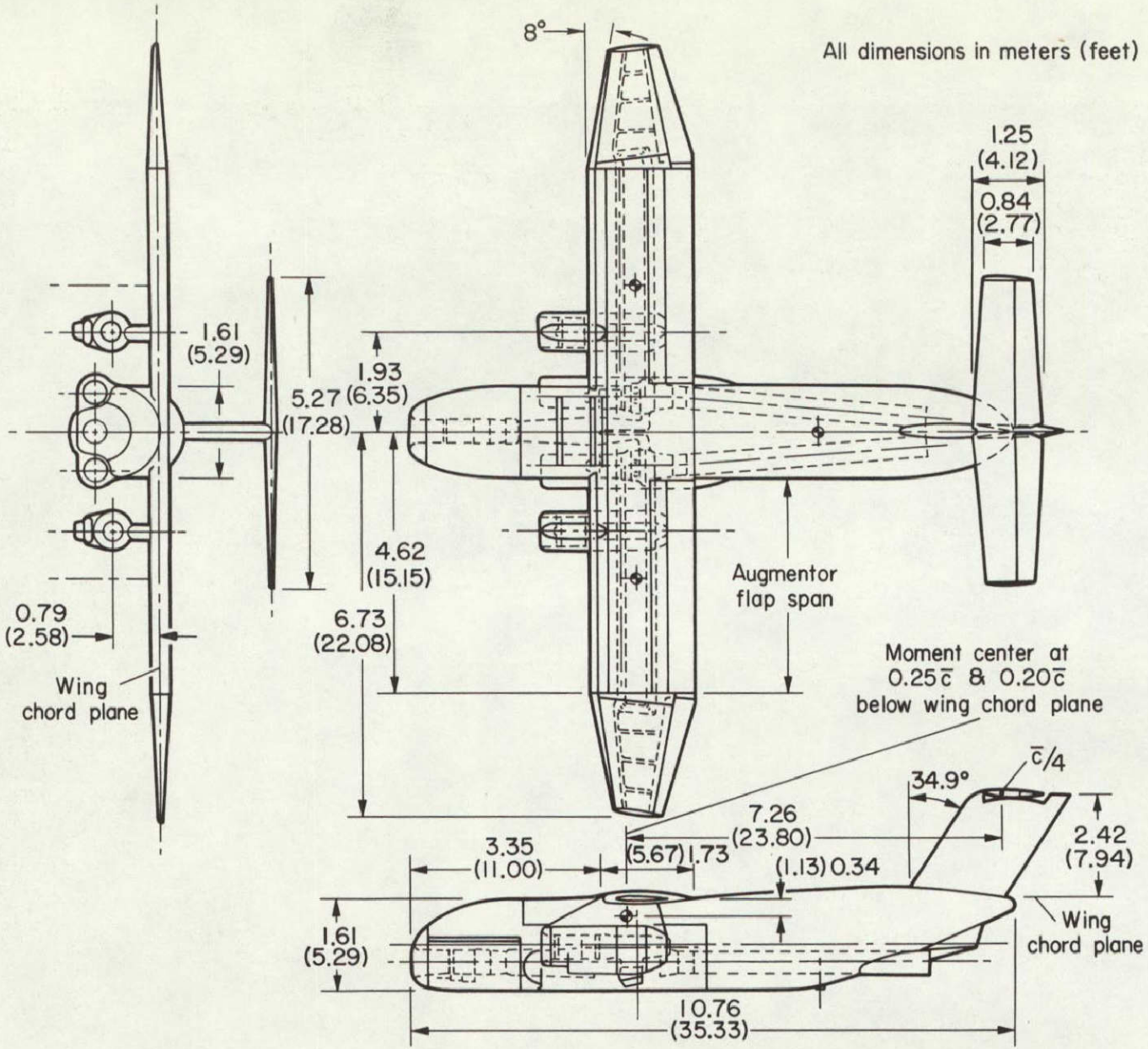

(a) Three-view drawing of the model.

Figure 2.- Geometric details of the model.

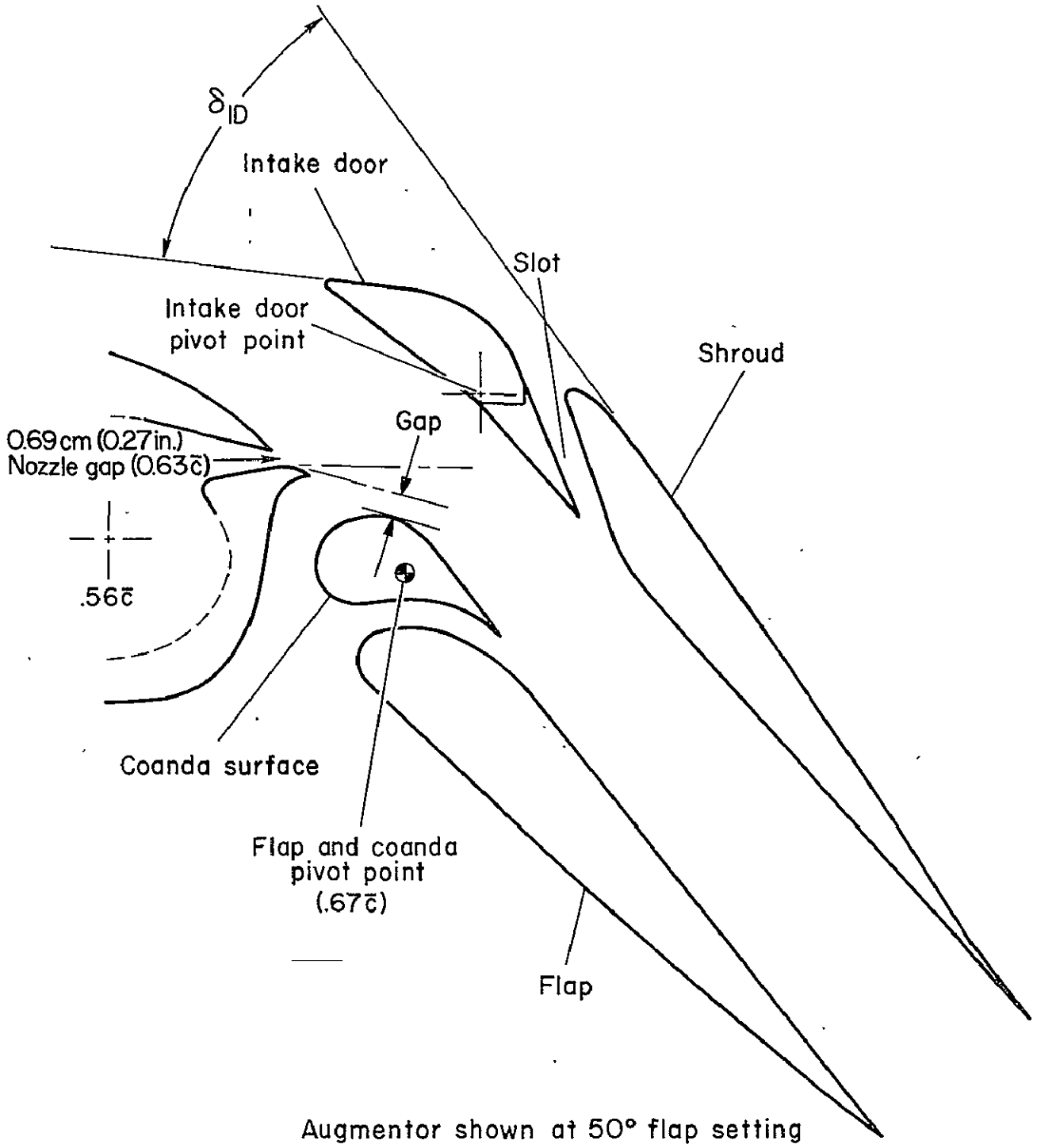

(b) Augmentor geometry.

Figure 2.- Continued.

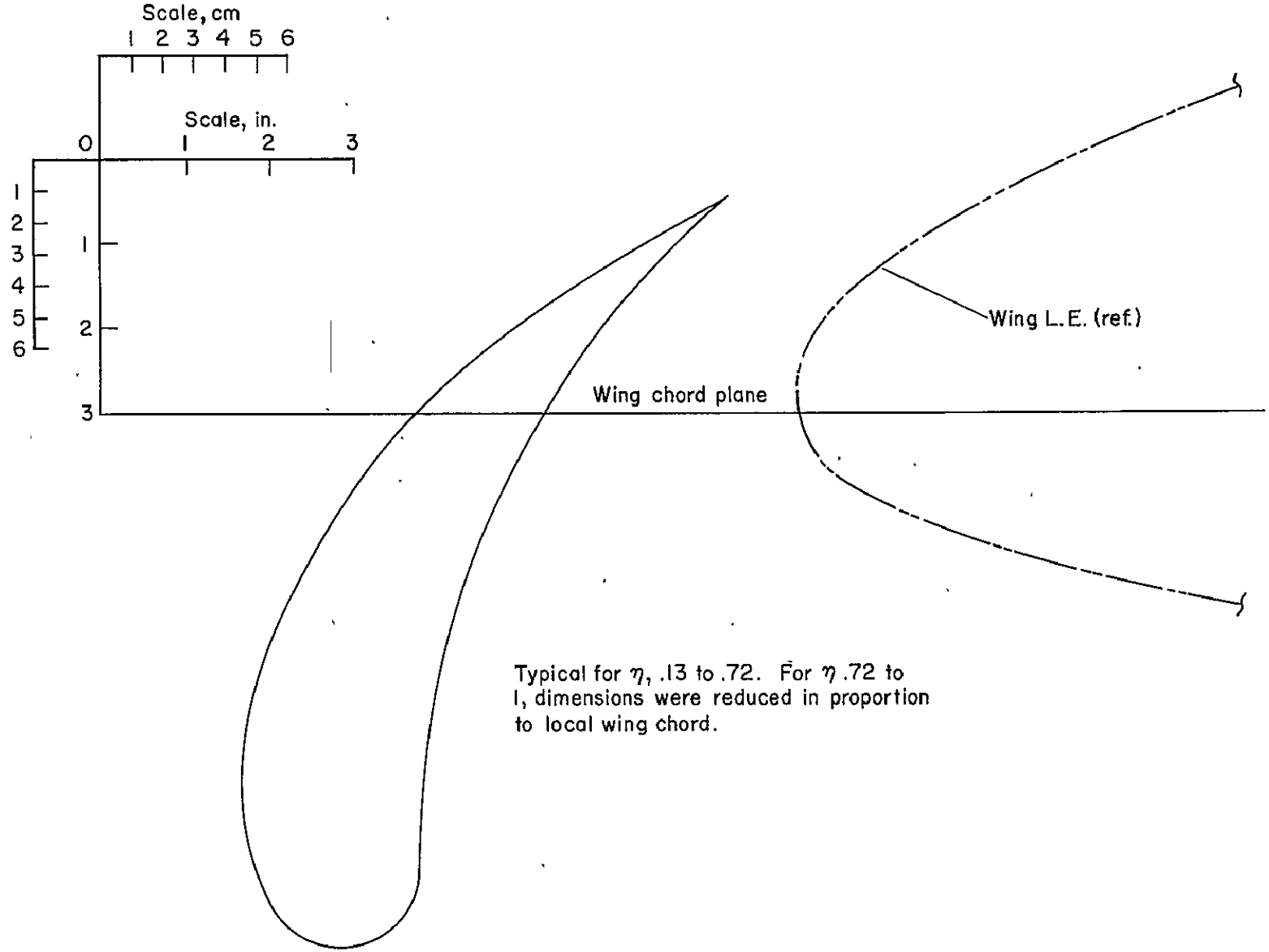

(c) Details of leading-edge slat.

Figure 2.- Continued.

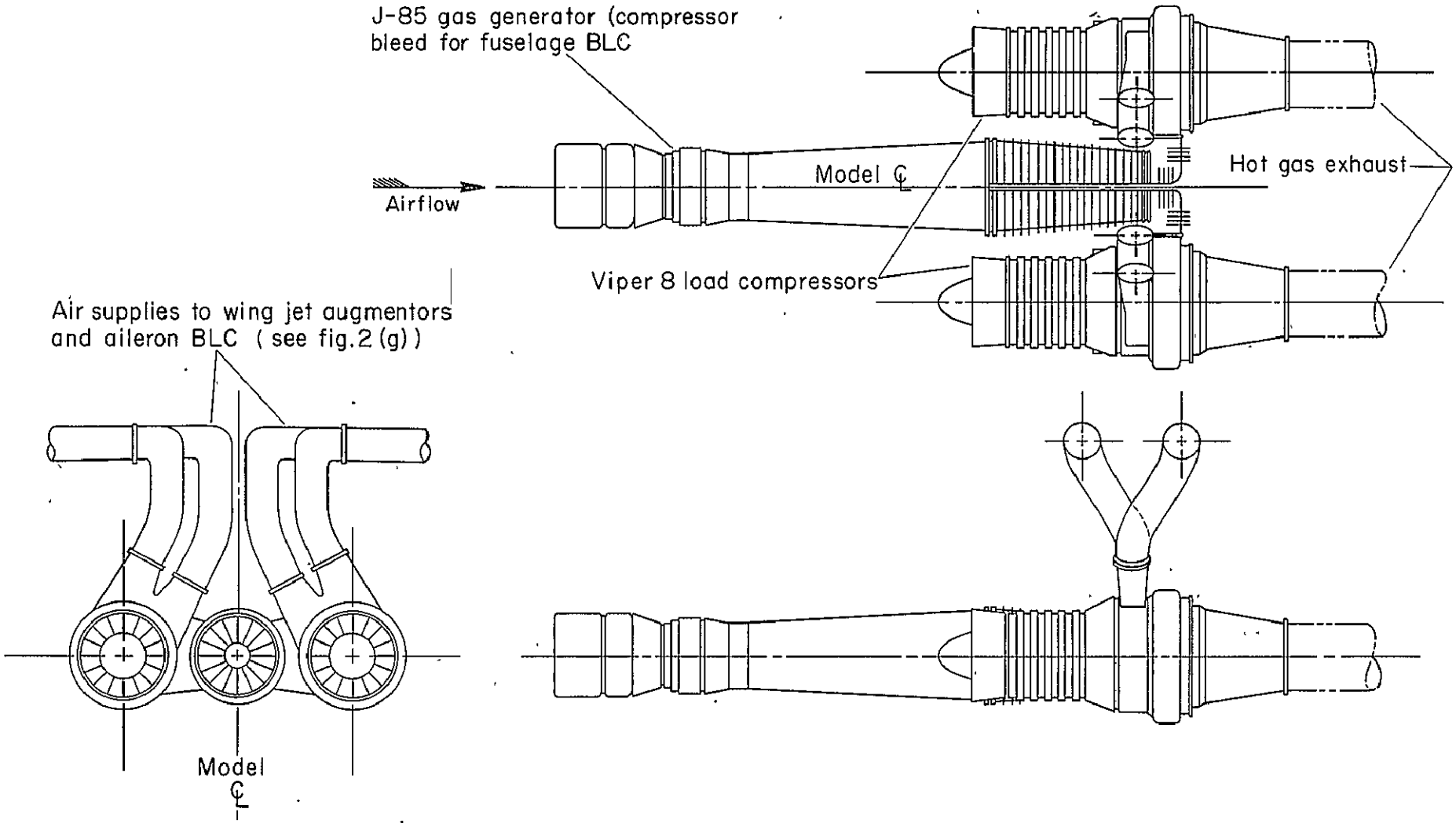

(d) Augmentor air compressor system.

Figure 2.- Continued.

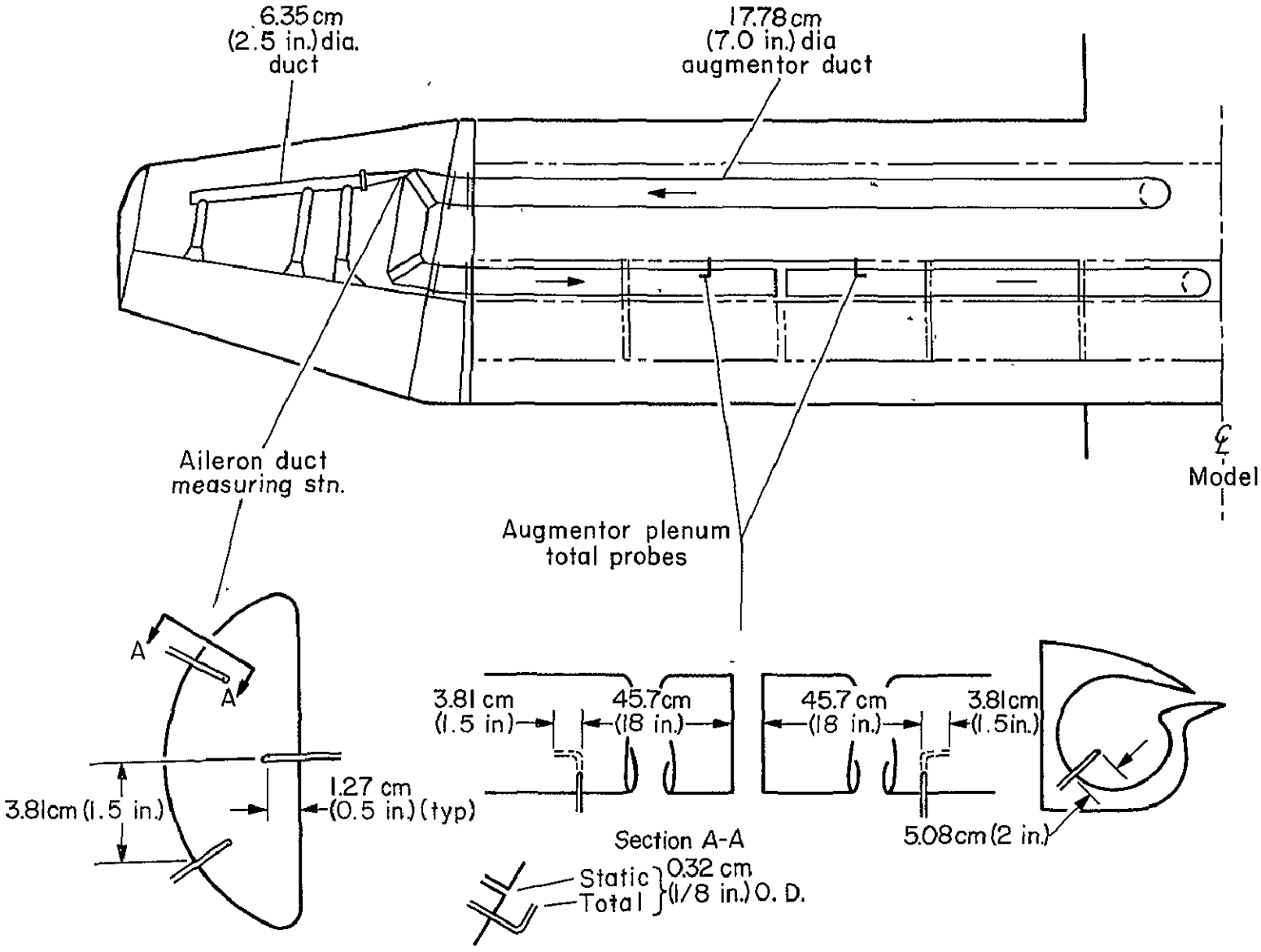

(e) Augmentor and aileron duct system.

Figure 2.- Continued.

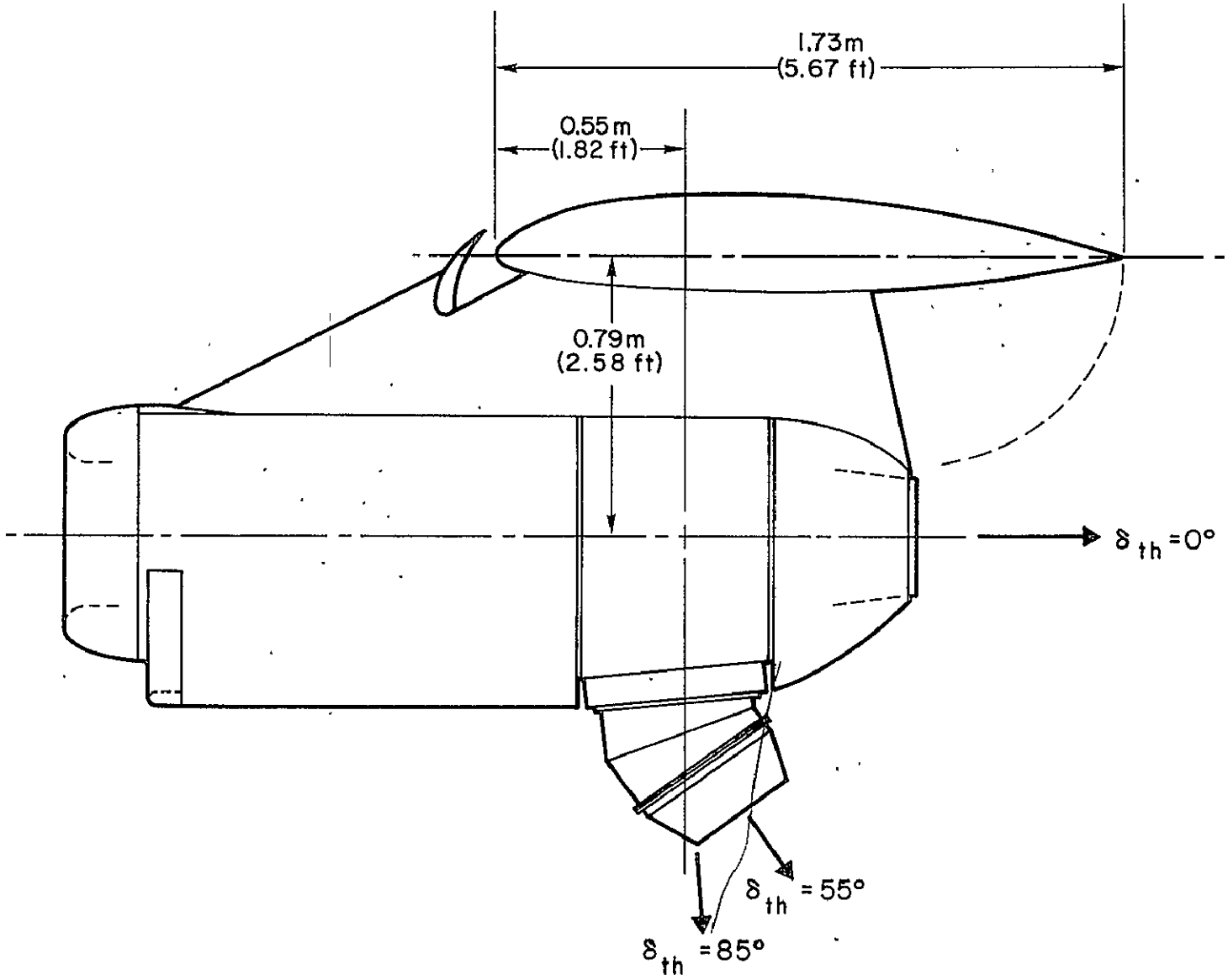

(f) J85 nacelle and thrust diverter nozzle.

Figure 2.- Continued.

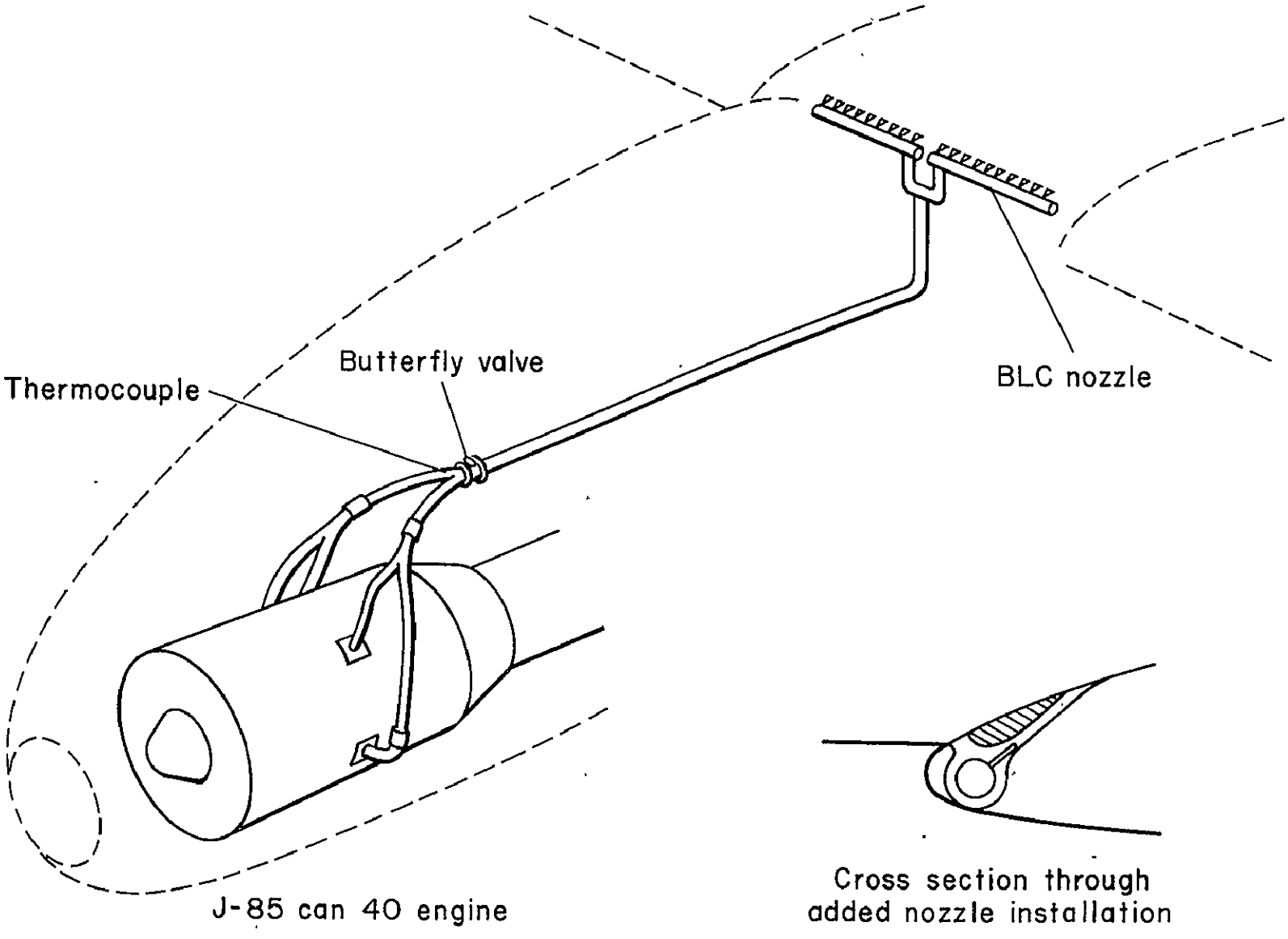

(g) Fuselage BLC system.

Figure 2.- Continued.

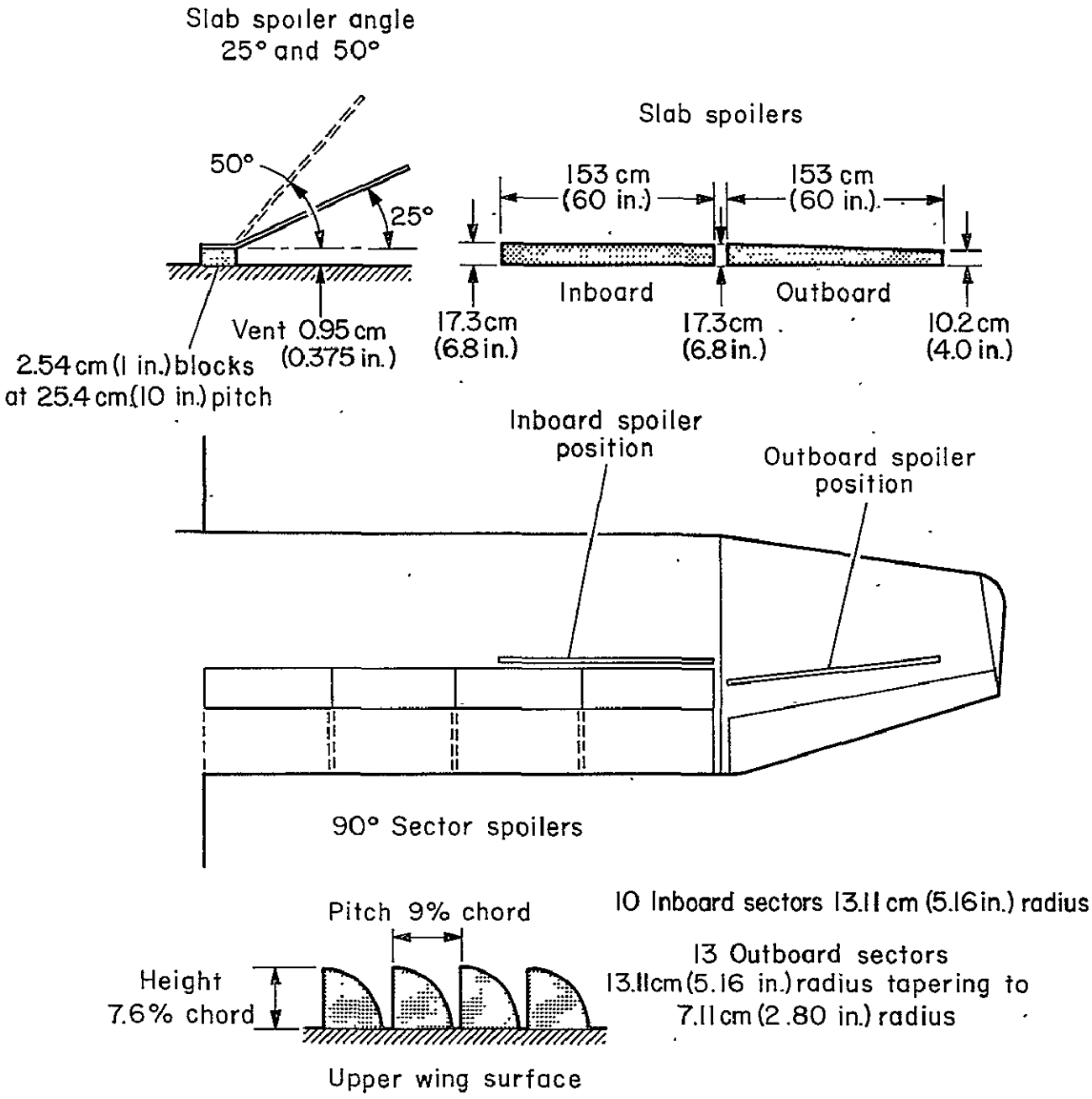

(h) General arrangement of spoilers.

Figure 2.- Continued.

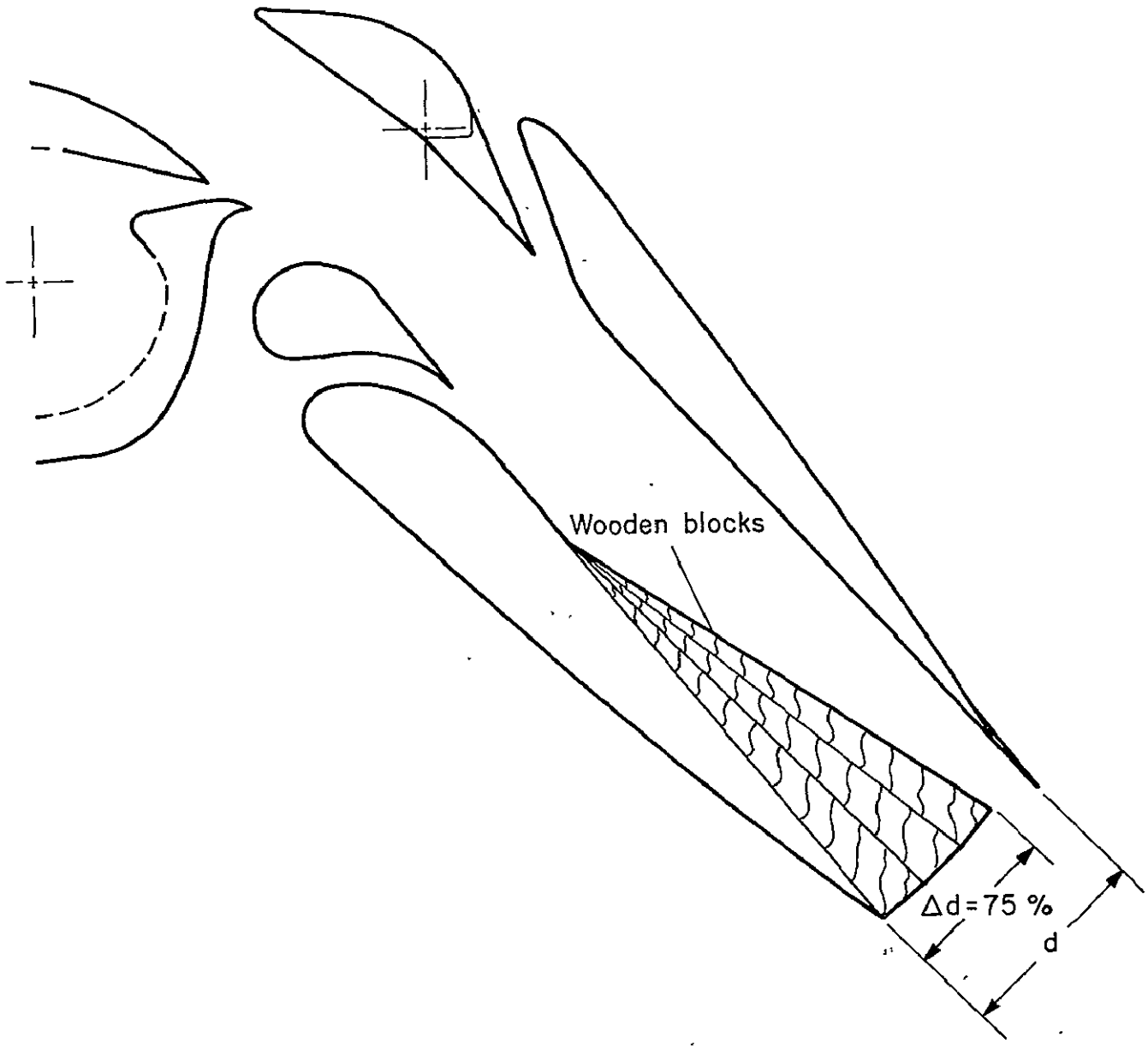

(i) Augmentor throttle system.

Figure 2.- Continued.

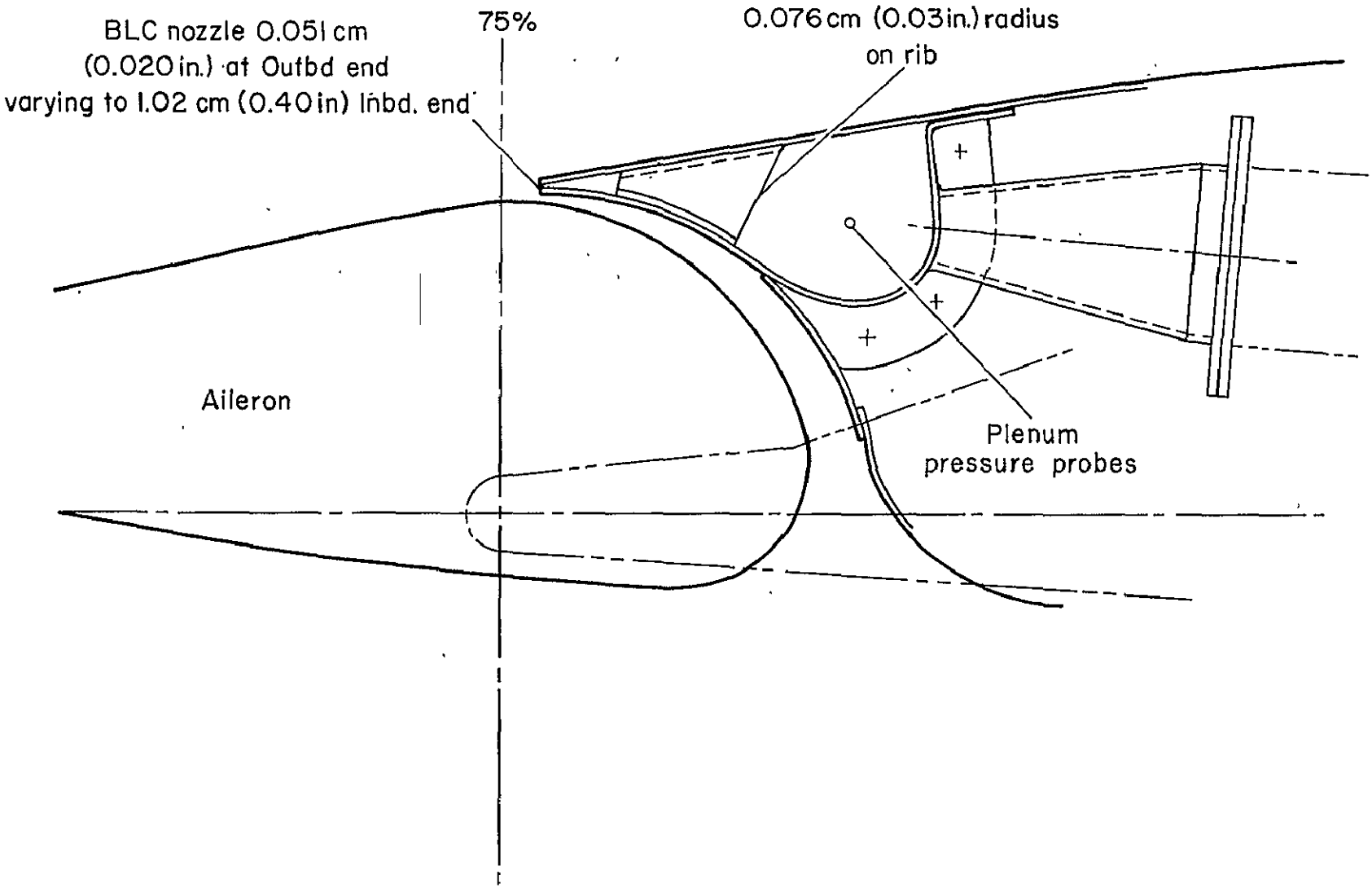

(j) Typical section through aileron blowing system.

Figure 2.- Concluded.

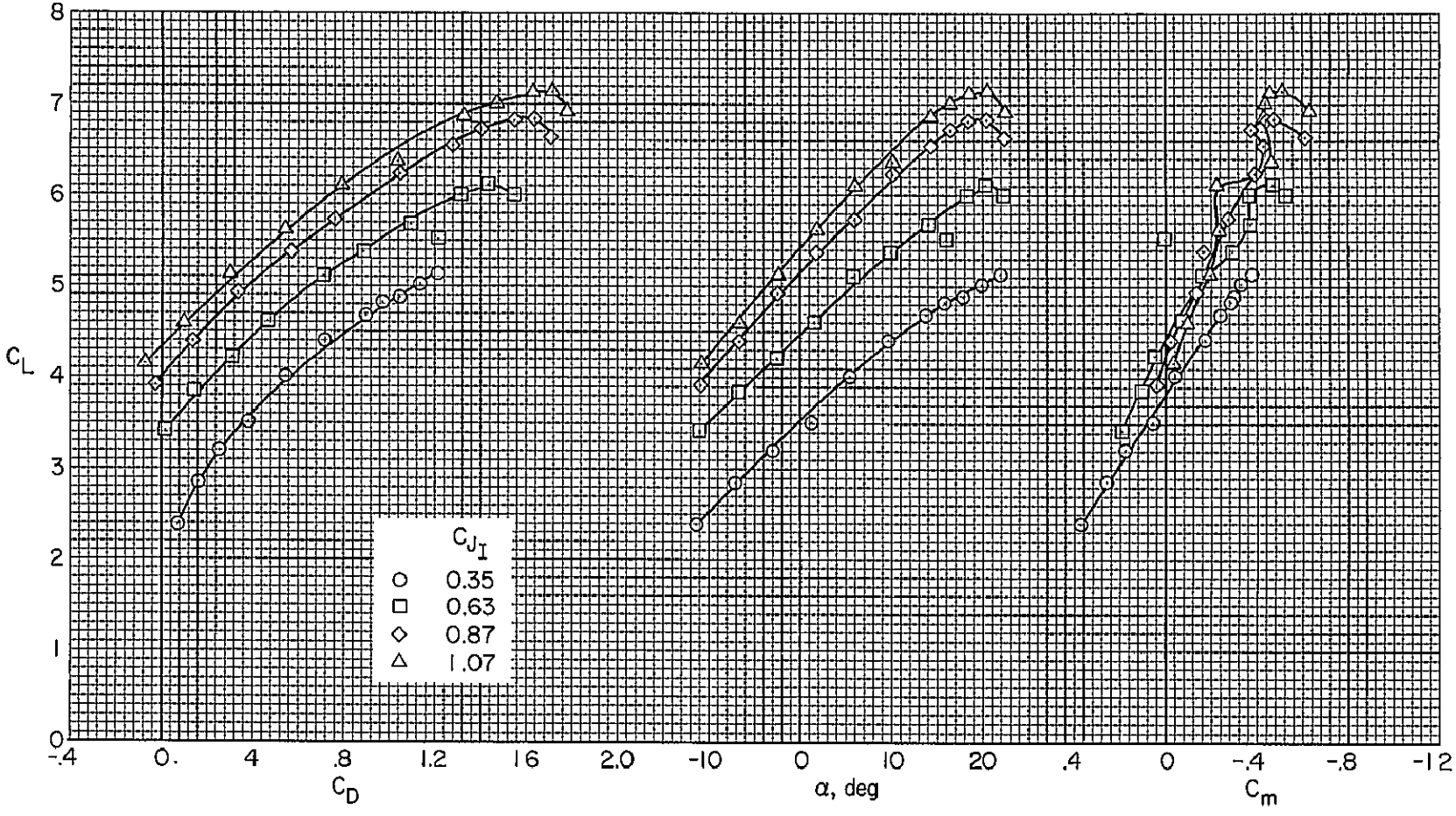

(a) Fuselage BLC on, $\delta_{th} = 85^{\circ}$, $\delta_a = 45/45$.

Figure 3.- The effect of C_{J_I} on the longitudinal characteristics of the model with $\delta_f = {}^{I}75^{\circ}$; $C_{T_{th}} = 0.81$, $i_t = -4^{\circ}$, $\delta_e = 0^{\circ}$.

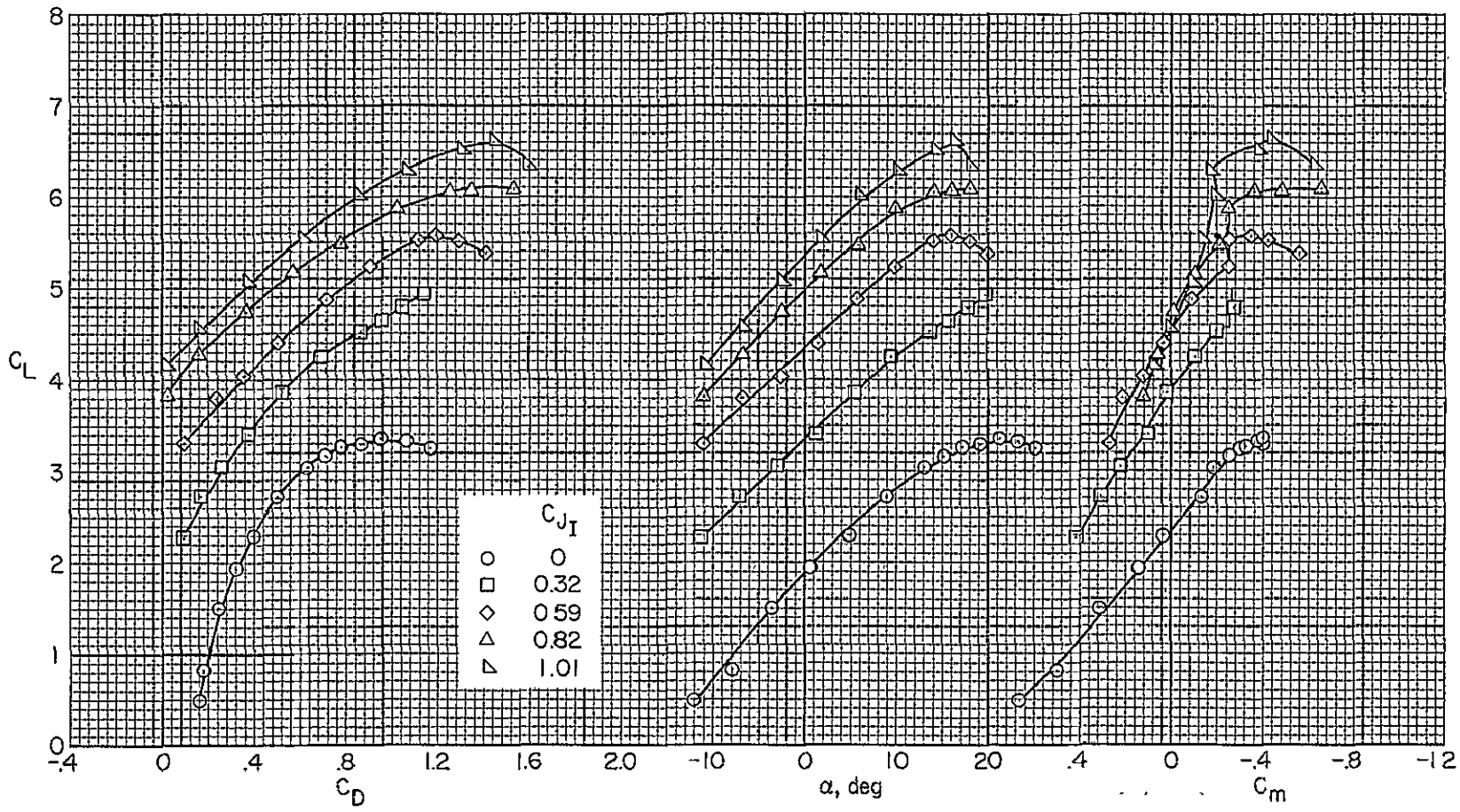

(b) Fuselage BLC off, $\delta_{th} = 100^{\circ}$, $\delta_a = 45/45$.

Figure 3.- Continued.

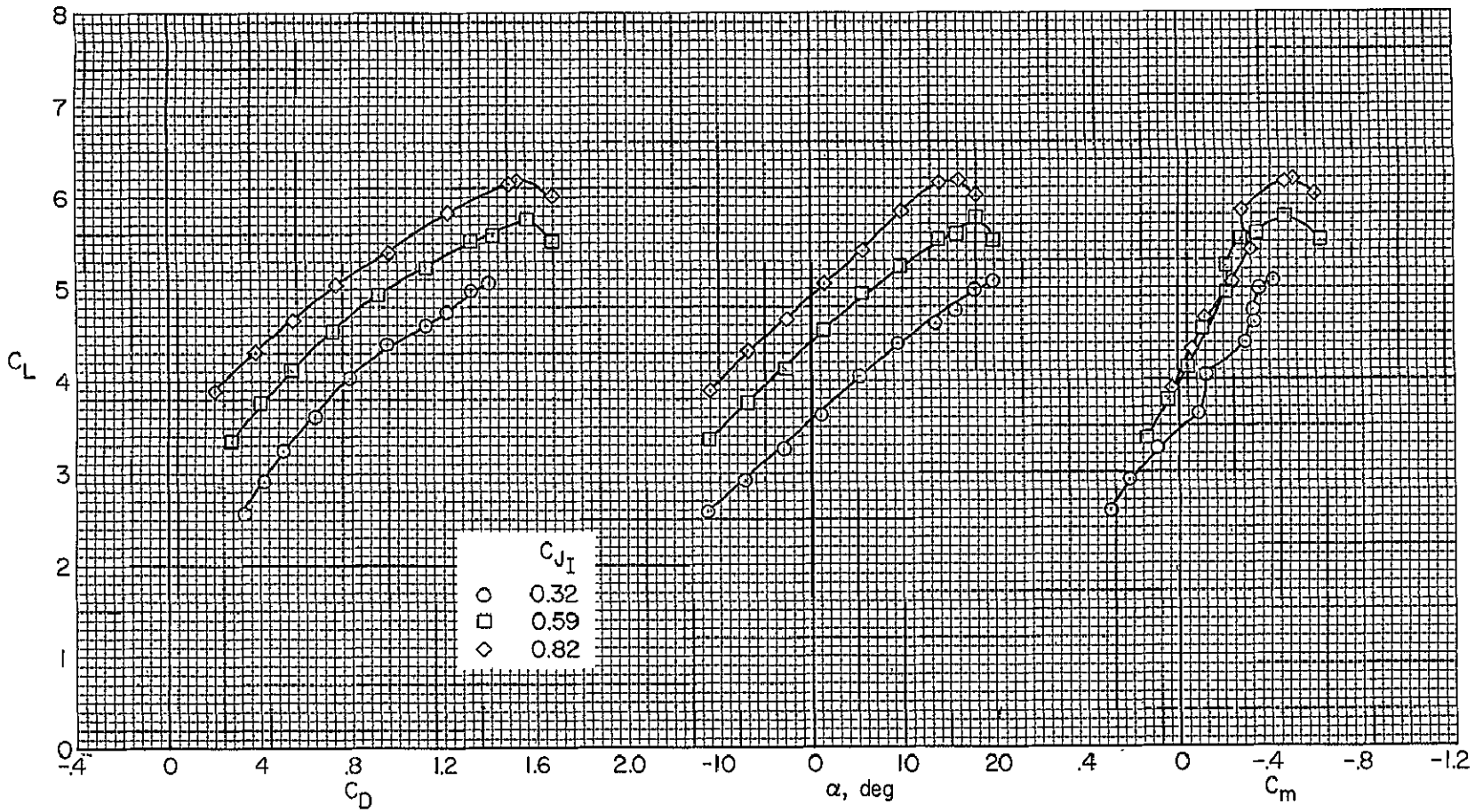

(c) Fuselage BLC off, $\delta_{th} = 100^{o}$, $\delta_{a} = 45/45$.

Figure 3.- Continued

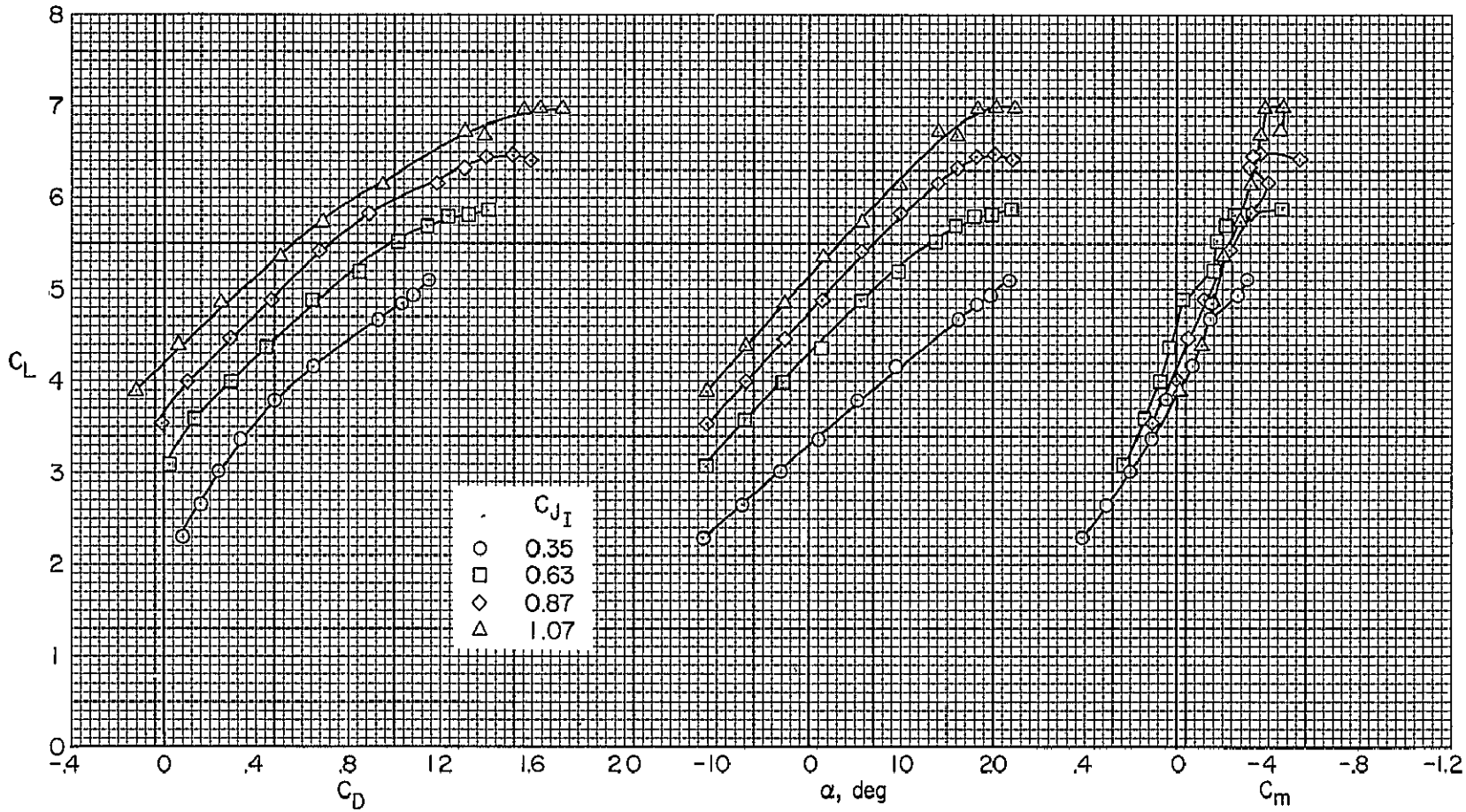

(d) Fuselage BLC on, $\delta_{th} = 85^{o}$, $\delta_{a} = 20/20$.

Figure 3.- Concluded.

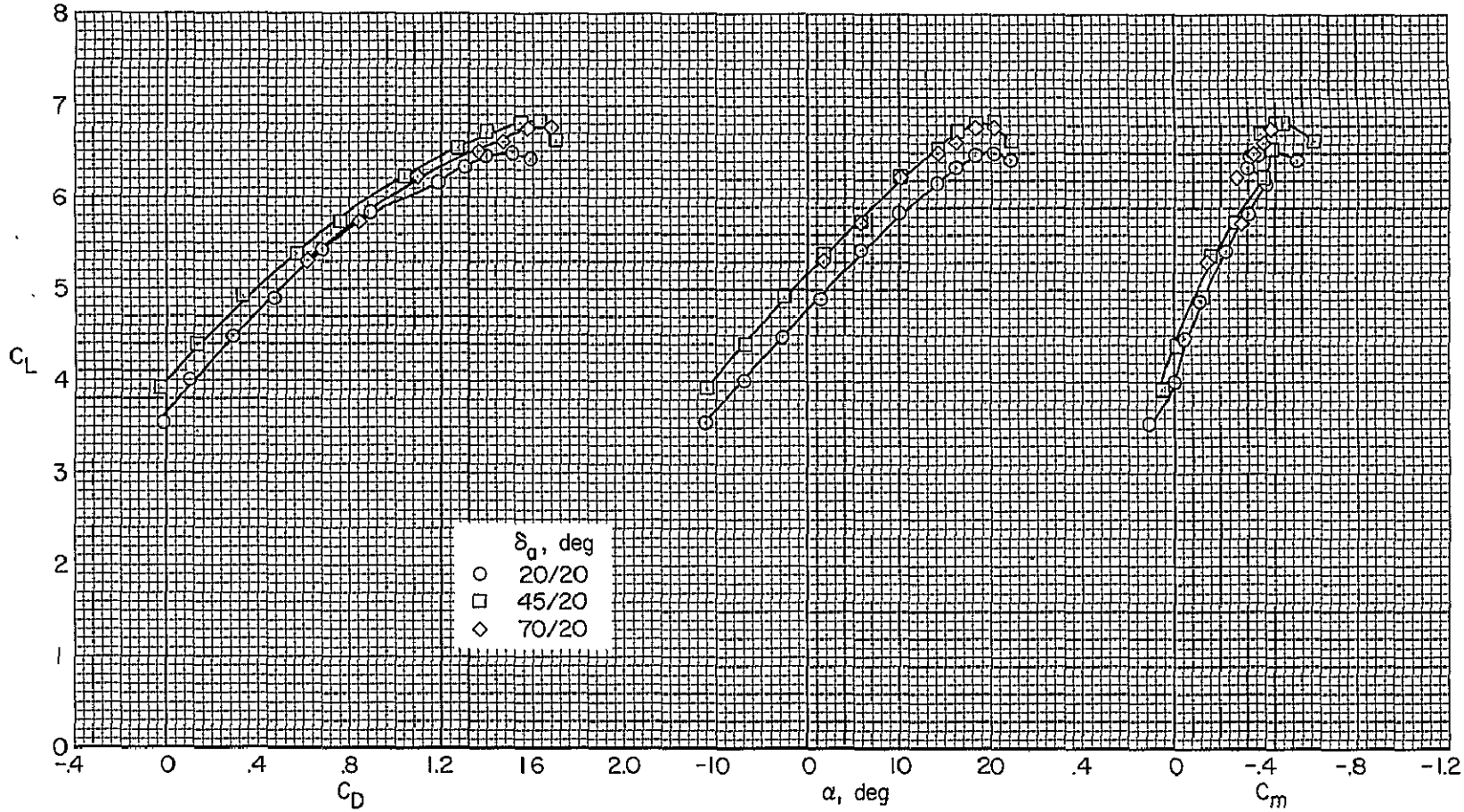

Figure 4.- The effect of symmetrical aileron droop on the longitudinal characteristics of the model with $\delta_f = 75^o$; $C_{J_I} = 0.87$, $\delta_{th} = 85^o$, $C_{T_{th}} = 0.81$, $i_t = -4^o$, $\delta_e = 0^o$, BLC on.

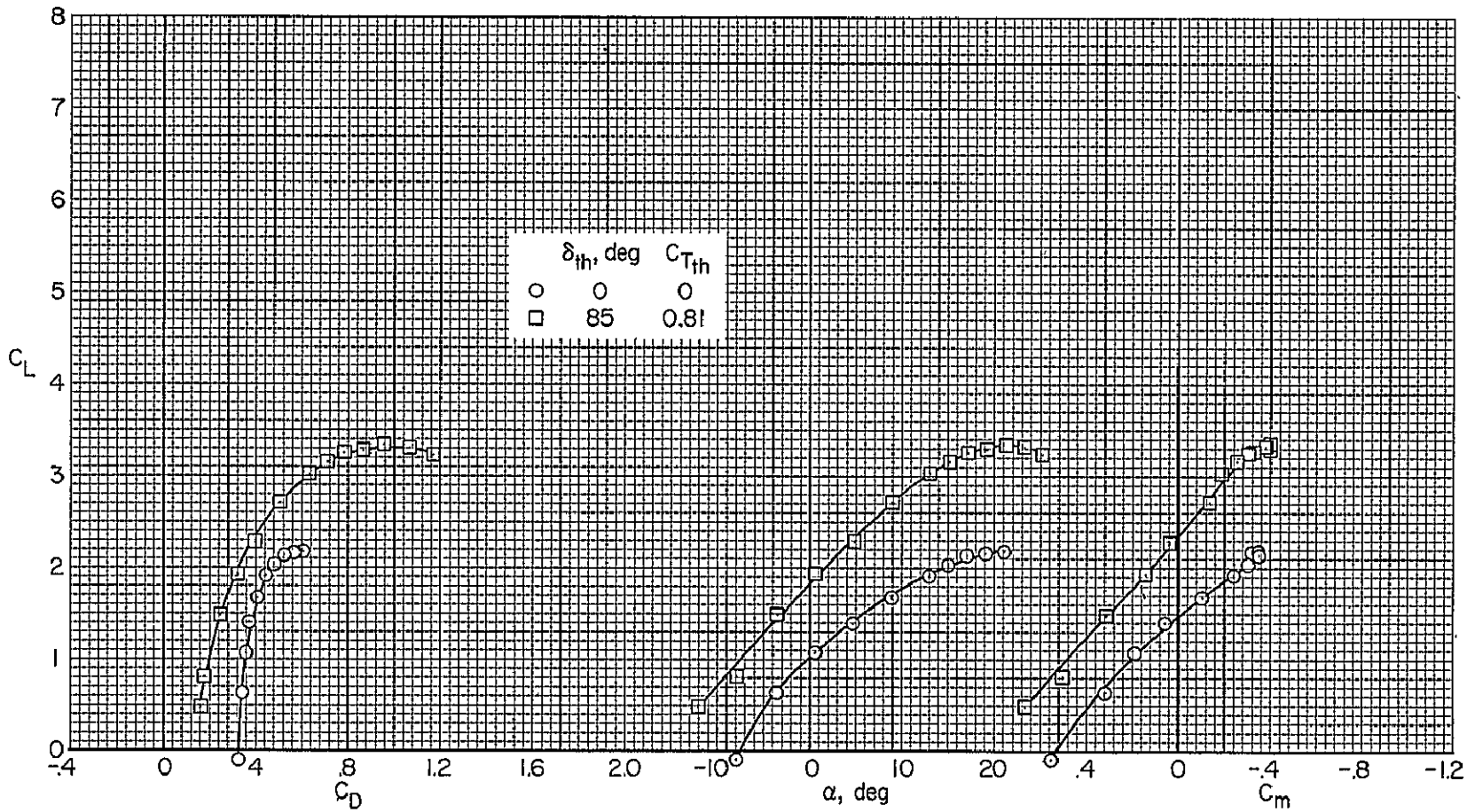

(a) Fuselage BLC off, $C_{J_I} = 0$.

Figure 5.- The effect of $C_{T_{th}}$ and δ_{th} on the longitudinal characteristics of the model with $\delta_f = 75^\circ$; $\delta_a = 45/45$, $i_t = -4^\circ$, $\delta_e = 0^\circ$.

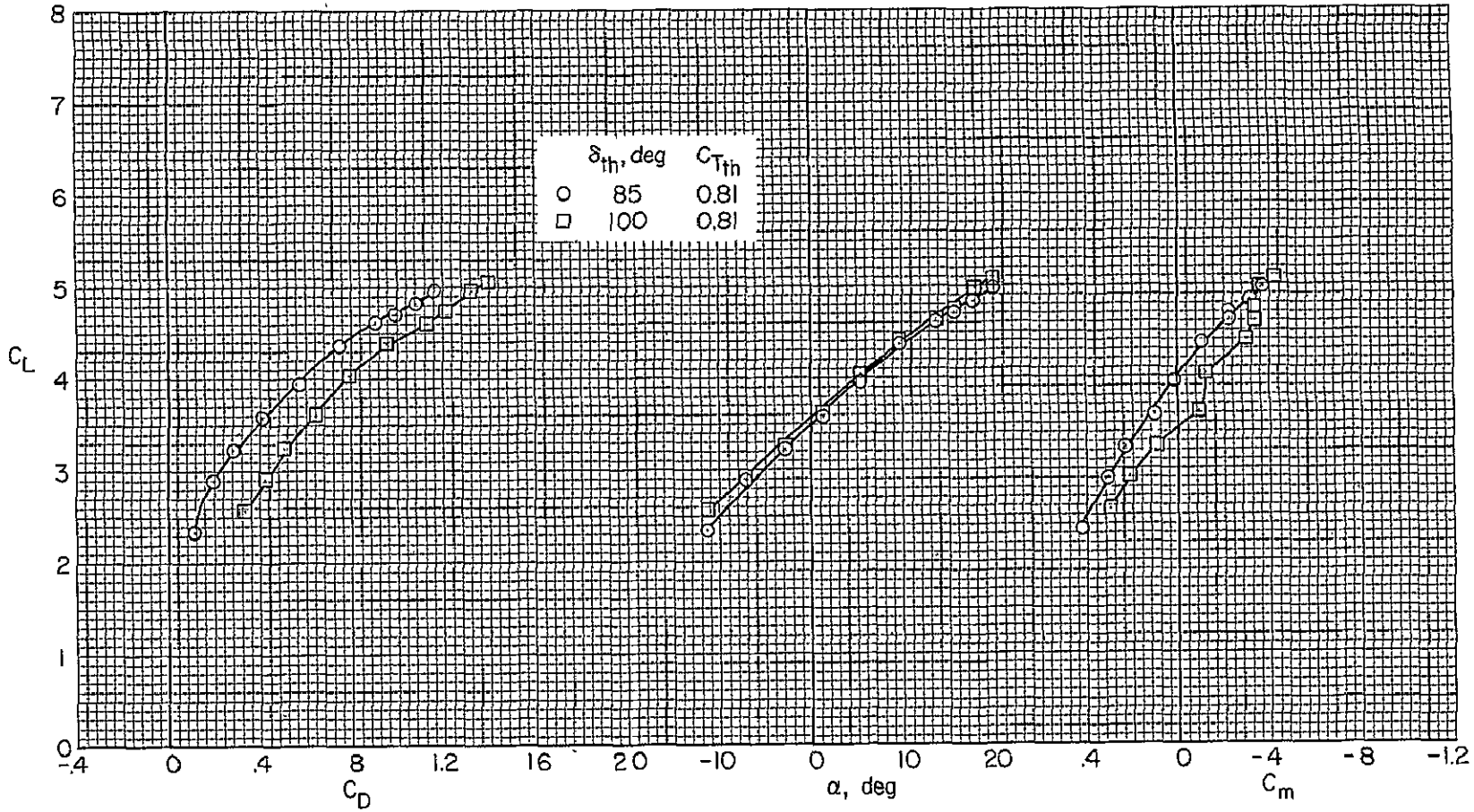

(b) Fuselage BLC off, $C_{J_I} = 0.32$.

Figure 5.- Continued.

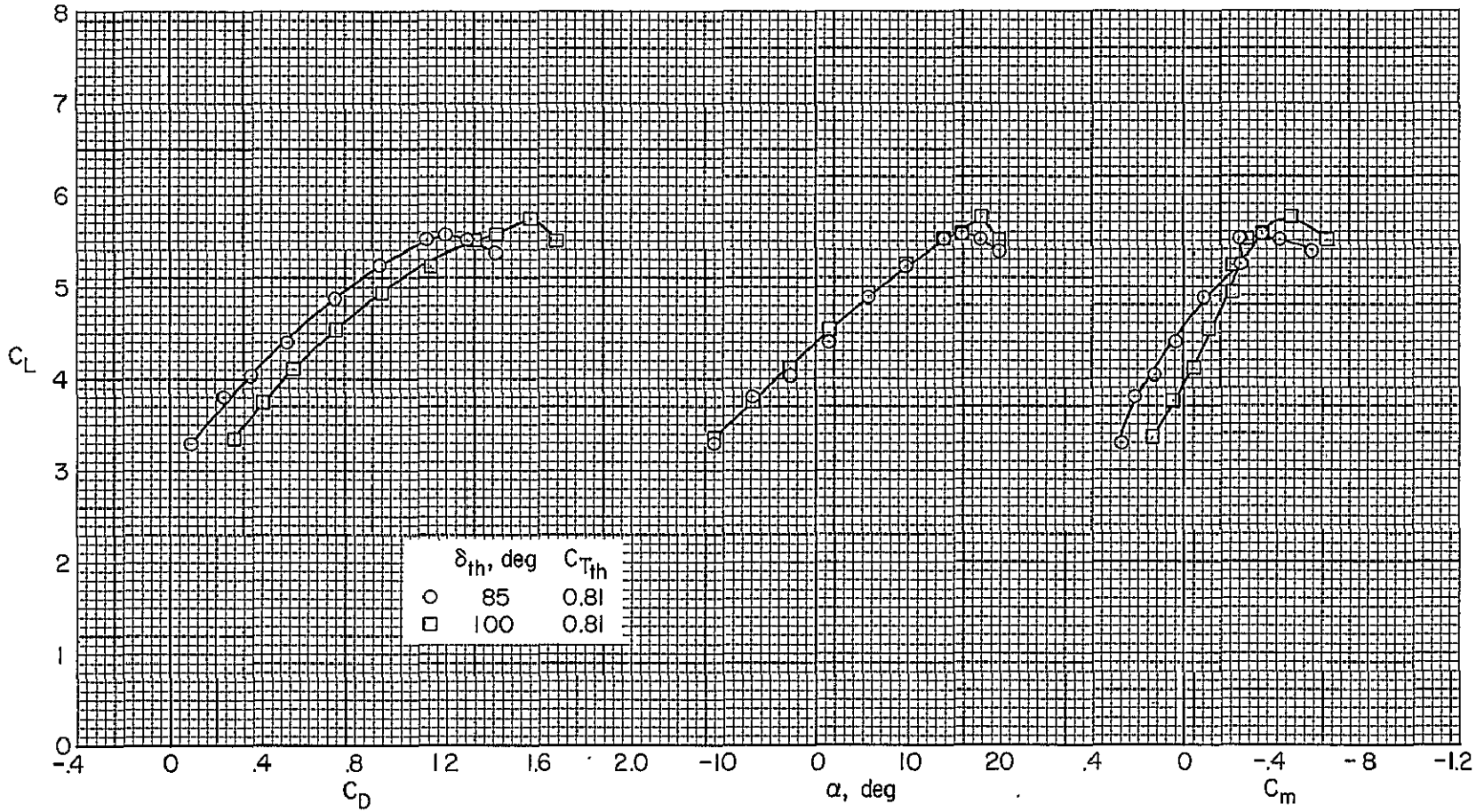

(c) Fuselage BLC off, C_{J_I} = 0.58.

Figure 5.- Continued.

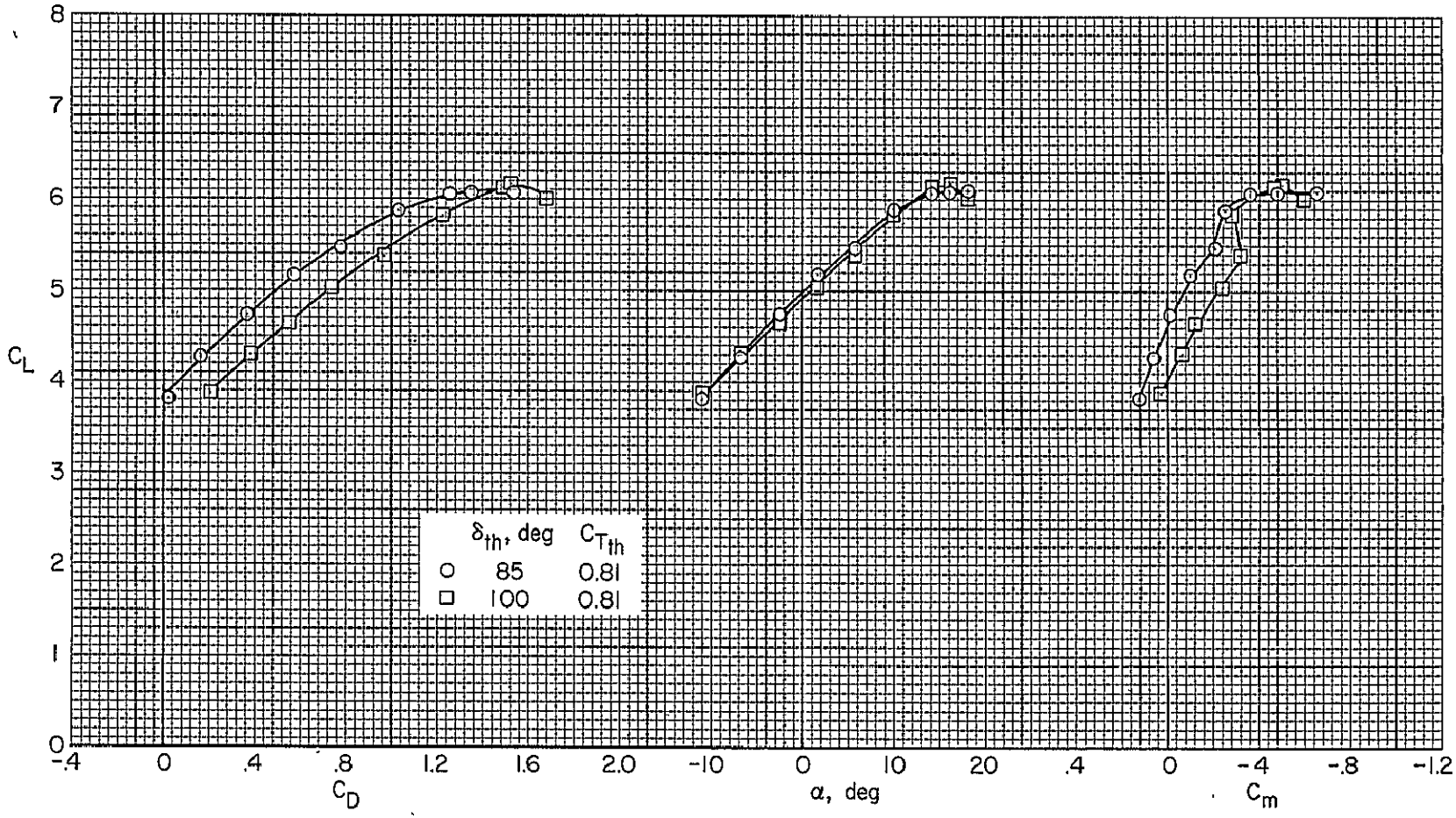

(d) Fuselage BLC off, $C_{J_I} = 0.82$.

Figure 5.- Continued.

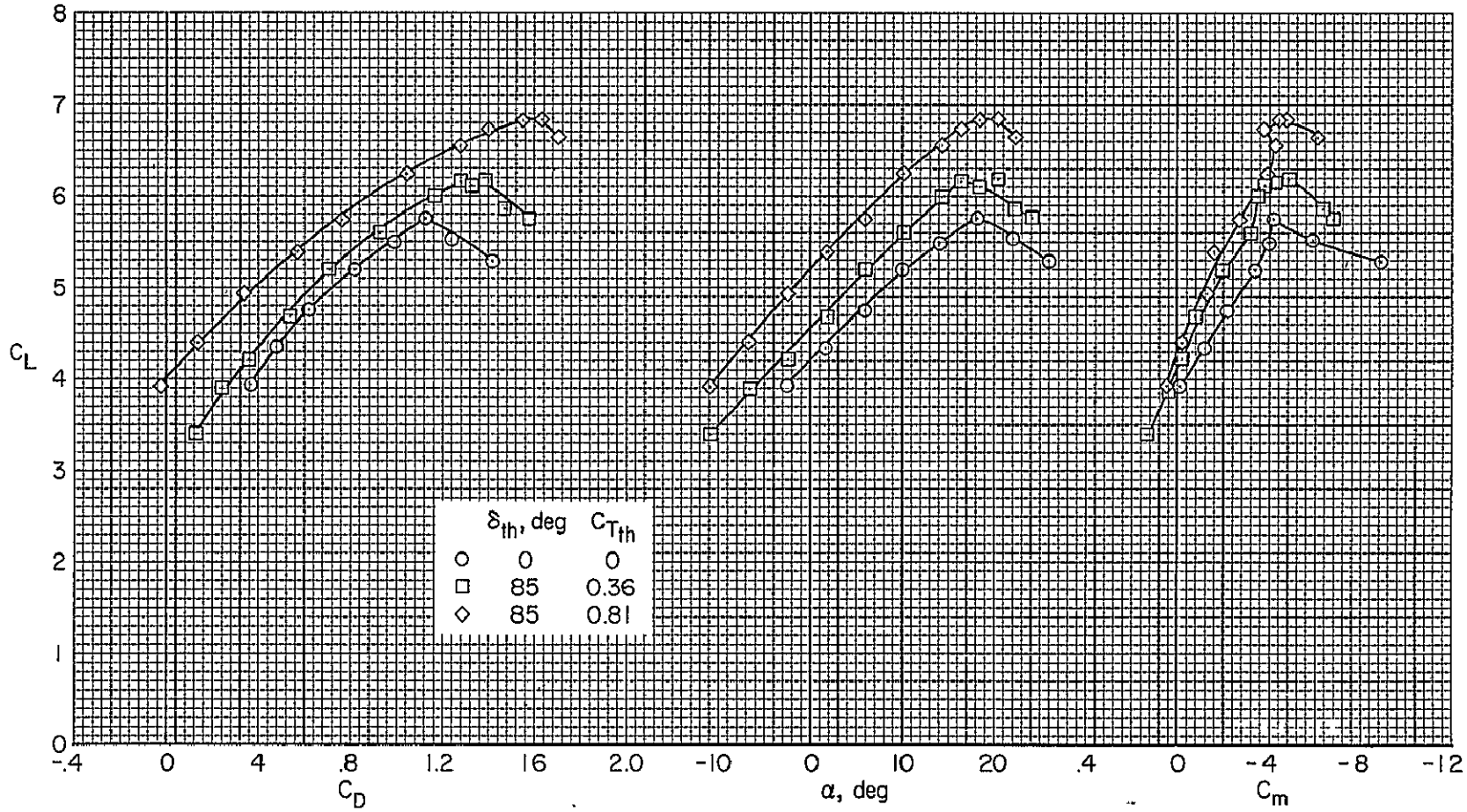

(e) Fuselage BLC on, $C_{J_I} = 0.85$.

Figure 5.- Concluded.

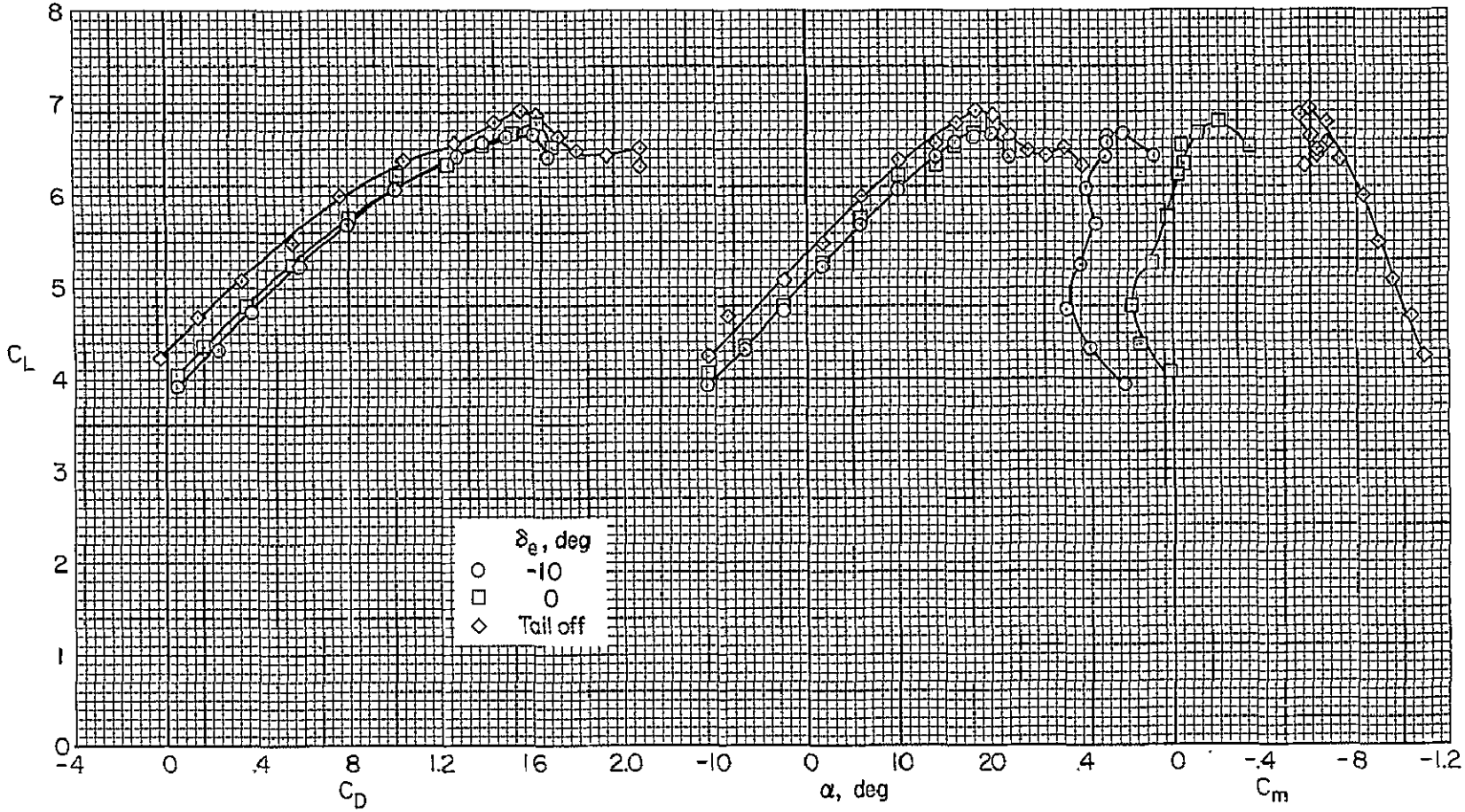

(a) $i_t = -9^o$.

Figure 6.- The effect of δ_e on the longitudinal characteristics of the model with $\delta_f = 75^o$; $C_{J_I} = 0.87$, $\delta_a = 45/45$, $C_{T_{th}} = 0.81$, $\delta_{th} = 85^o$, BLC on.

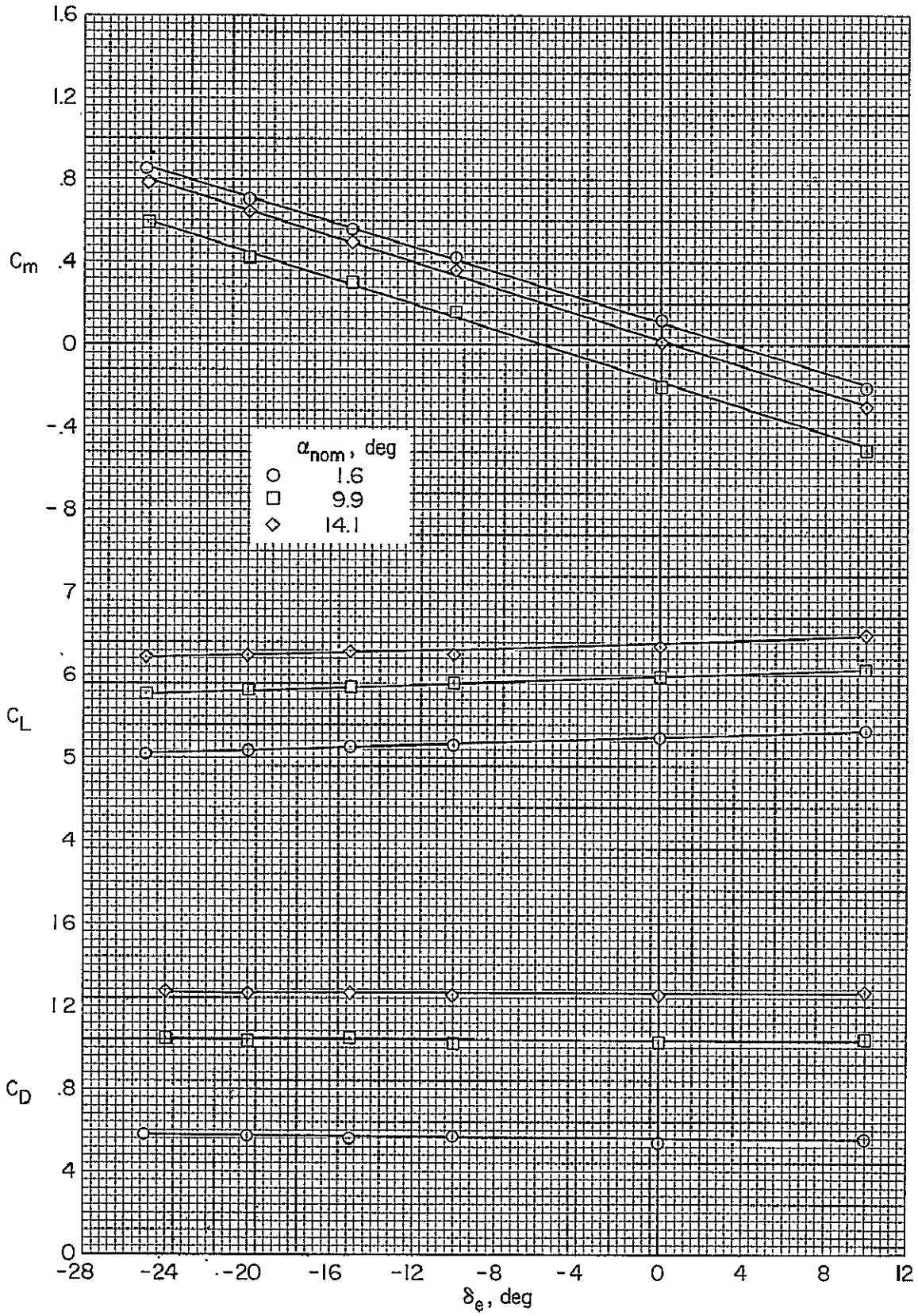

(b) $i_t = -9^\circ$, constant α.

Figure 6.- Continued.

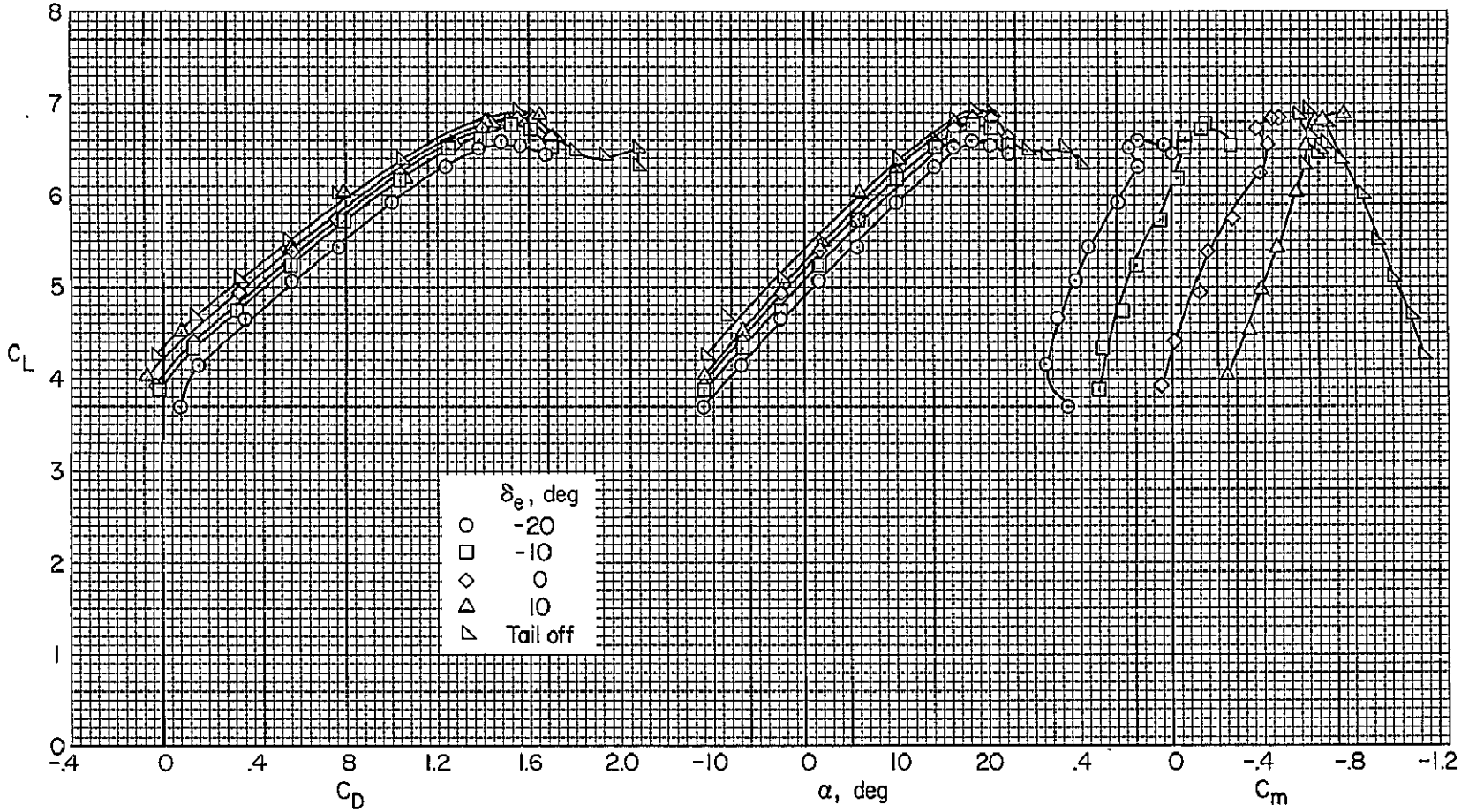

(c) $i_t = -4^\circ$.

Figure 6.- Continued.

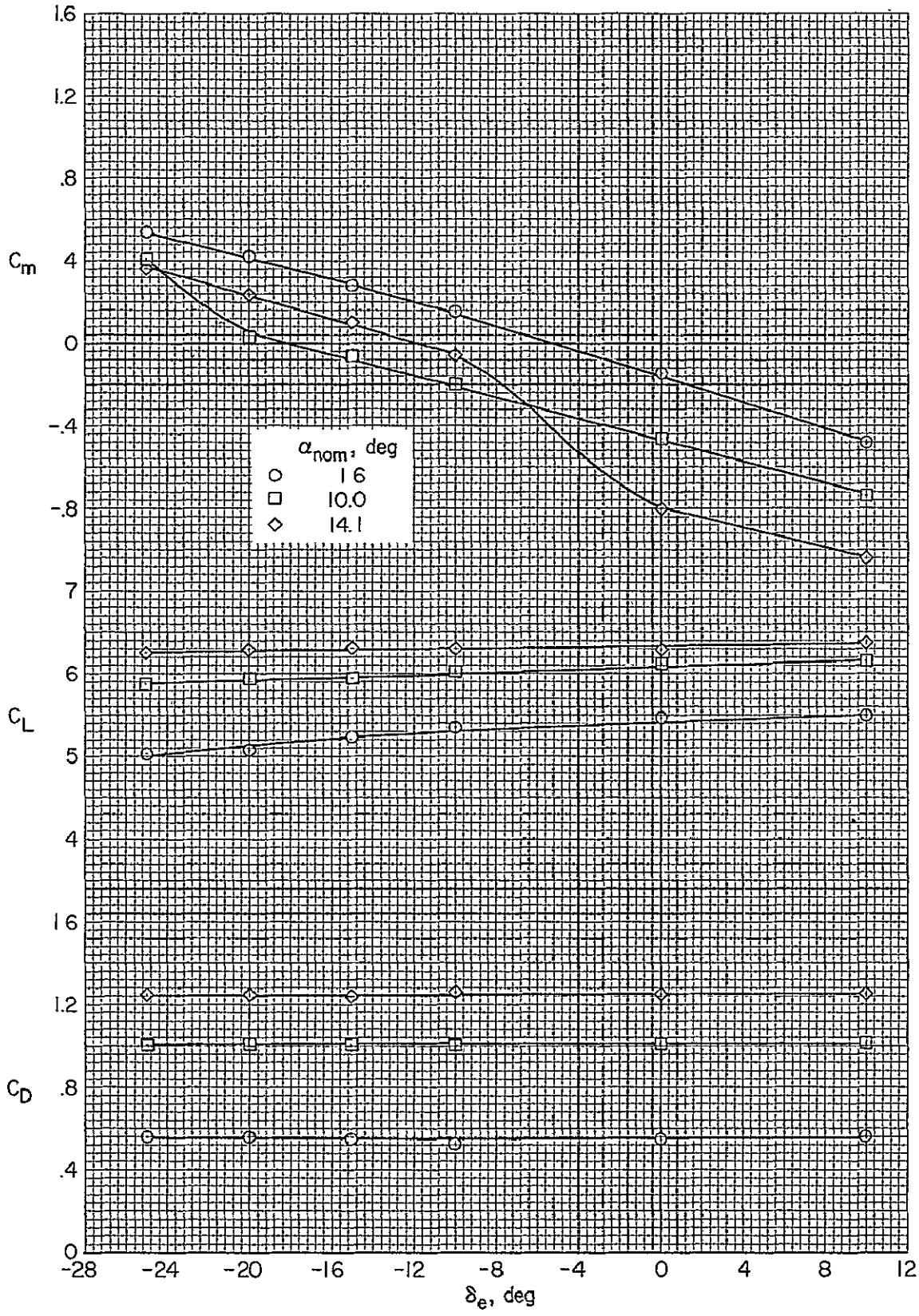

(d) $i_t = -4^\circ$, constant α.

Figure 6.- Continued.

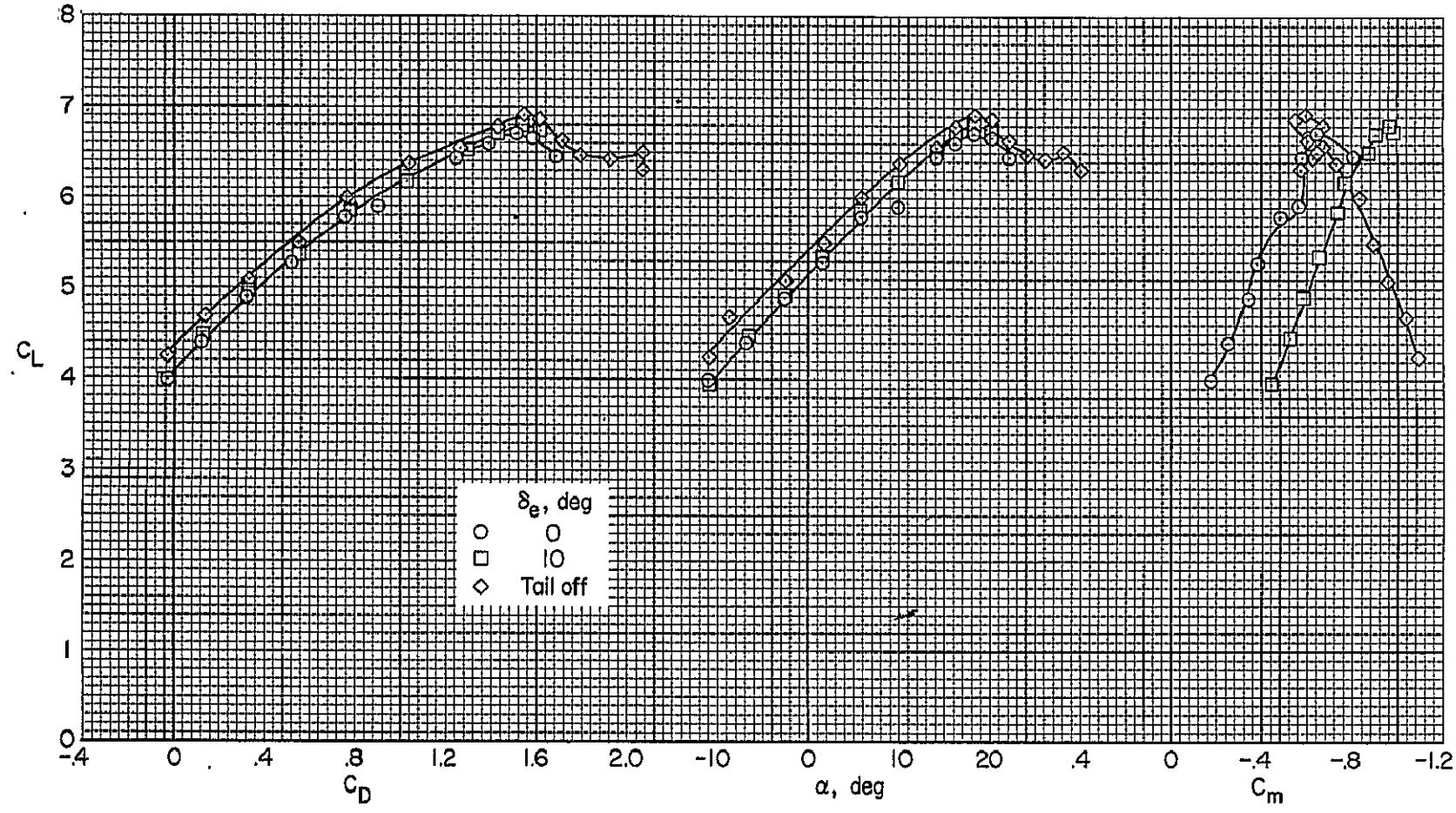

(e) $i_t = 1^\circ$.

Figure 6.- Continued.

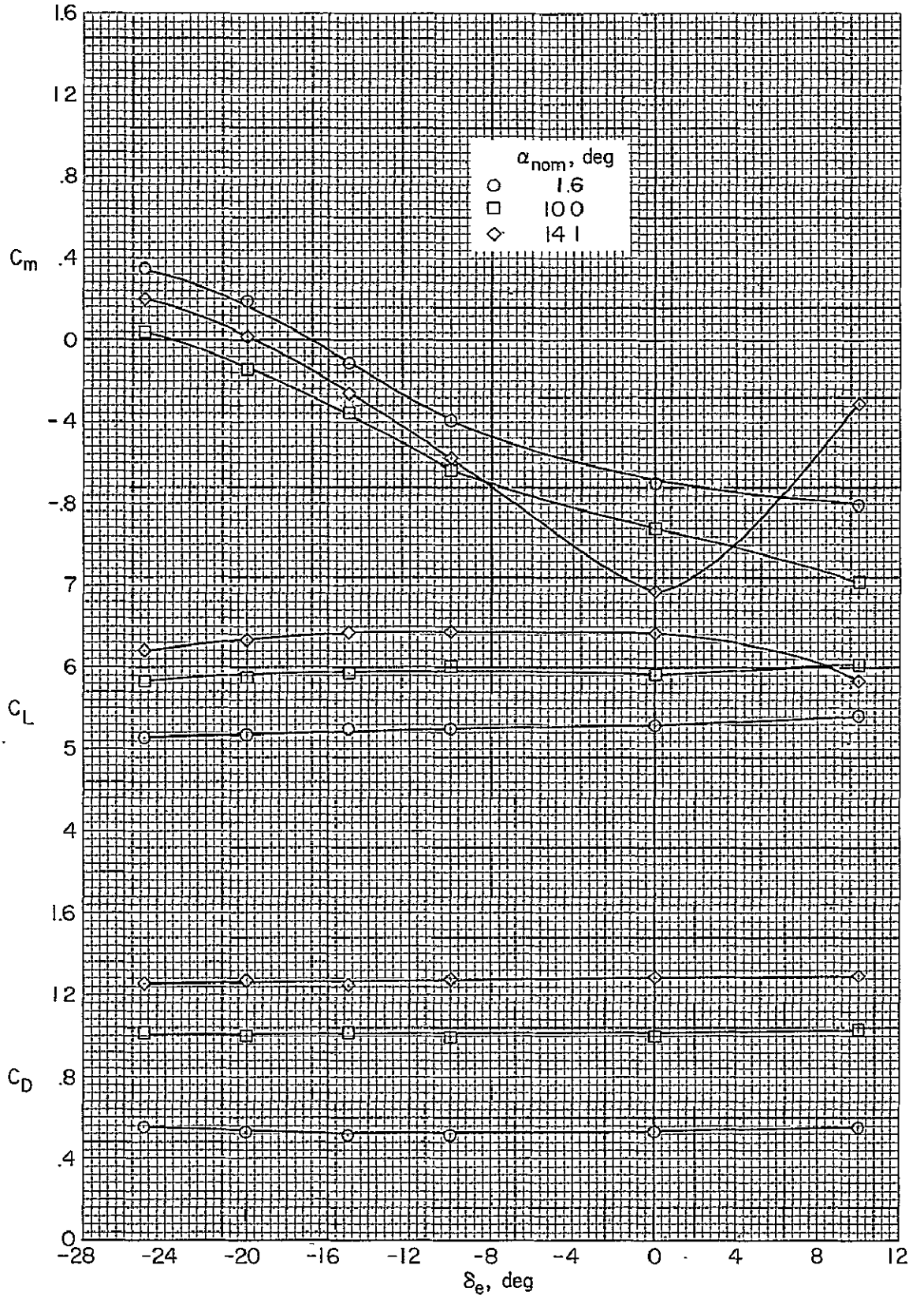

(f) $i_t = 1^\circ$.

Figure 6.- Concluded.

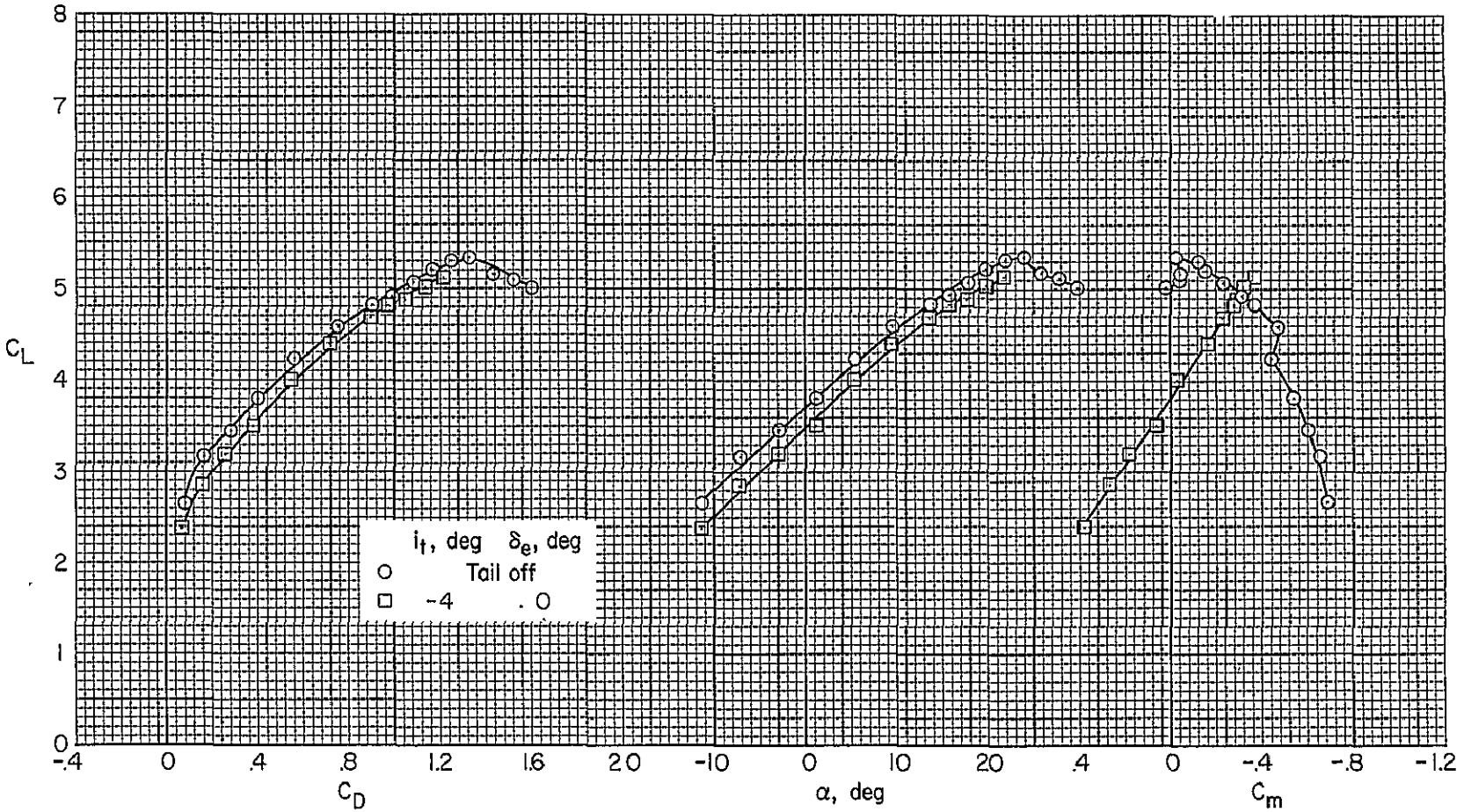

(a) Fuselage BLC on, $C_{J_I} = 0.32$.

Figure 7.- The effect of the horizontal tail on the longitudinal characteristics of the model with $\delta_f = 75^\circ$; $C_{T_{th}} = 0.81$, $\delta_{th} = 85^\circ$, $\delta_a = 45/45$.

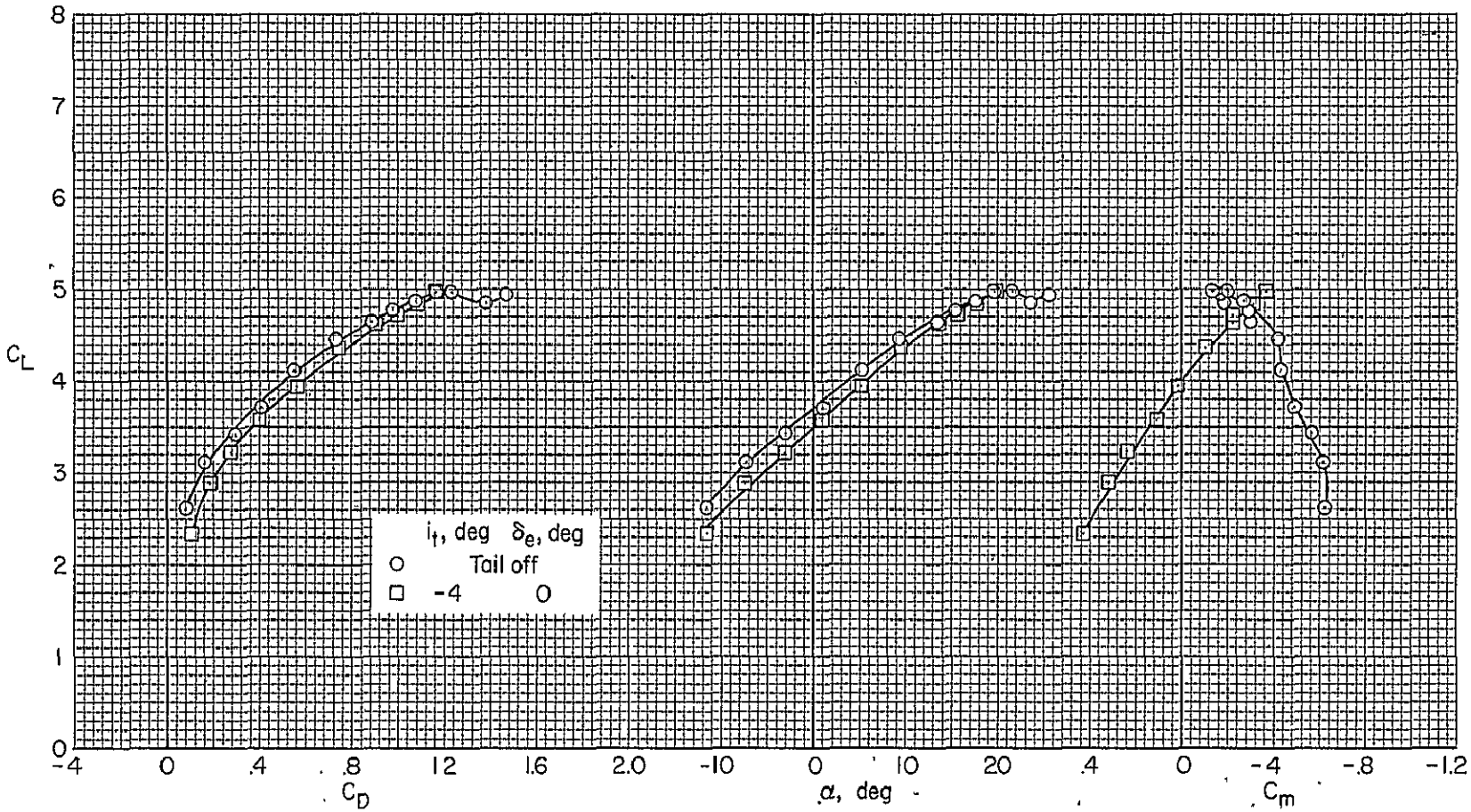

(b) Fuselage BLC off, $C_{J_I} = 0.32$.

Figure 7.- Continued.

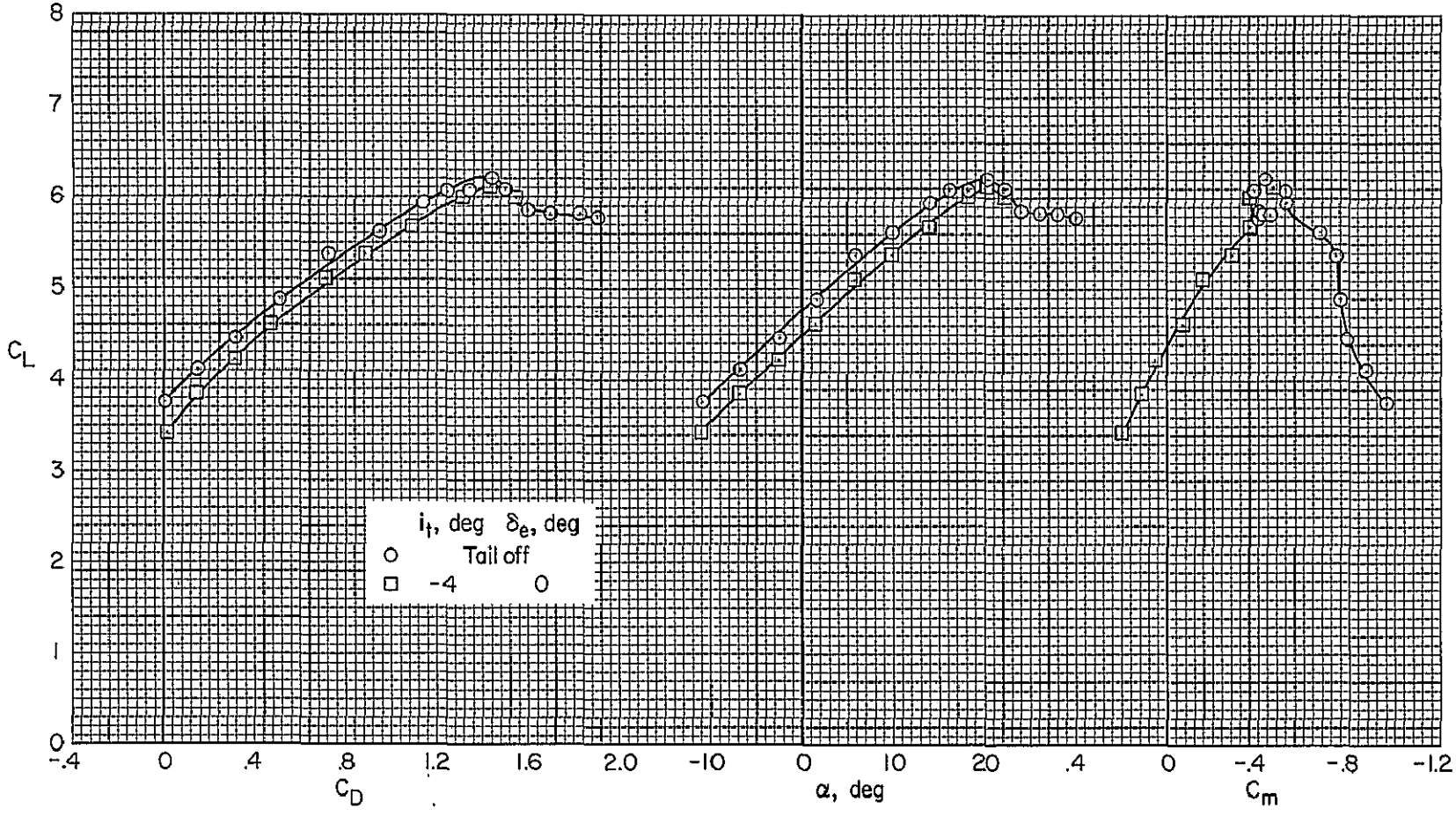

(c) Fuselage BLC on, $C_{J_I} = 0.63$.

Figure 7.- Continued.

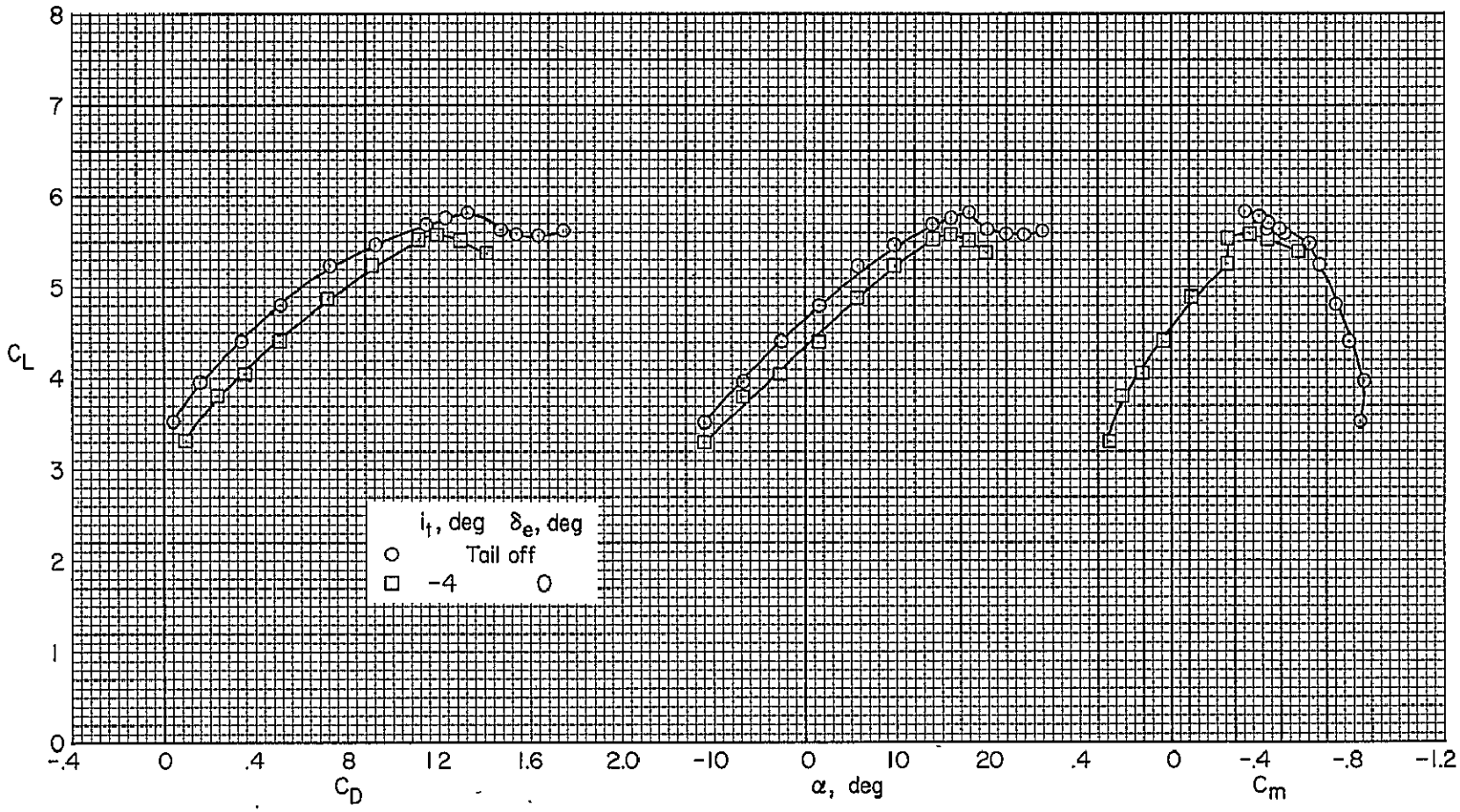

(d) Fuselage BLC off, $C_{J_I} = 0.59$.

Figure 7.- Continued.

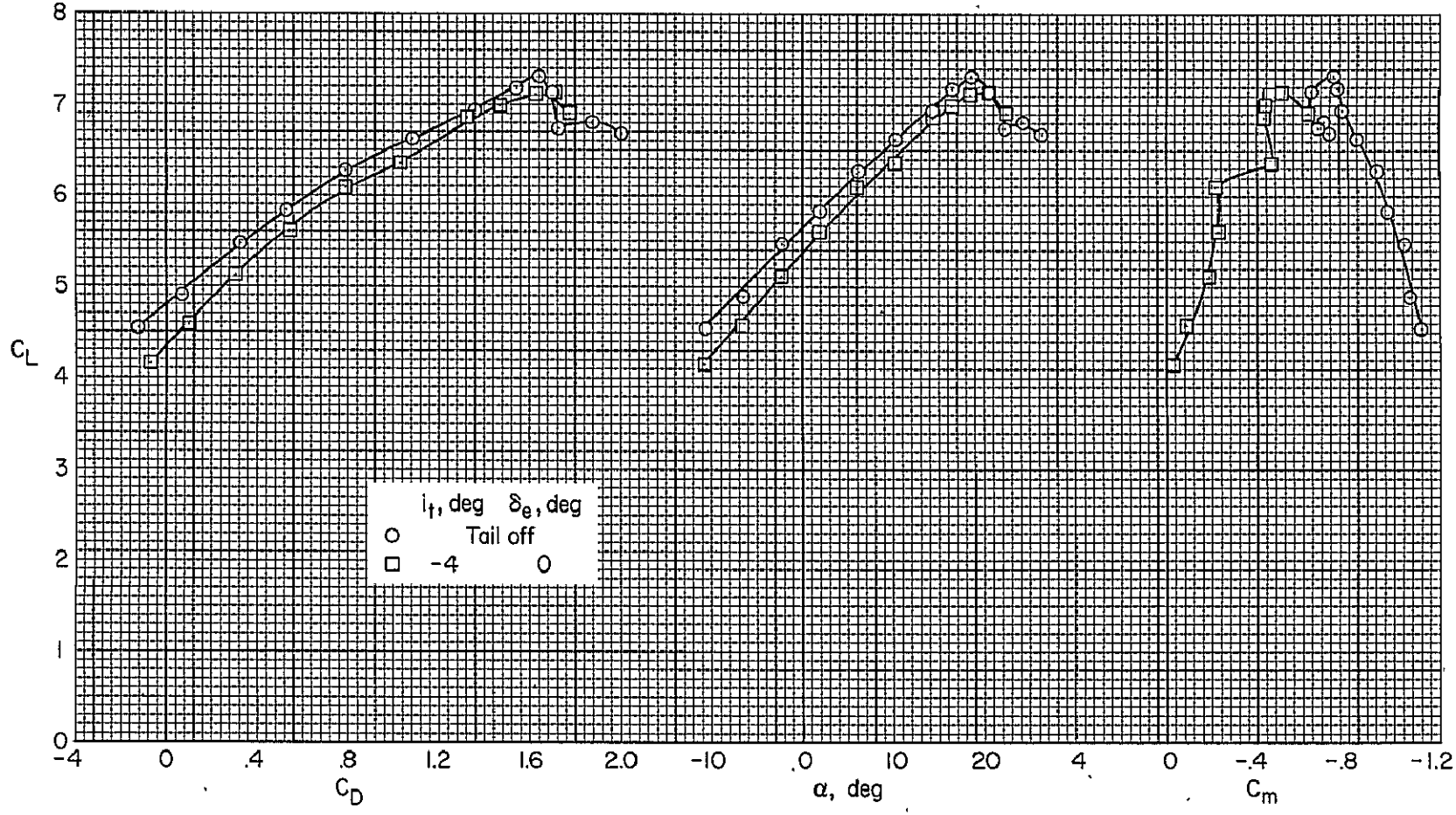

(e) Fuselage BLC on, $C_{J_I} = 1.07$.

Figure 7.- Concluded.

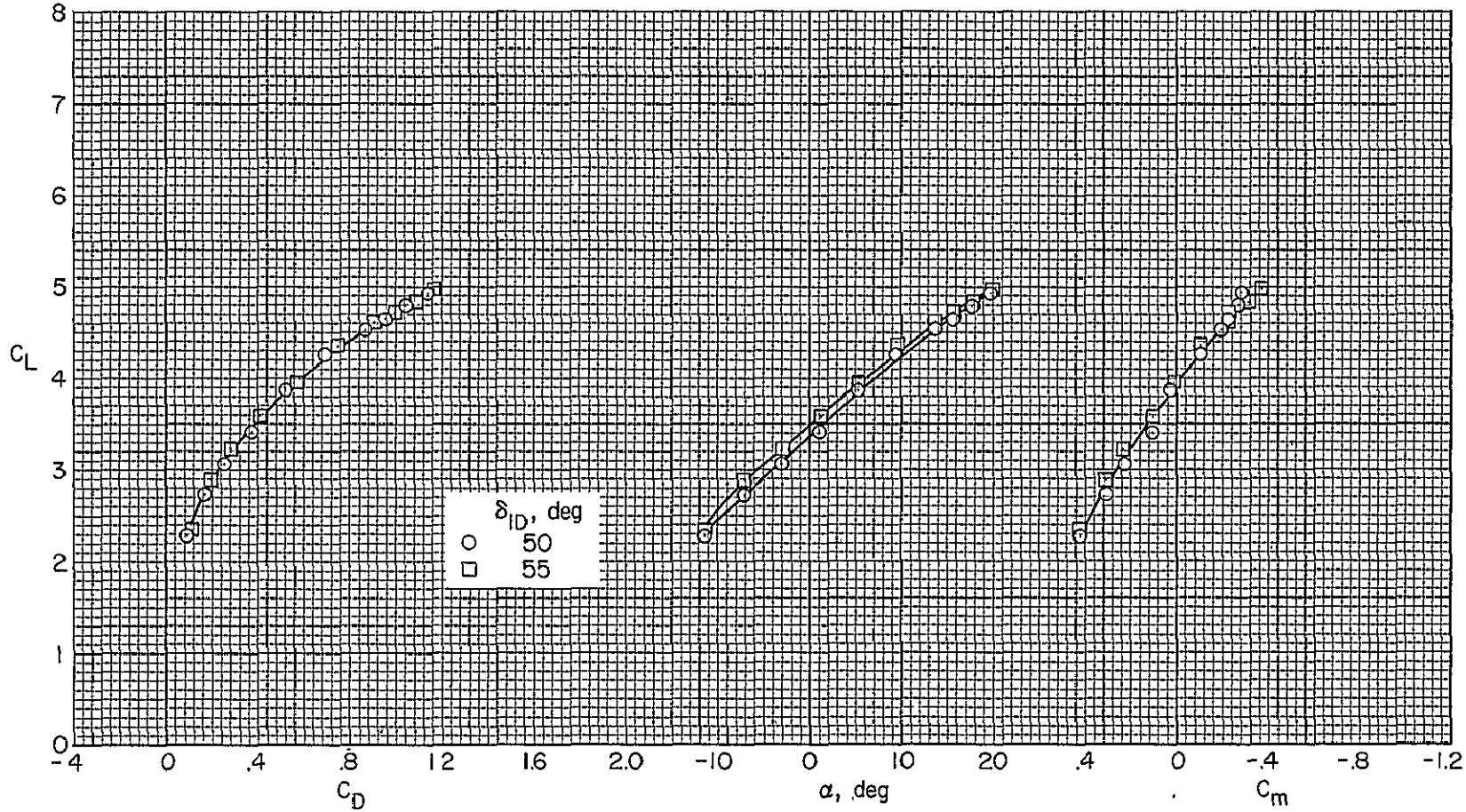

(a) $C_{J_I} = 0.32$, $i_t = -4^\circ$, $\delta_e = 0^\circ$.

Figure 8.- The effect of the intake door angle on the longitudinal characteristics of the model with $\delta_f = 75^\circ$; $C_{T_{th}} = 0.81$, $\delta_{th} = 85^\circ$, $\delta_a = 45/45$, BLC off.

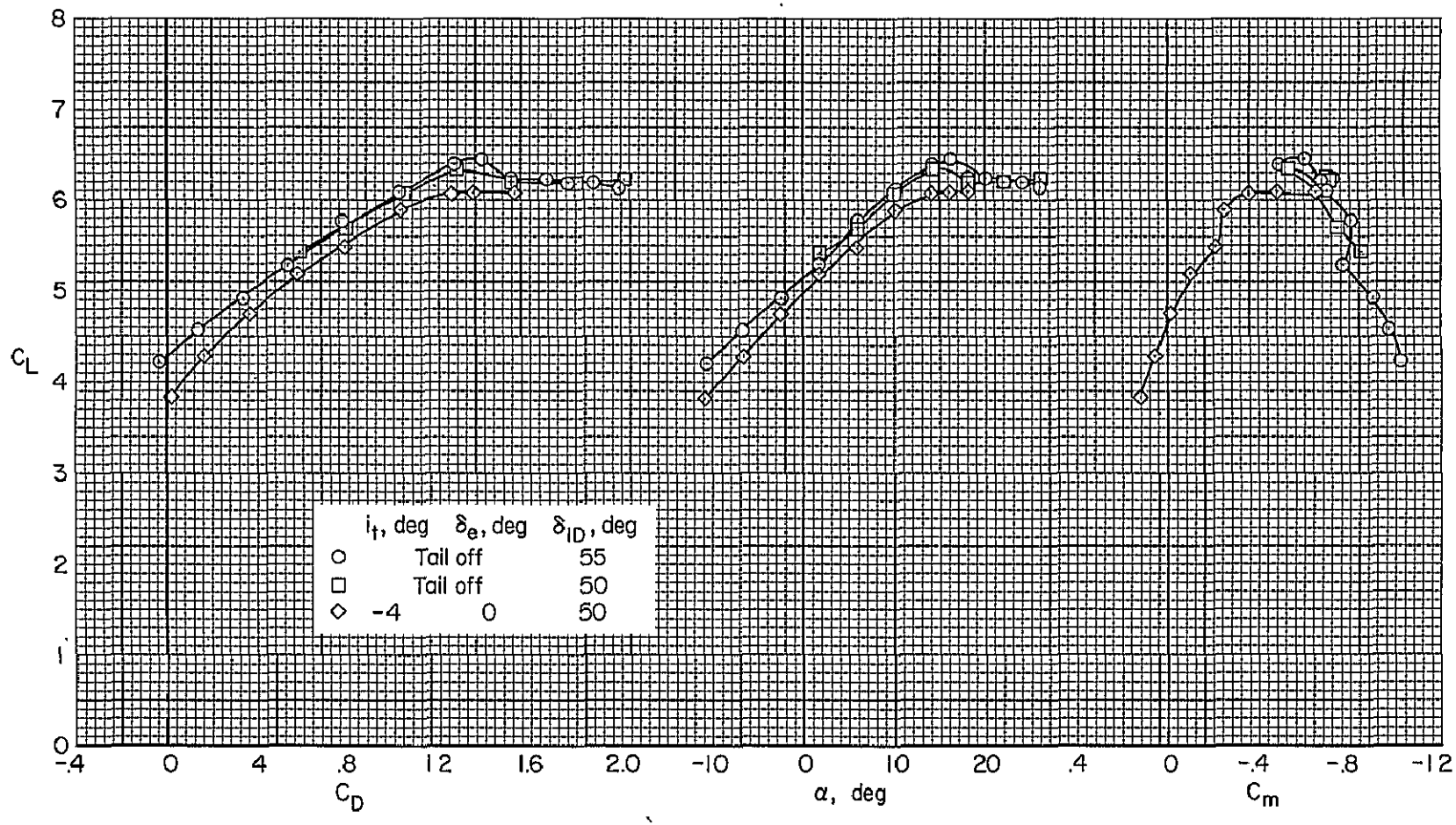

(b) $C_{J_I} = 0.82$.

Figure 8.- Concluded.

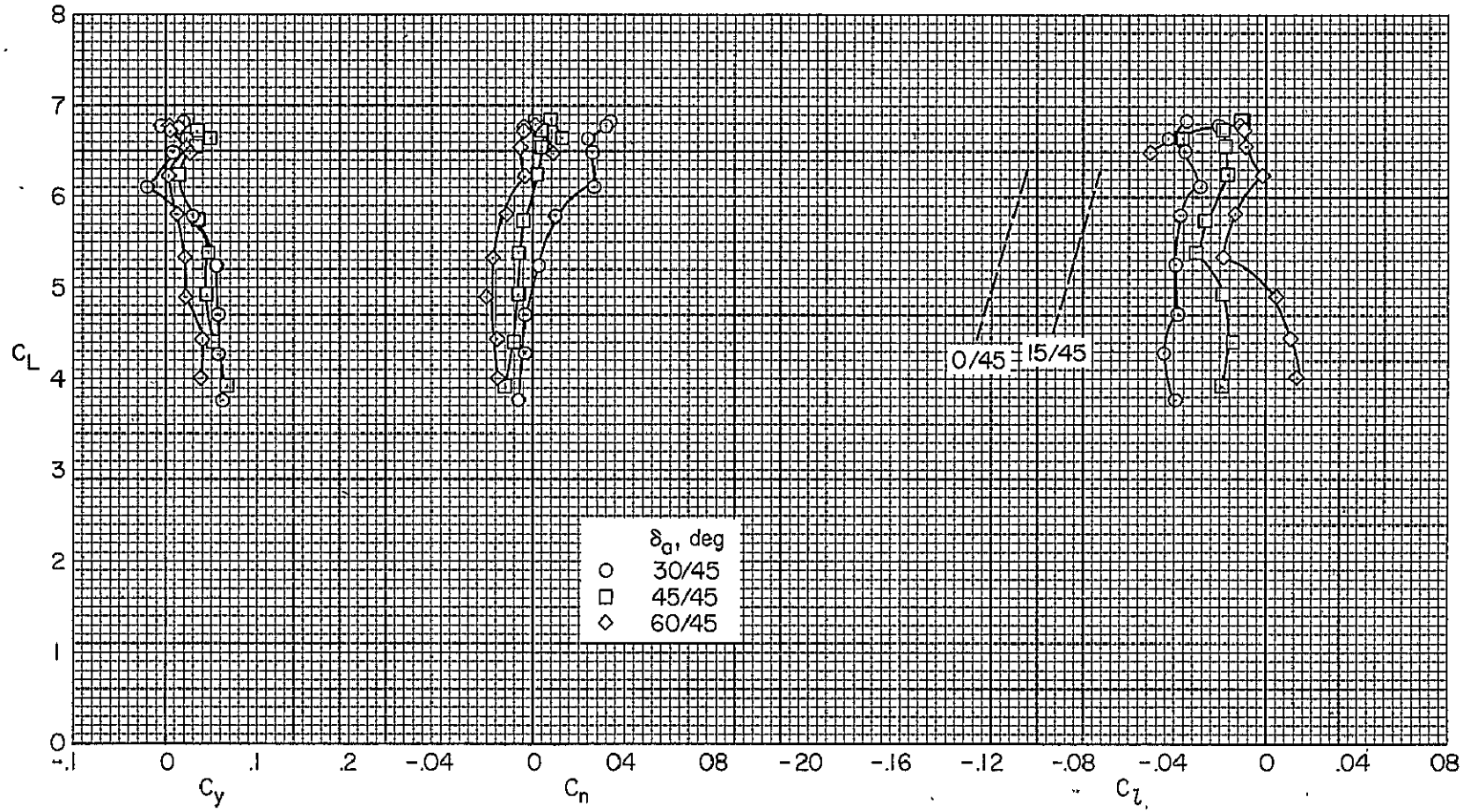

(a) Fuselage BLC on, $C_{J_I} = 0.78$.

Figure 9.- The effect of differential aileron deflection on the lateral-directional characteristics of the model with $\delta_f = 75^\circ$; $C_{T_{th}} = 0.81$, $\delta_{th} = 85^\circ$, $i_t = -4^\circ$, $\delta_e = 0^\circ$.

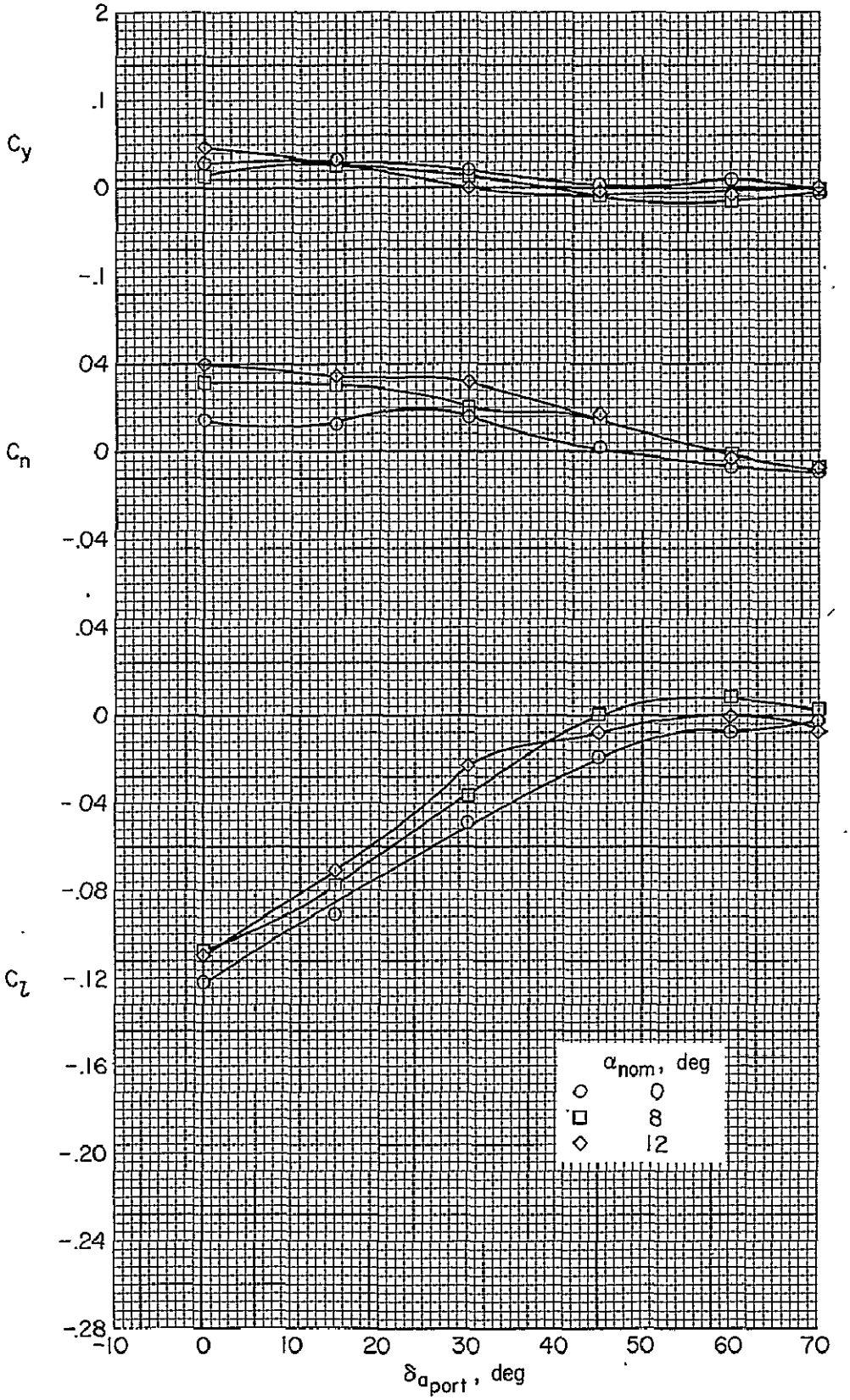

(b) Fuselage BLC on, $C_{J_I} = 0.78$, $\delta_{a_{stbd}} = 45^{o}$.

Figure 9.- Continued.

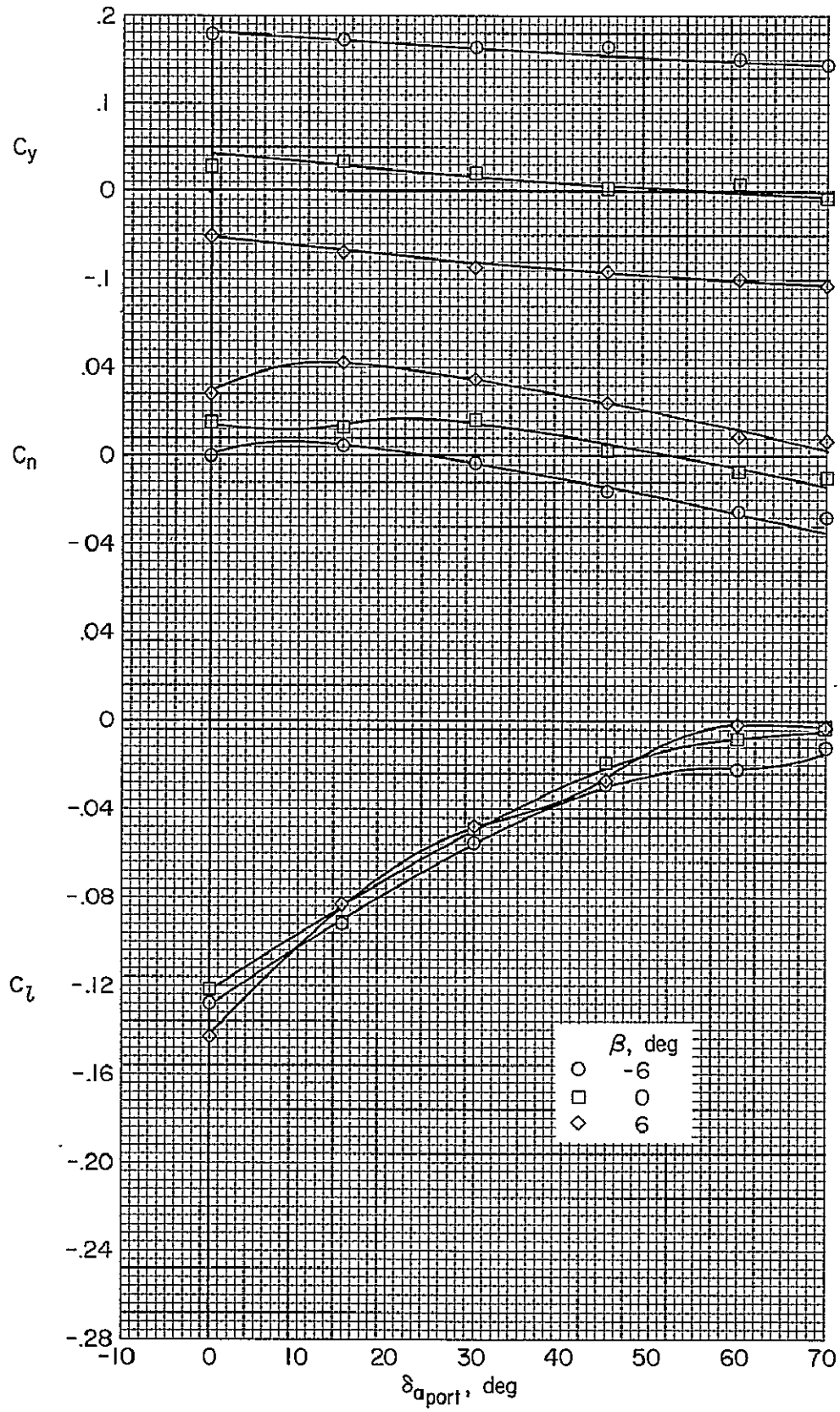

(c) Fuselage BLC on, $C_{J_I} = 0.88$, $\alpha = 0^\circ$, $\delta_{a_{stbd}} = 45^\circ$.

Figure 9.- Continued.

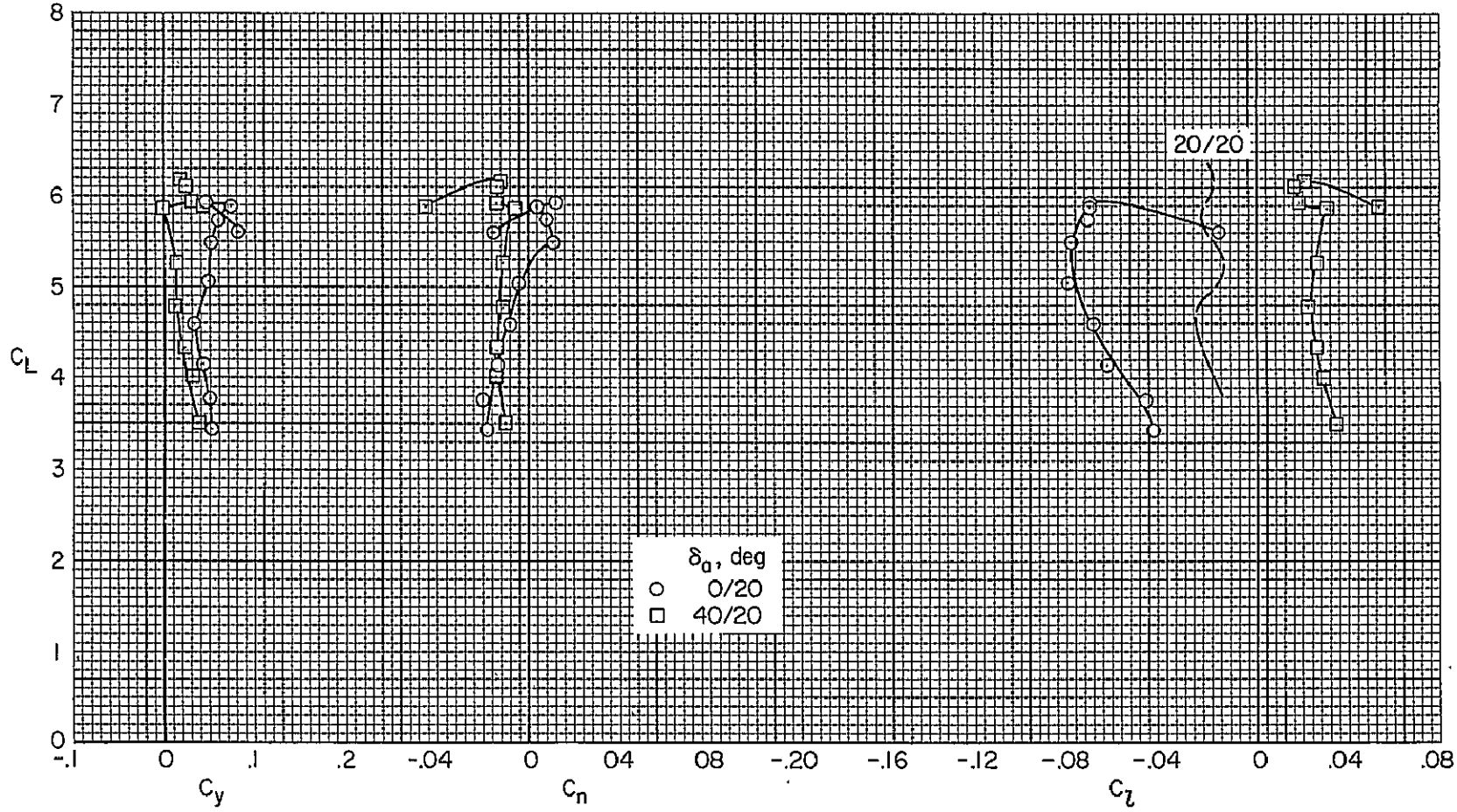

(d) Fuselage BLC off, C_{J_I} = 0.83.

Figure 9.- Continued.

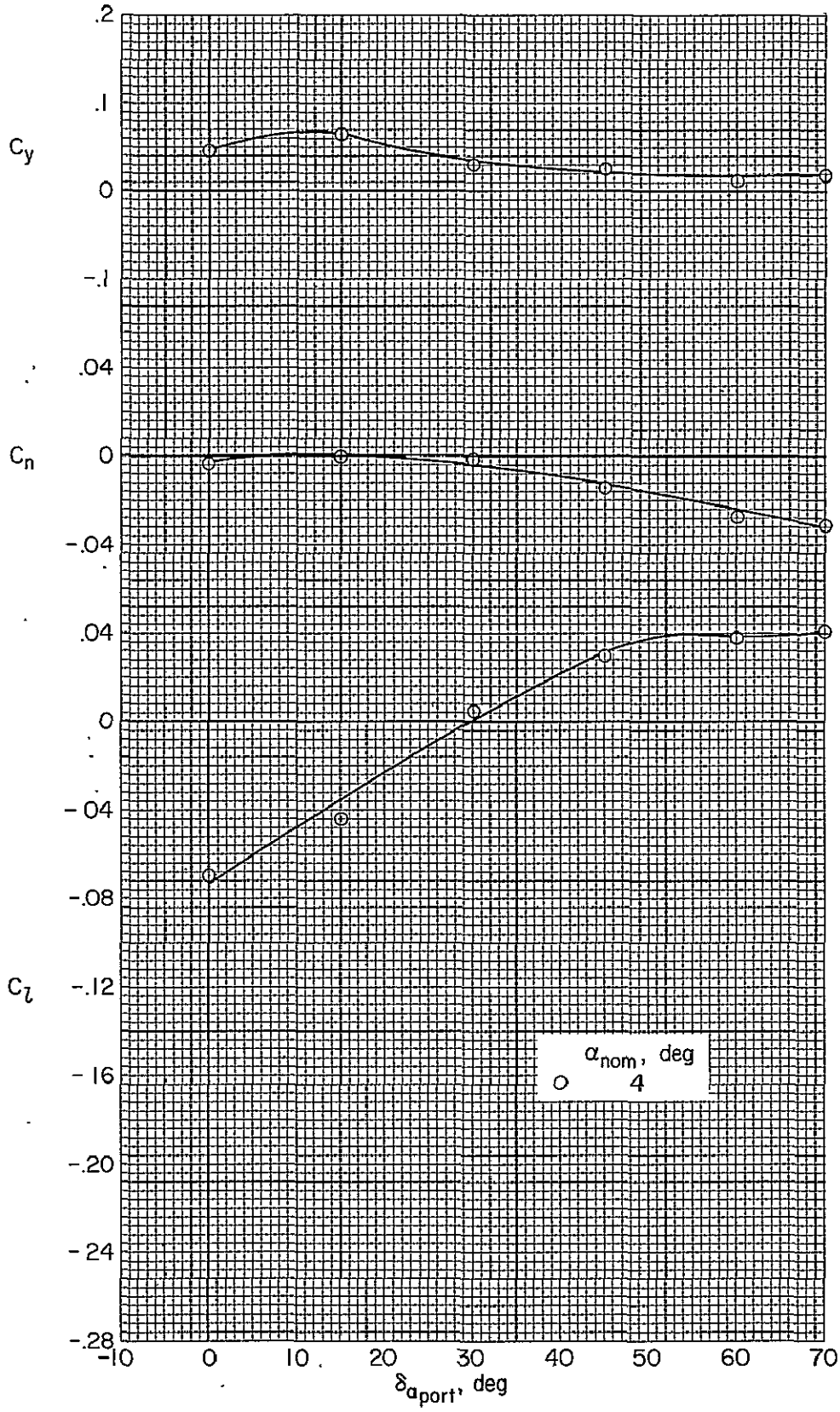

(e) Fuselage BLC off, $C_{J_I} \doteq 0.83$, $\delta_{a_{stbd}} = 20^{o}$.

Figure 9.- Concluded.

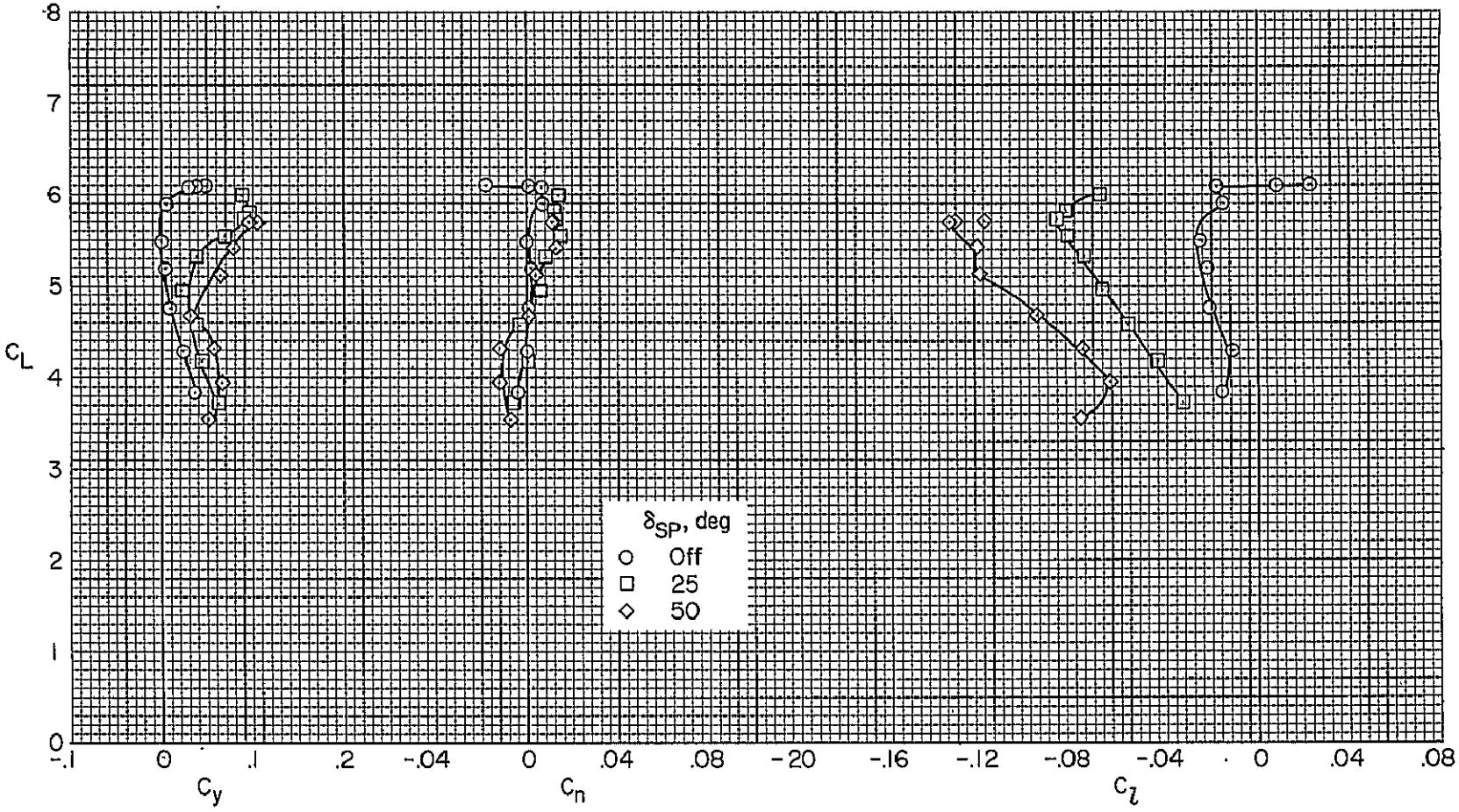

(a) Inboard panel spoilers, $C_{J_I} = 0.78$, $\delta_a = 45/45$.

Figure 10.- The effect of spoiler deflection on the lateral-directional characteristics of the model with $\delta_f = 75^o$; $C_{T_{th}} = 0.81$, $\delta_{th} = 85^o$, BLC off, $i_t = -4^o$, $\delta_e = 0^o$.

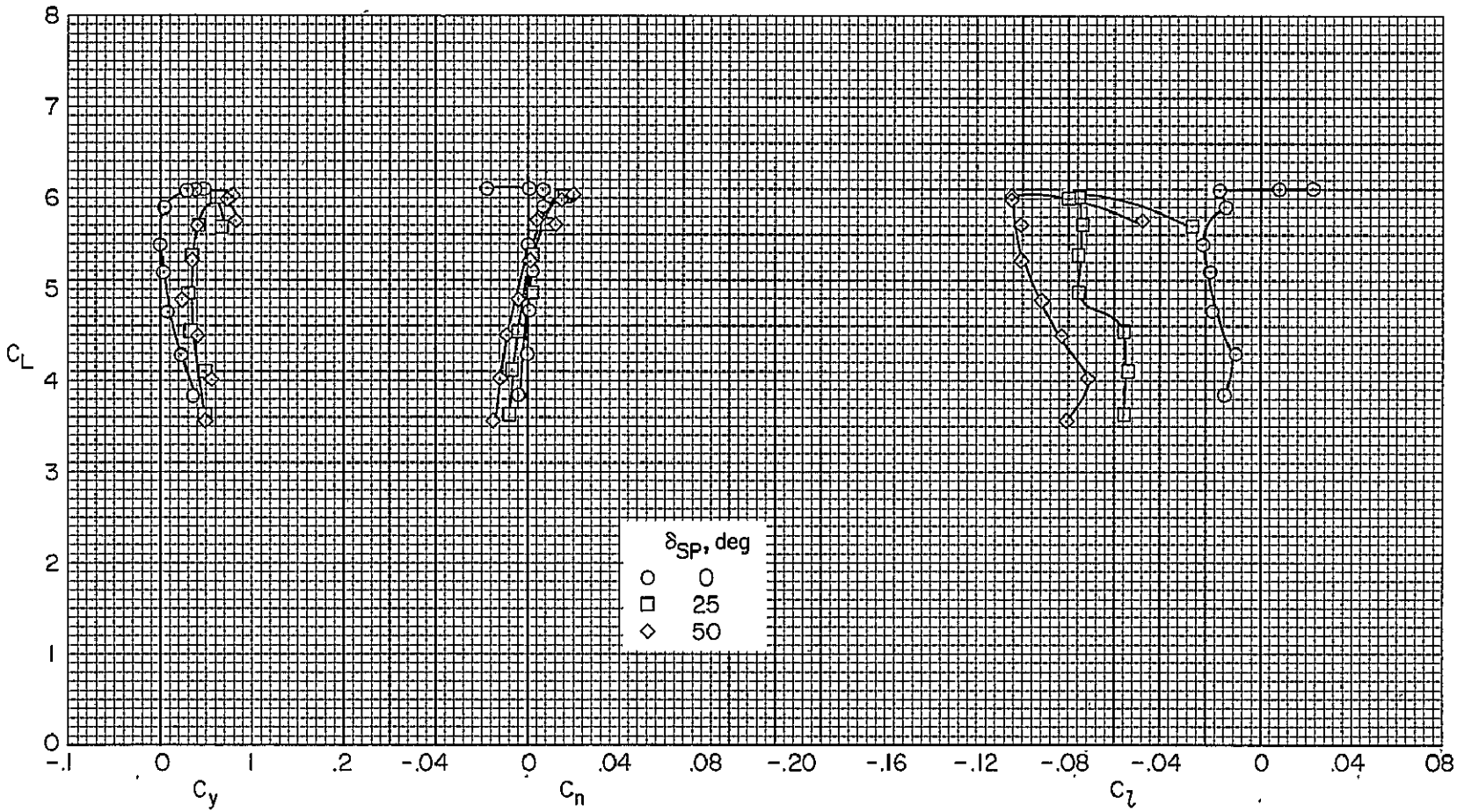

(b) Outboard panel spoilers, $C_{J_I} = 0.78$, $\delta_a = 45/45$.

Figure 10.- Continued.

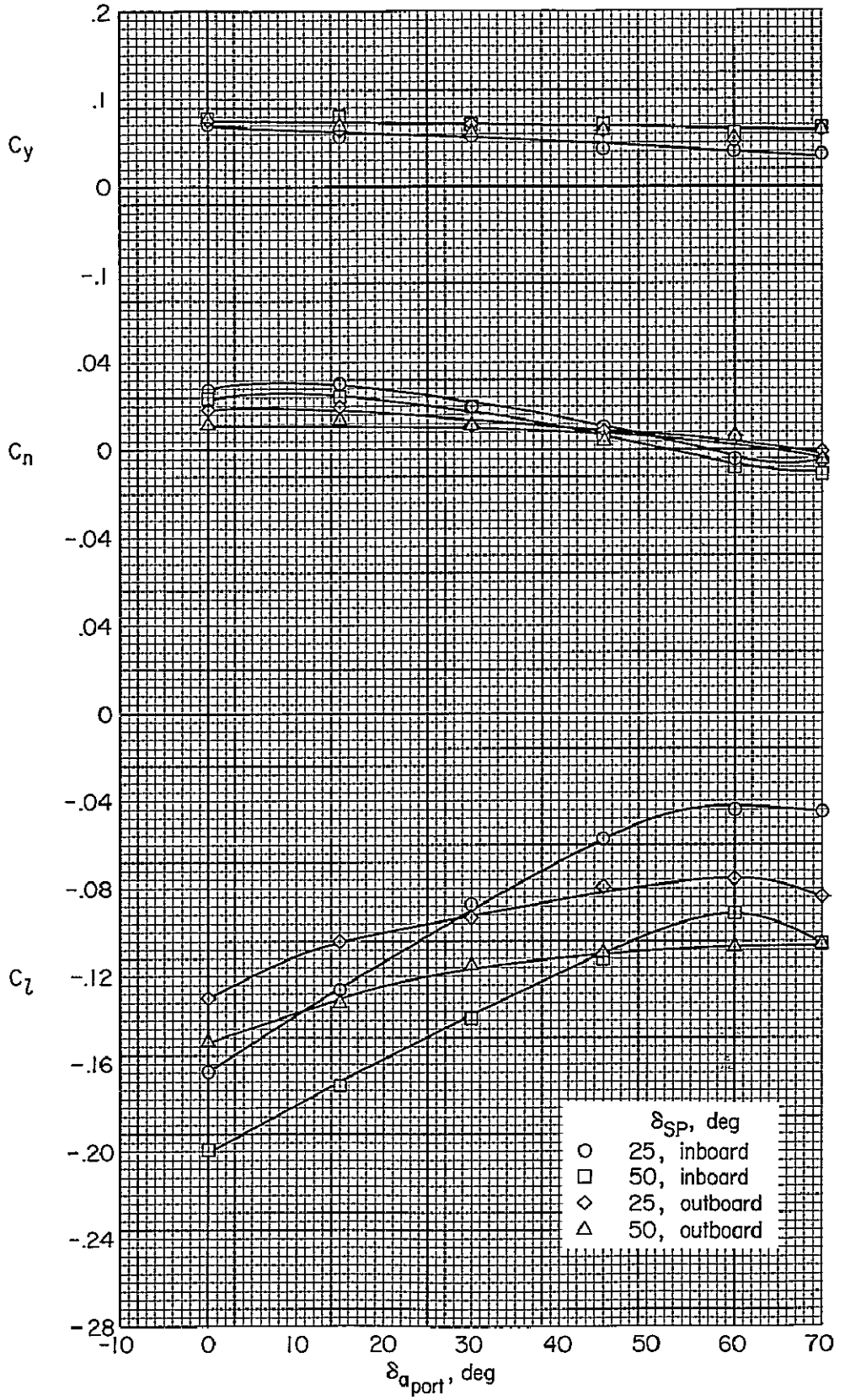

(c) Inboard and outboard spoilers, $C_{J_I} = 0.78$, $\delta_{a_{stbd}} = 45^\circ$, $\alpha = 4^\circ$.

Figure 10.- Continued.

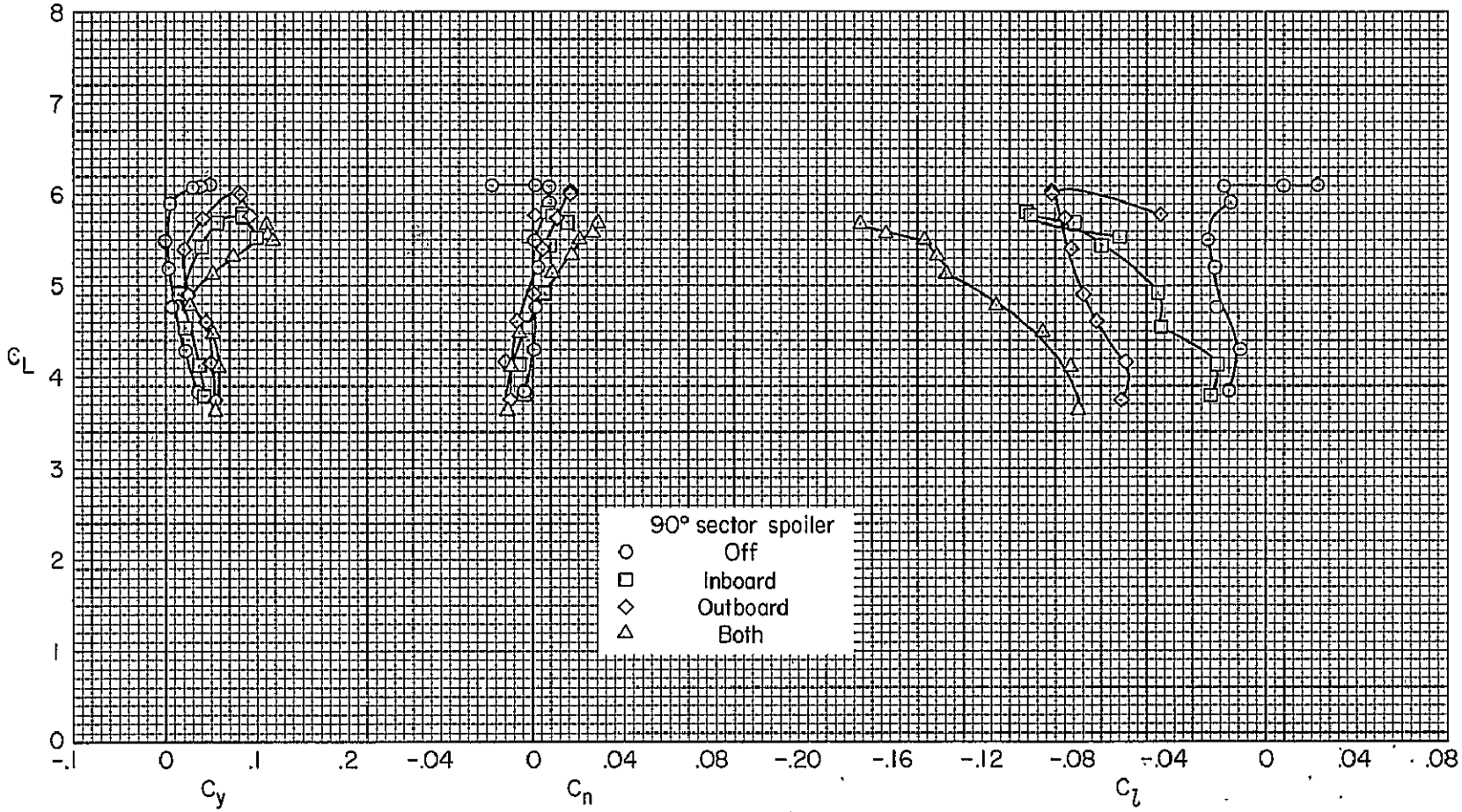

(d) Inboard and outboard sector spoilers, $C_{J_I} = 0.78$, $\delta_a = 45/45$.

Figure 10.- Continued.

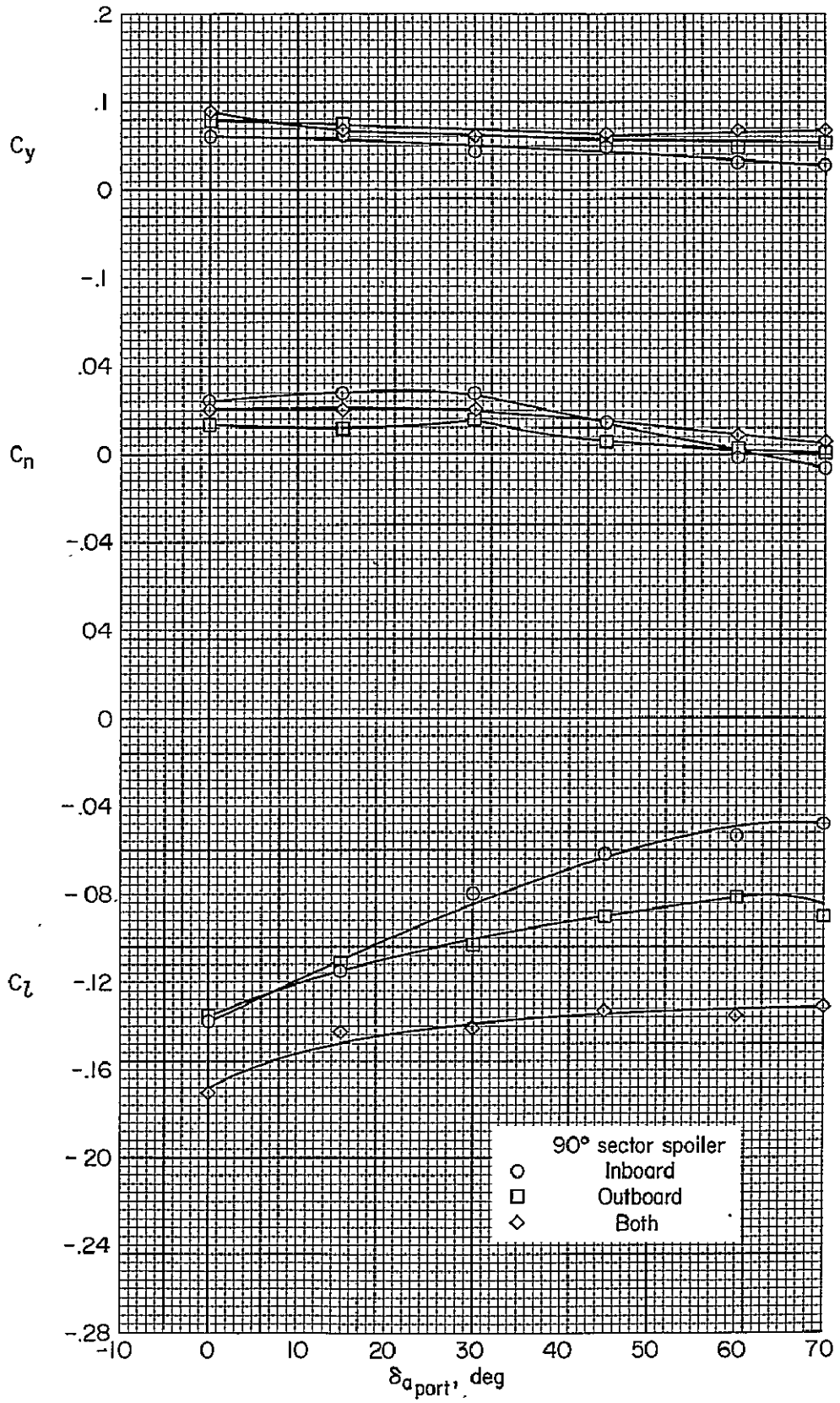

(e) Inboard and outboard sector spoilers, $C_{J_I} = 0.78$, $\delta_{a_{stbd}} = 45^{\circ}$, $\alpha = 4^{\circ}$.

Figure 10.- Concluded.

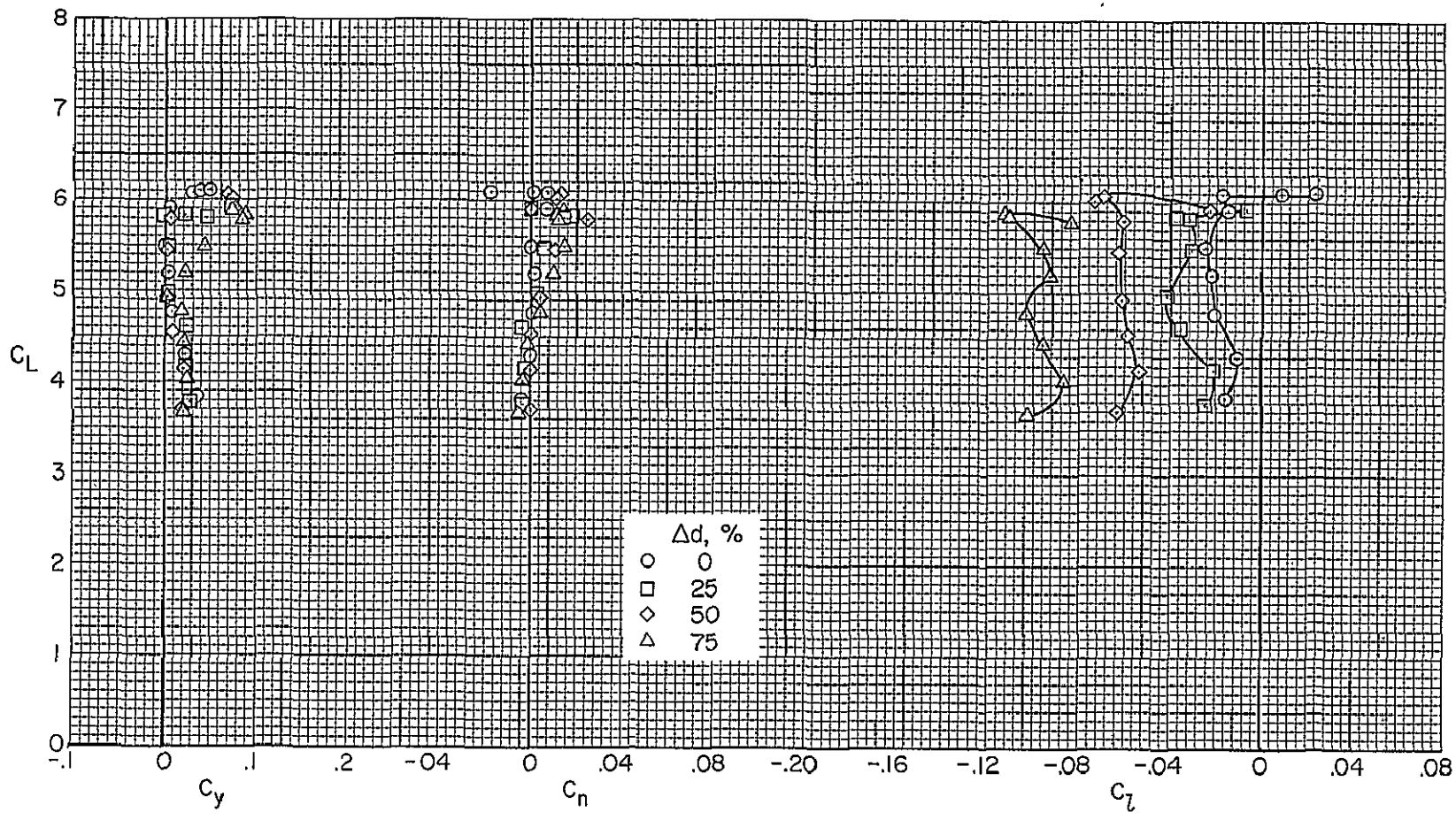

(a) Throttling of outboard 25% of flap semispan, $C_{J_I} = 0.78$, $\delta_a = 45/45$.

Figure 11.- The effect of augmentor throttling on the lateral directional characteristics of the model with $\delta_f = 75^o$; BLC off, $C_{T_{th}} = 0.81$, $\delta_{th} = 85^o$, $i_t = -4^o$, $\delta_e = 0^o$.

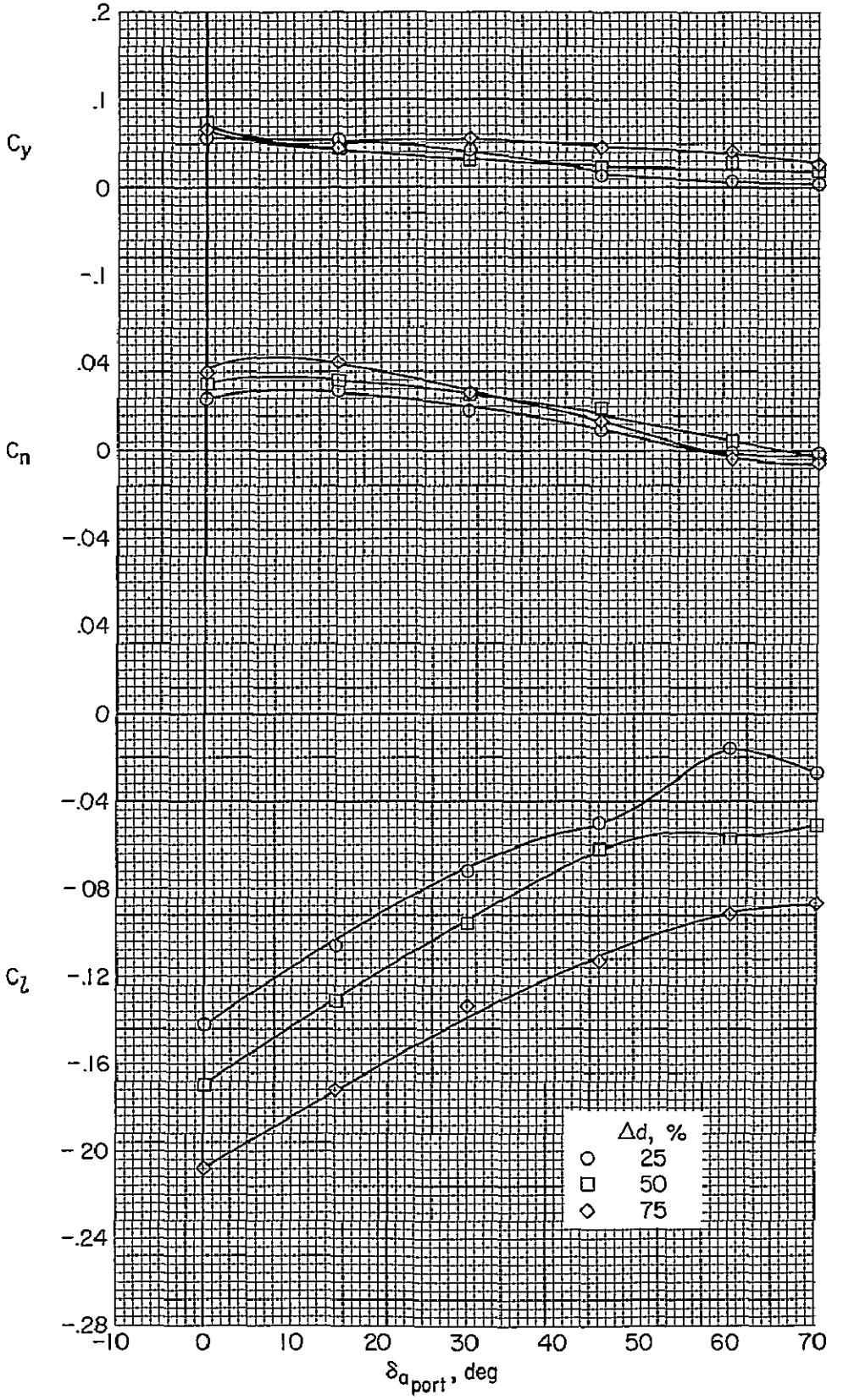

(b) Throttling of outboard 25% of flap semispan, $C_{J_I} = 0.78$, $\alpha = 4^o$, $\delta_{a_{stbd}} = 45^o$.

Figure 11.- Continued.

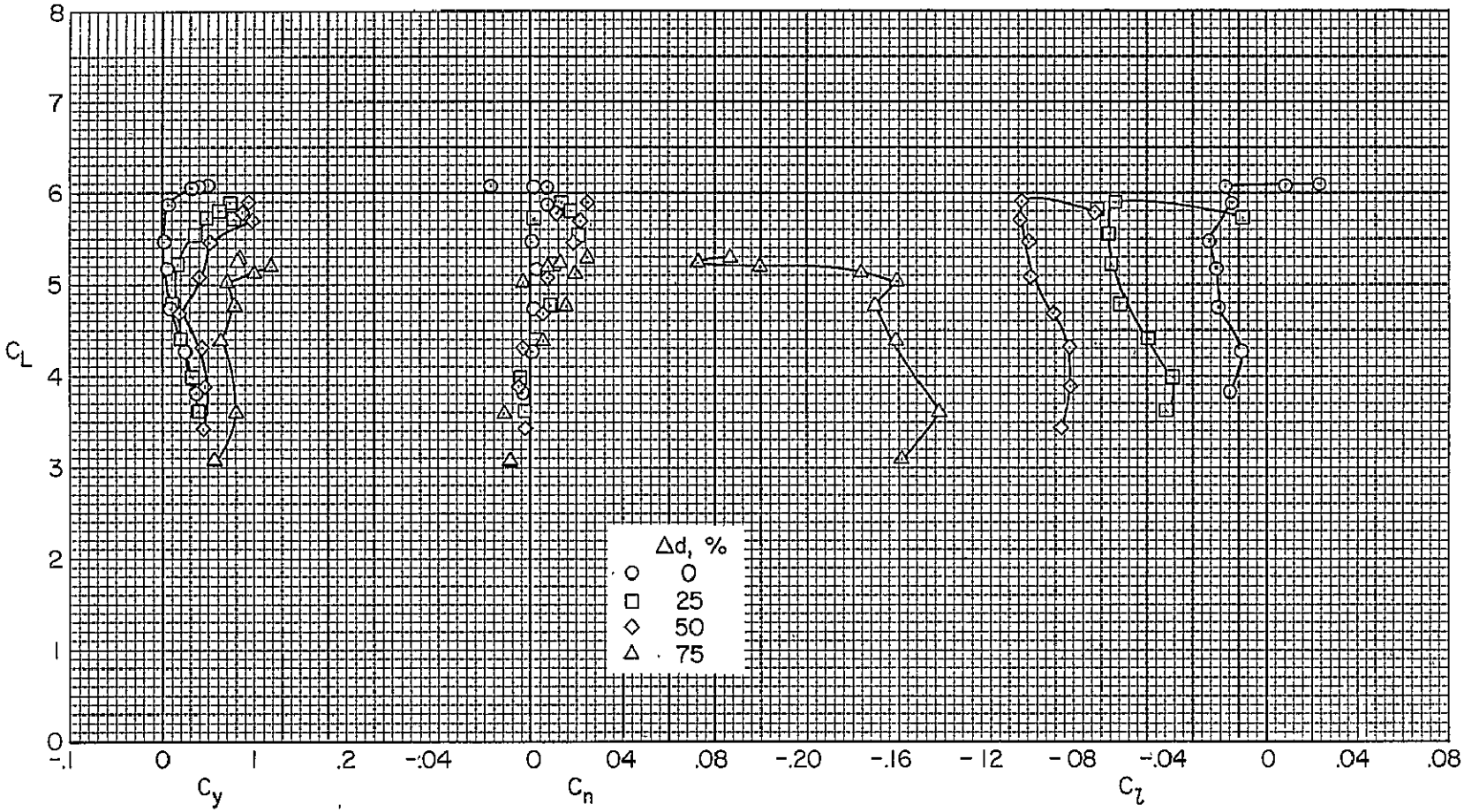

(c) Throttling of outboard 50% of flap semispan, C_{J_I} = 0.78, δ_a = 45/45.

Figure 11.- Continued.

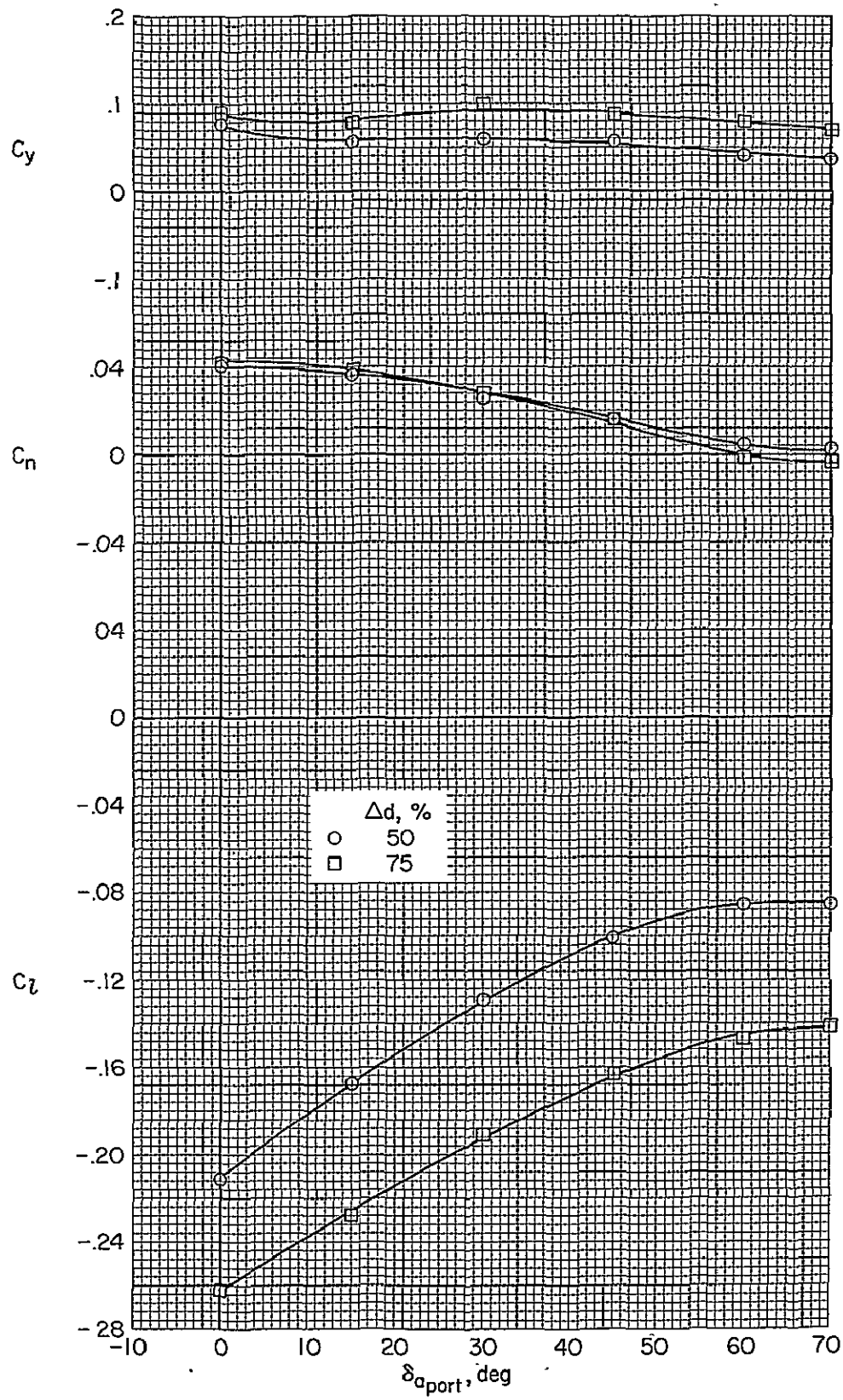

(d) Throttling of outboard 50% of flap semispan, $C_{J_I} = 0.78$, $\alpha = 4^\circ$, $\delta_{a_{stbd}} = 45^\circ$.

Figure 11.- Continued.

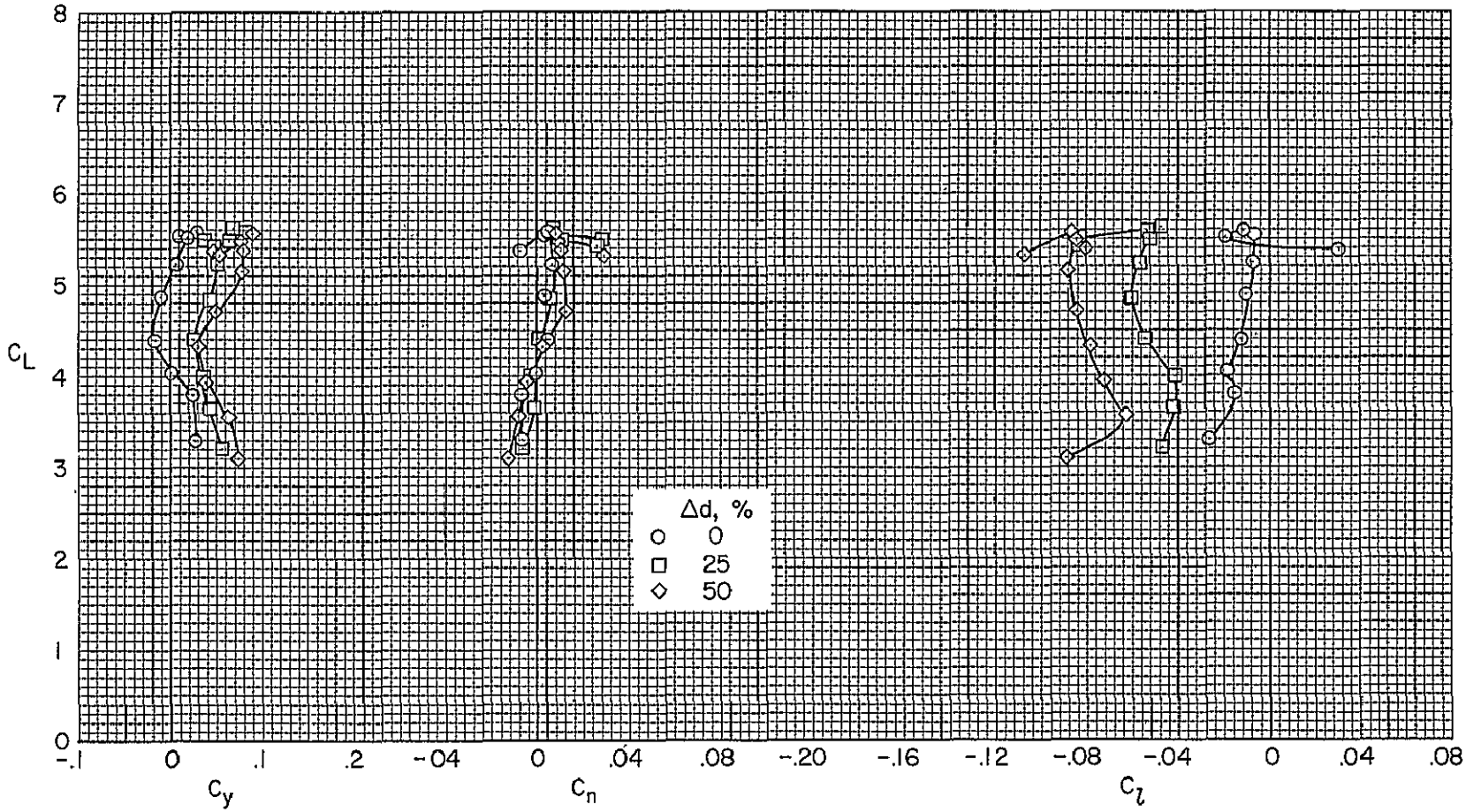

(e) Throttling of outboard 50% of flap semispan, $C_{J_I} = 0.57$, $\delta_a = 45/45$.

Figure 11.- Continued.

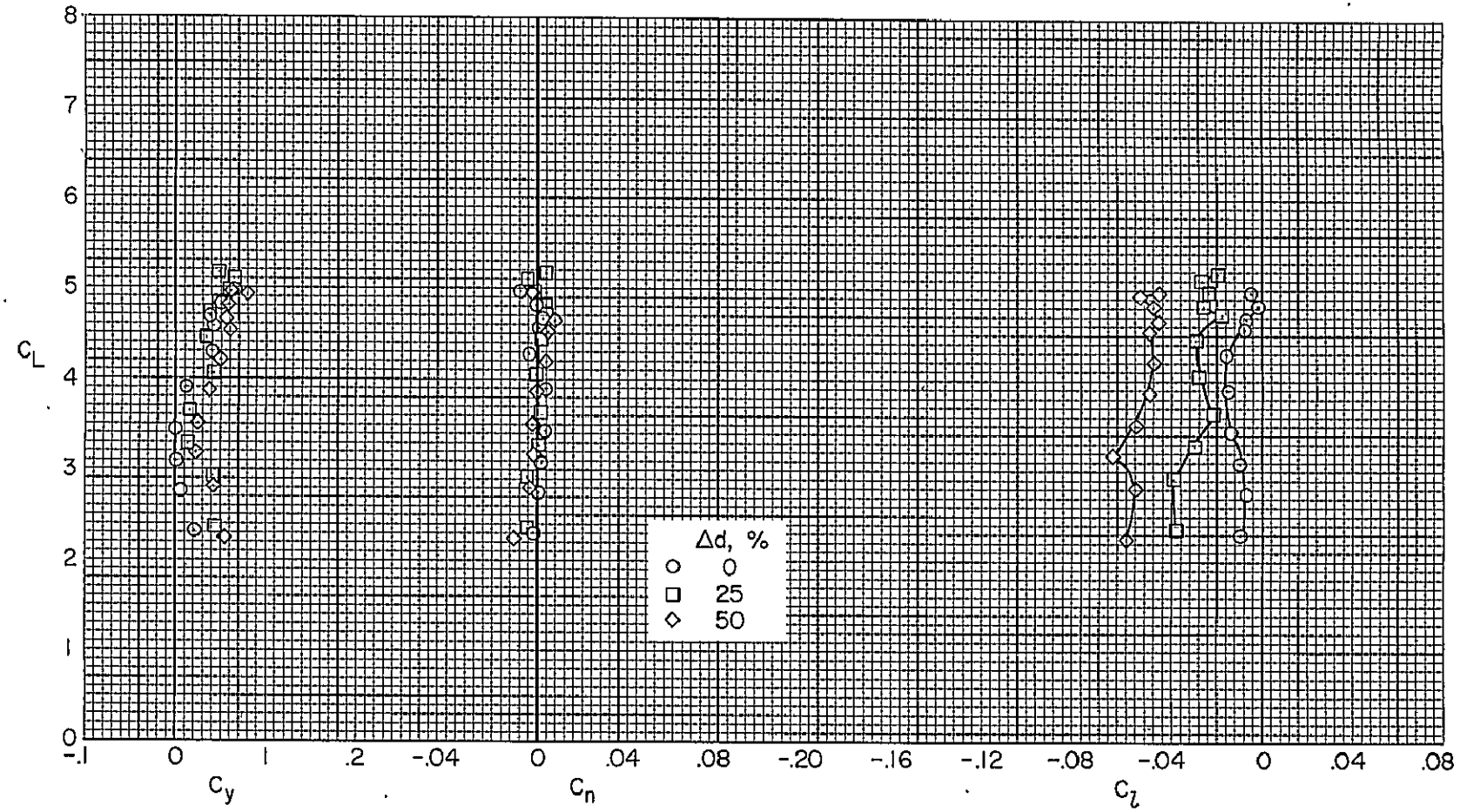

(f) Throttling of outboard 50% of flap semispan, $C_{J_I} = 0.30$, $\delta_a = 45/45$.

Figure 11.- Concluded.

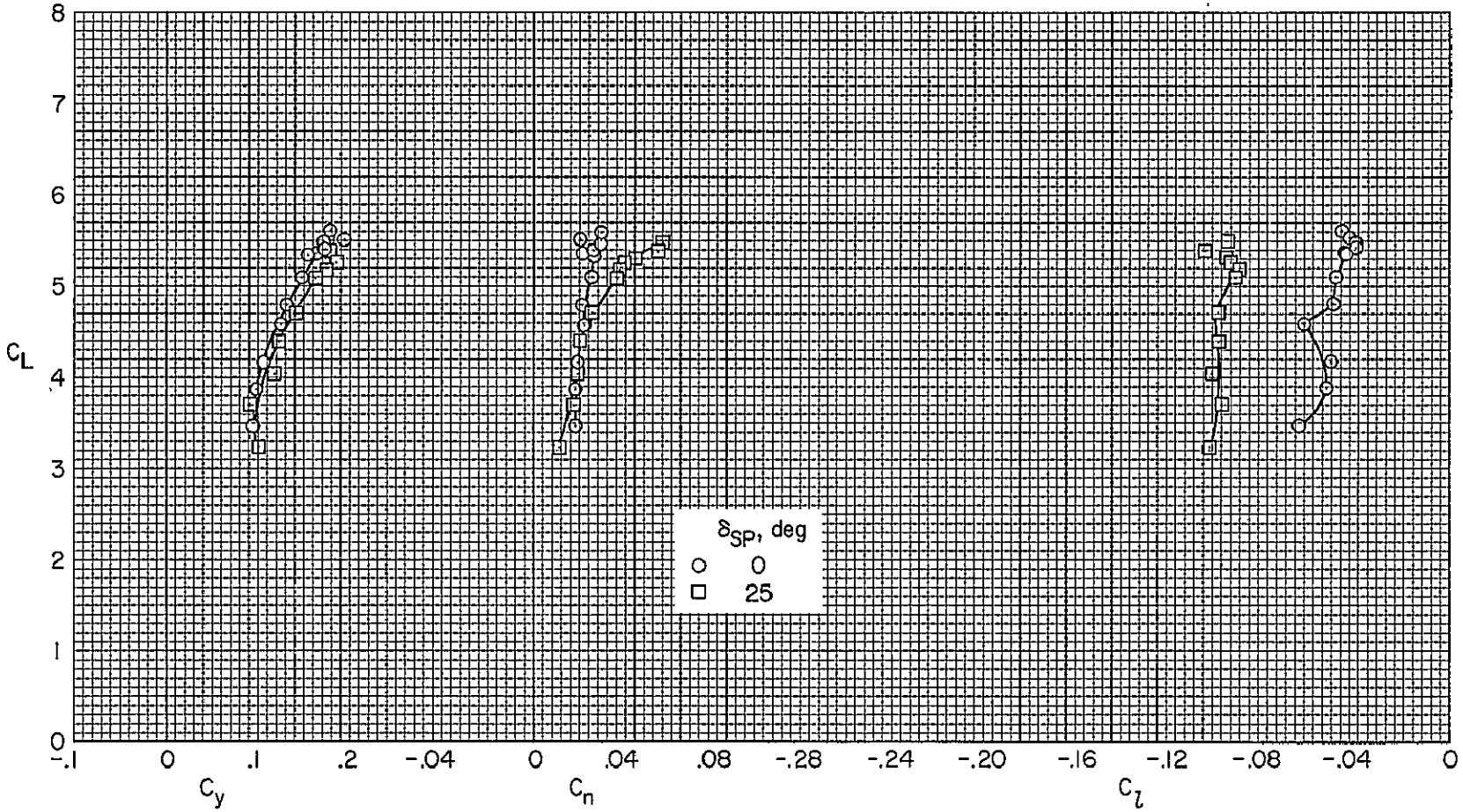

(a) $C_{J_I} = 0.62$, $\Delta d = 25\%$.

Figure 12.- The effect of outboard panel spoiler deflection on the lateral-directional characteristics of the model with varying augmentor throttling over the outboard 50% of the flap semispan; $\delta_f = 75^o$, $C_{T_{th}} = 0.81$, $\delta_{th} = 85^o$, BLC on, $\delta_a = 45/45$, $i_t = -4^o$, $\delta_e = 0^o$.

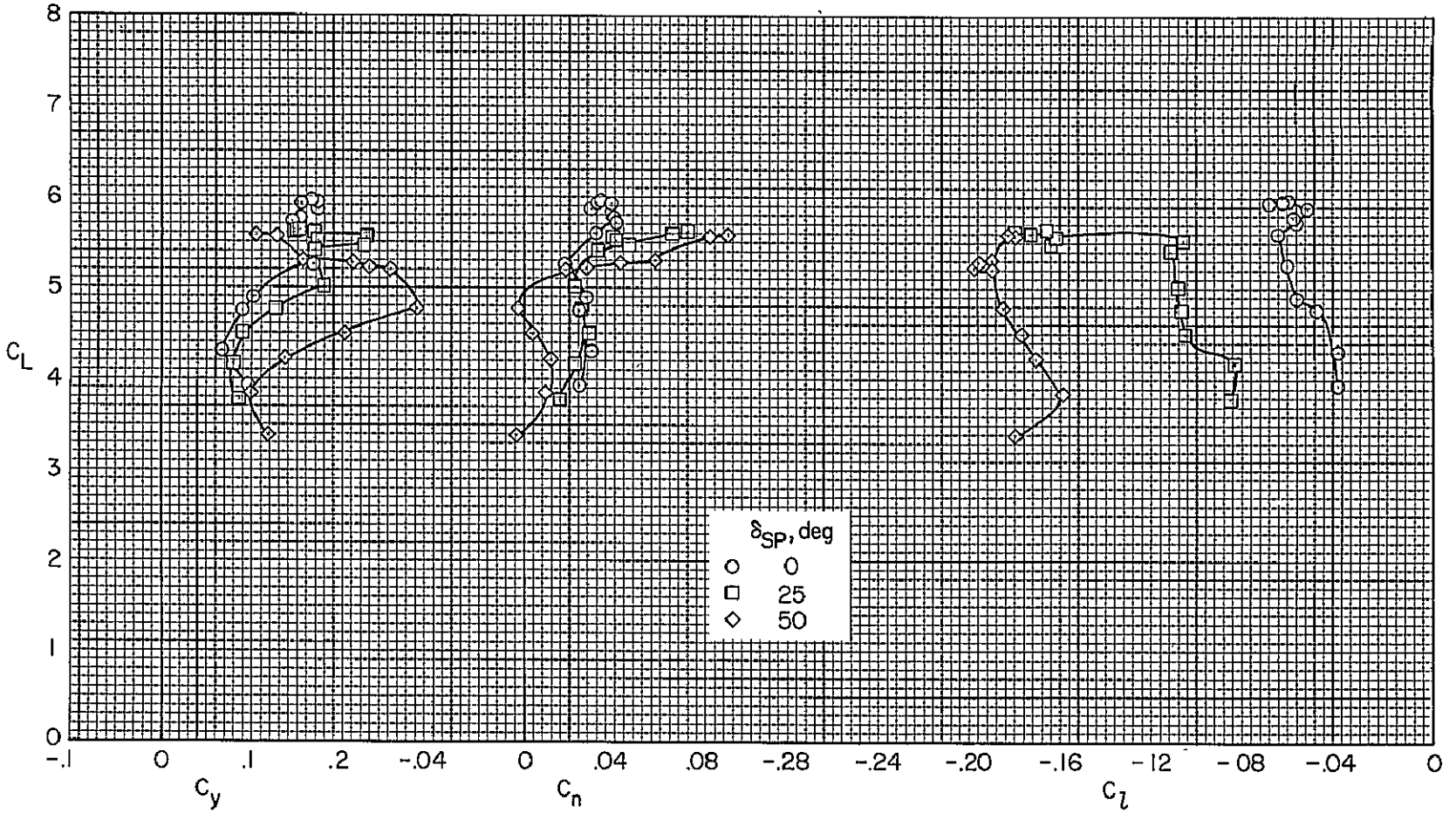

(b) C_{J_I} = 0.86, Δd = 25%.

Figure 12.- Continued.

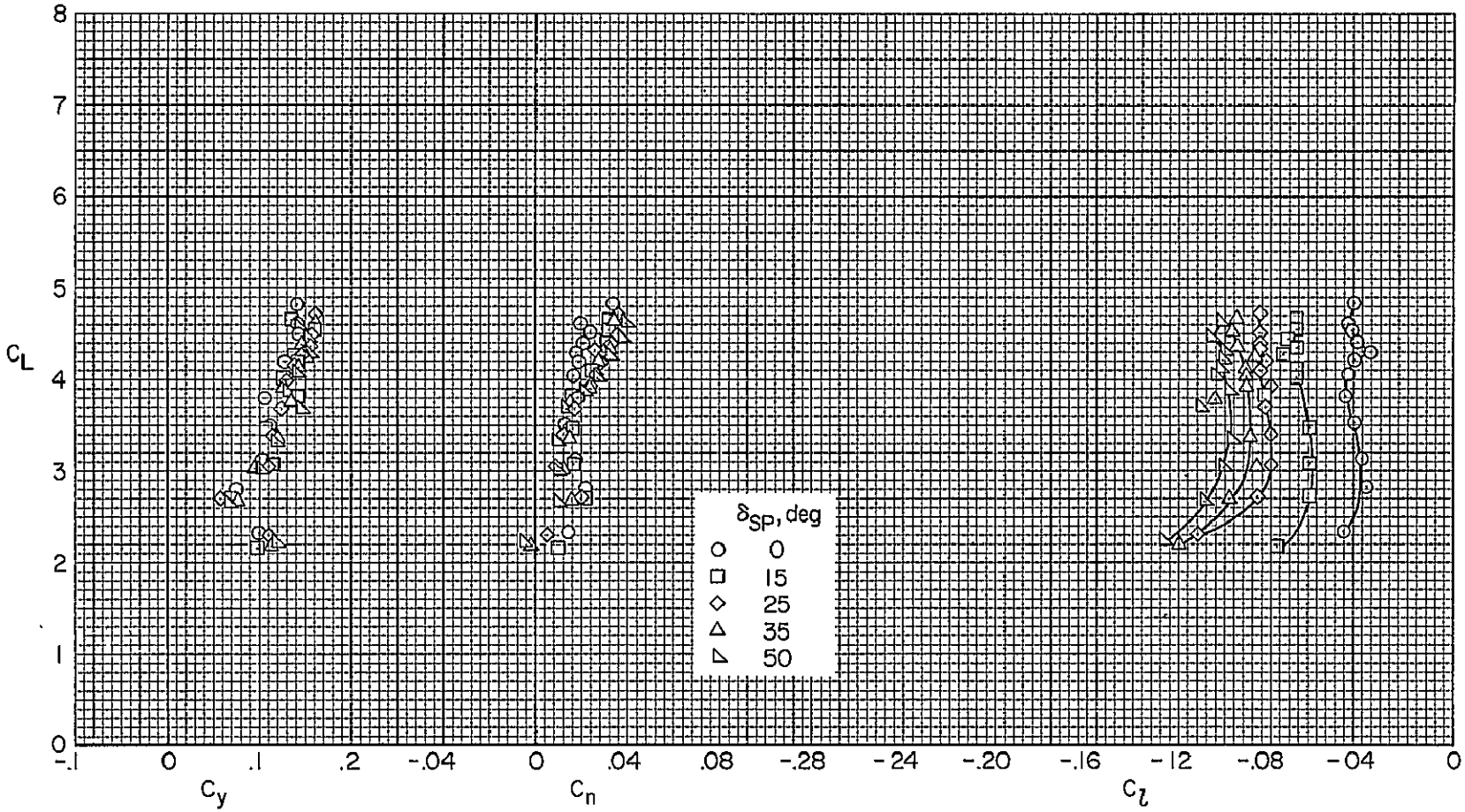

(c) $C_{J_I} = 0.35$, $\Delta d = 50\%$.

Figure 12.- Continued.

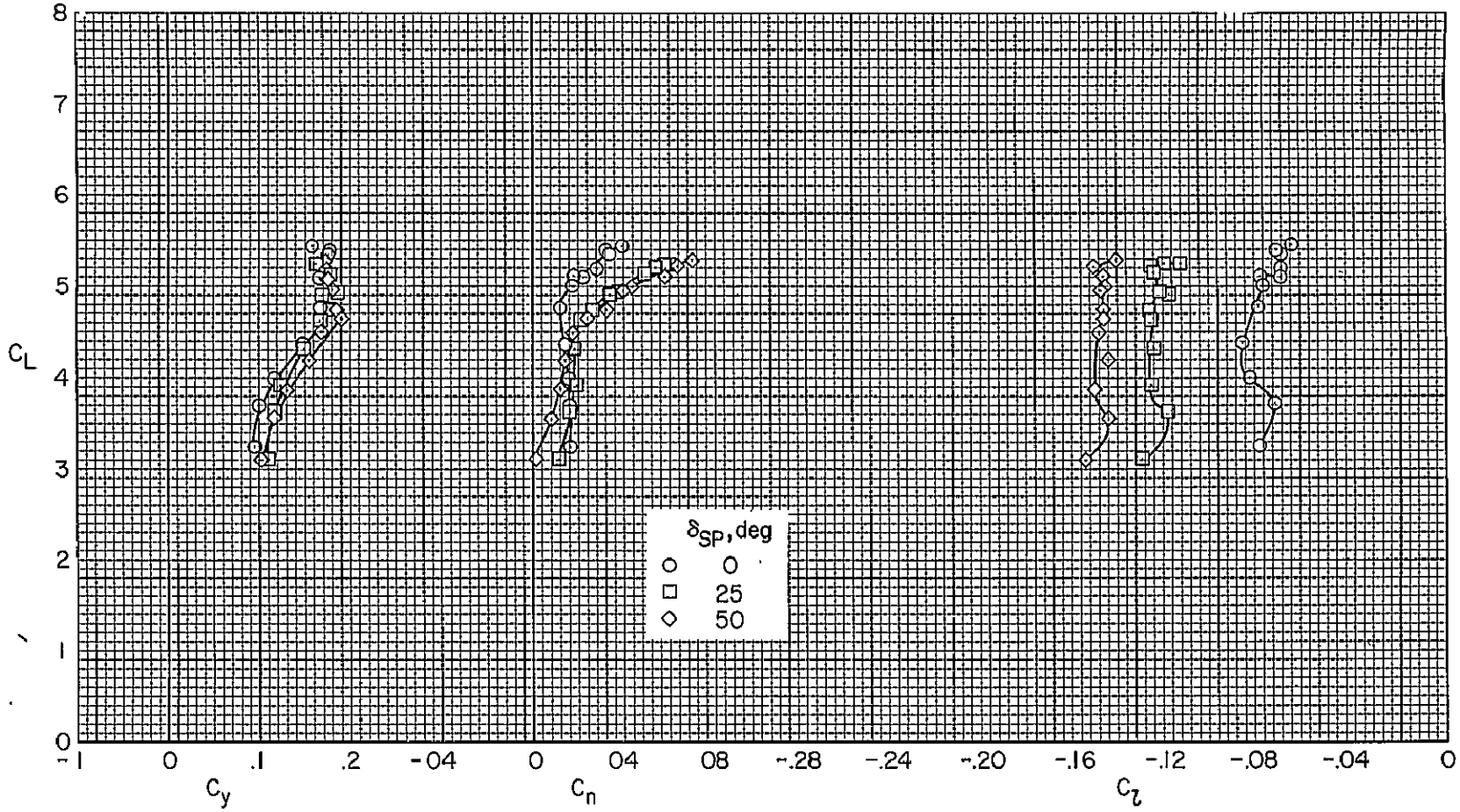

(d) C_{J_I} = 0.62, Δd = 50%.

Figure 12.- Continued.

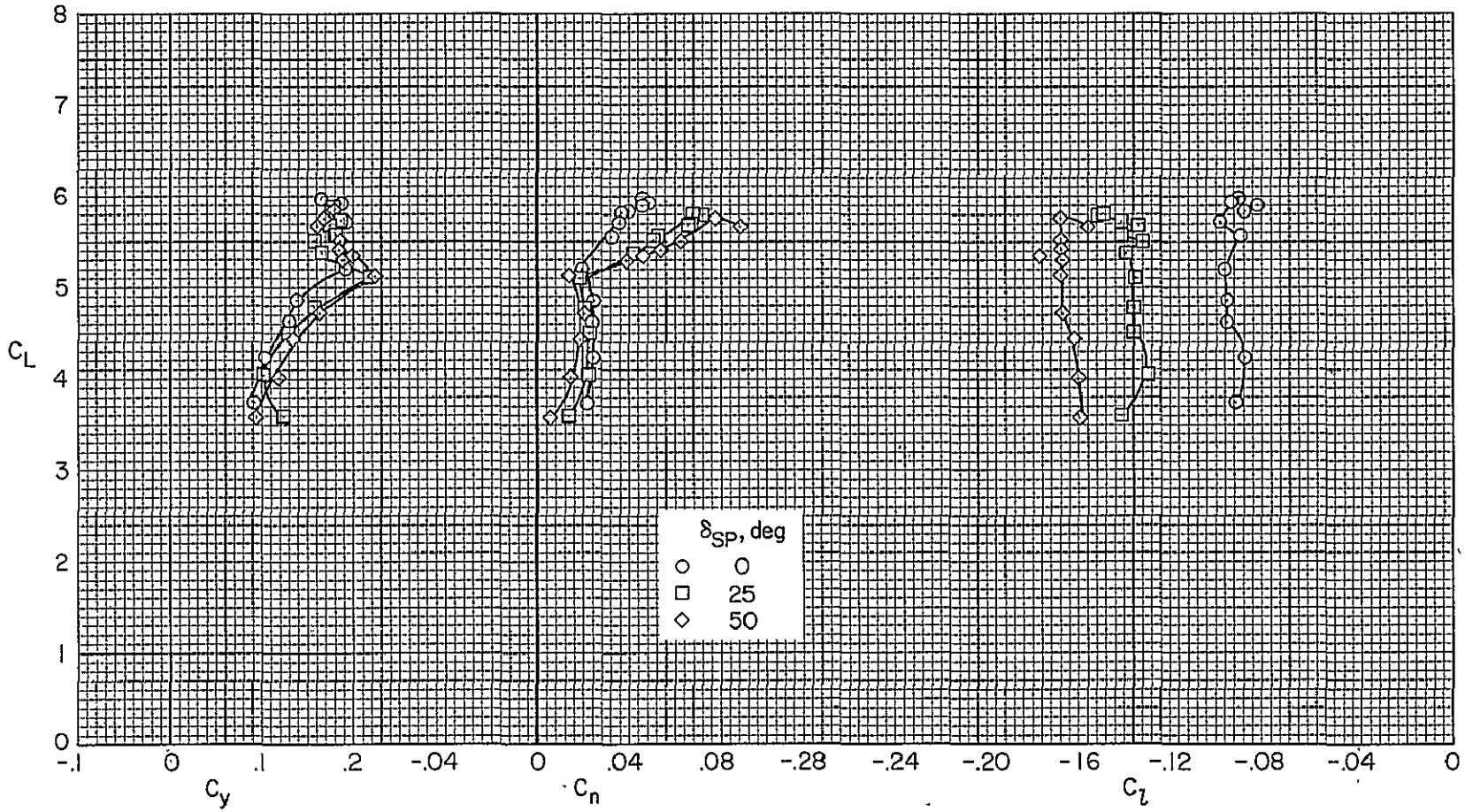

(e) C_{J_I} = 0.86, Δd = 50%.

Figure 12.- Continued.

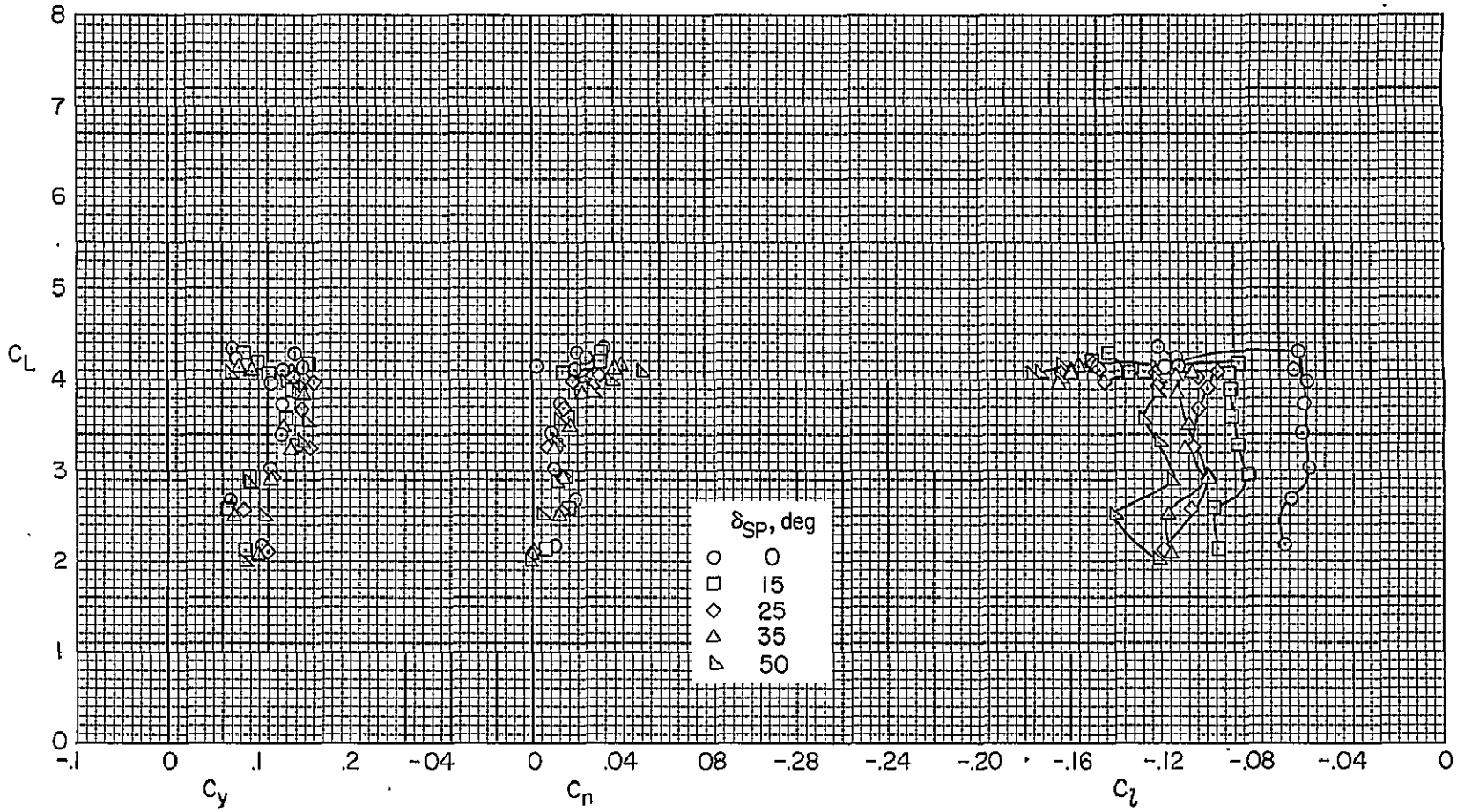

(f) $C_{J_I} = 0.35$, $\Delta d = 65\%$.

Figure 12.- Continued.

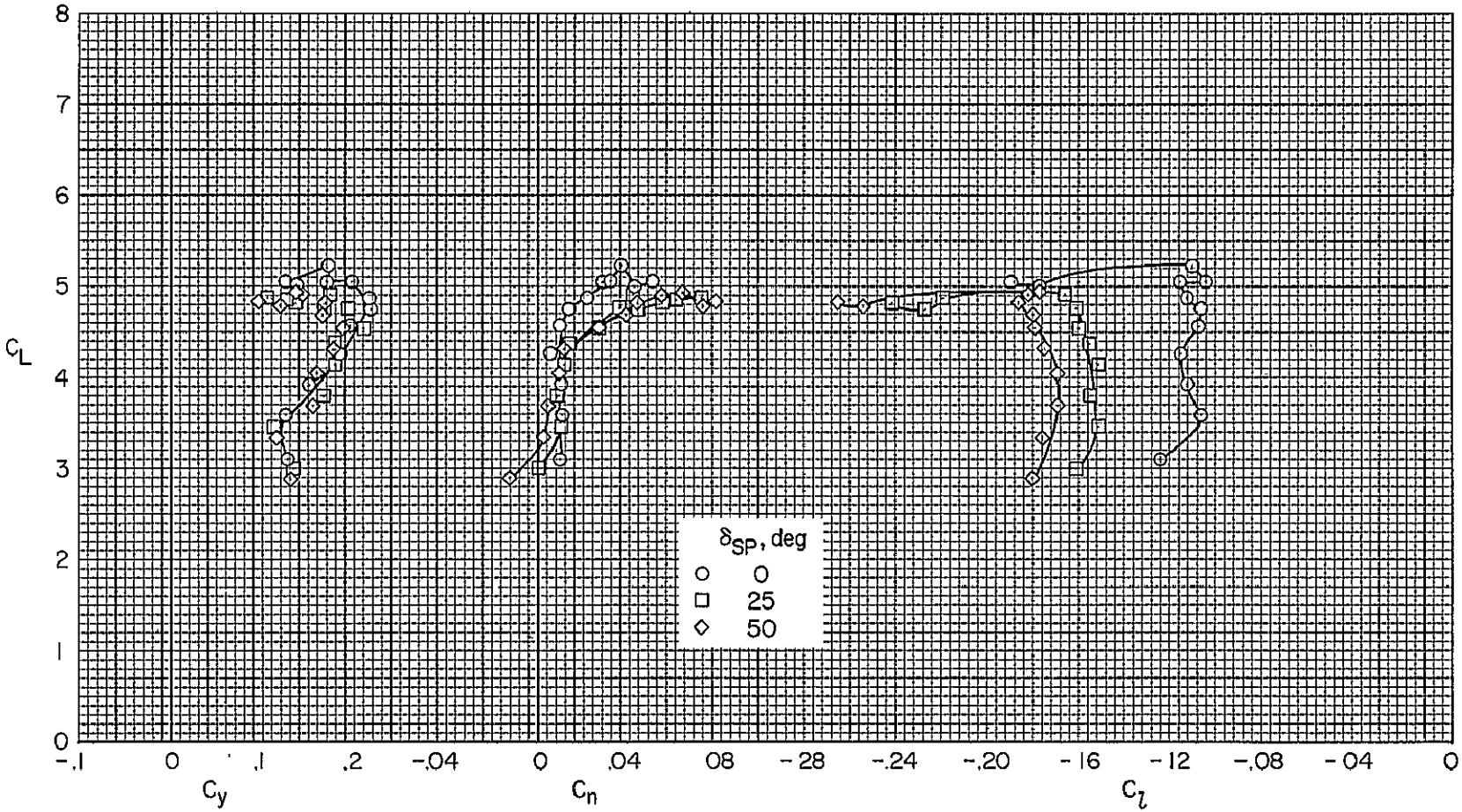

(g) C_{J_I} = 0.62, Δd = 65%.

Figure 12.- Continued.

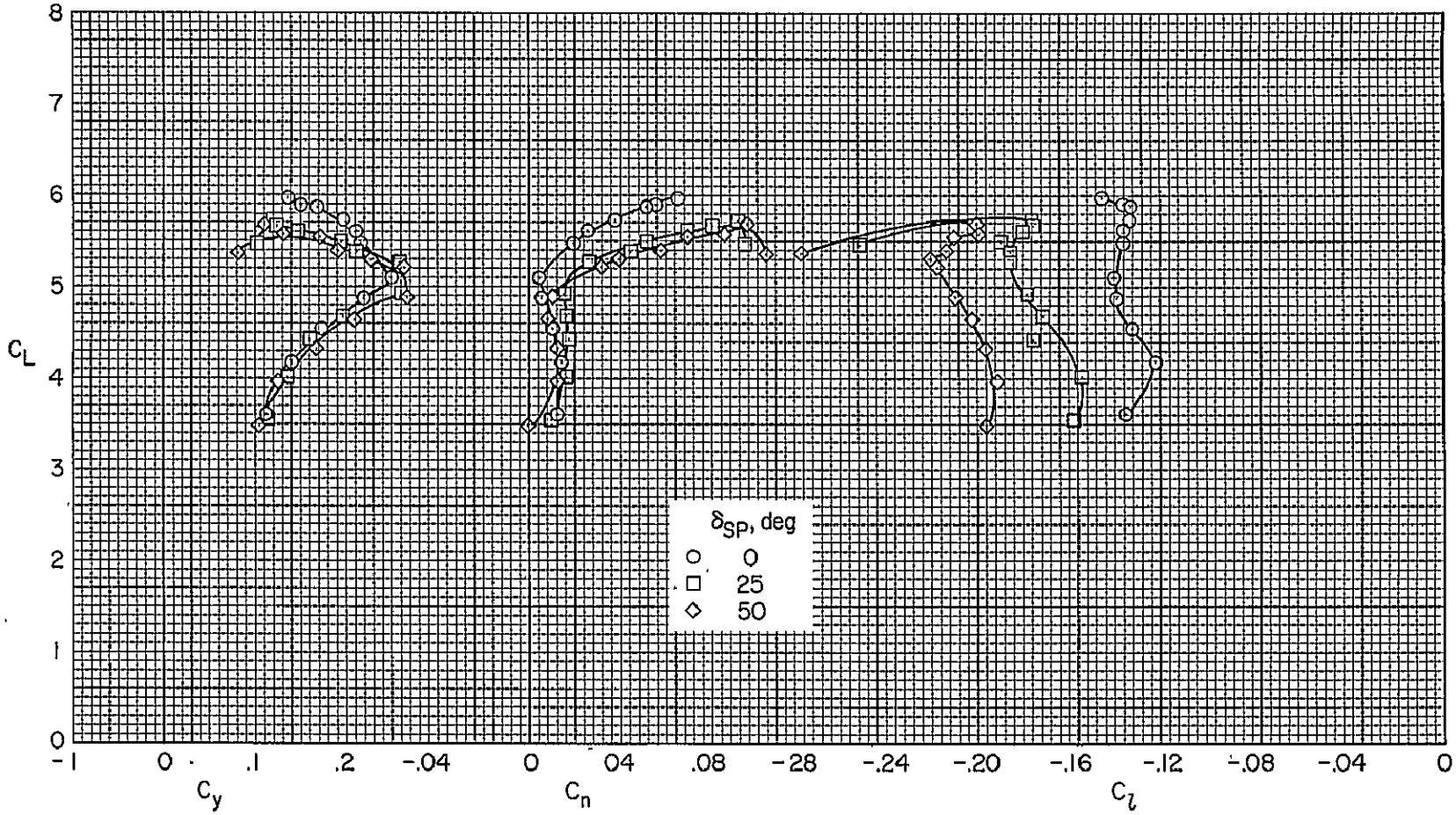

(h) $C_{J_I} = 0.86$, $\Delta d = 65\%$.

Figure 12.- Continued.

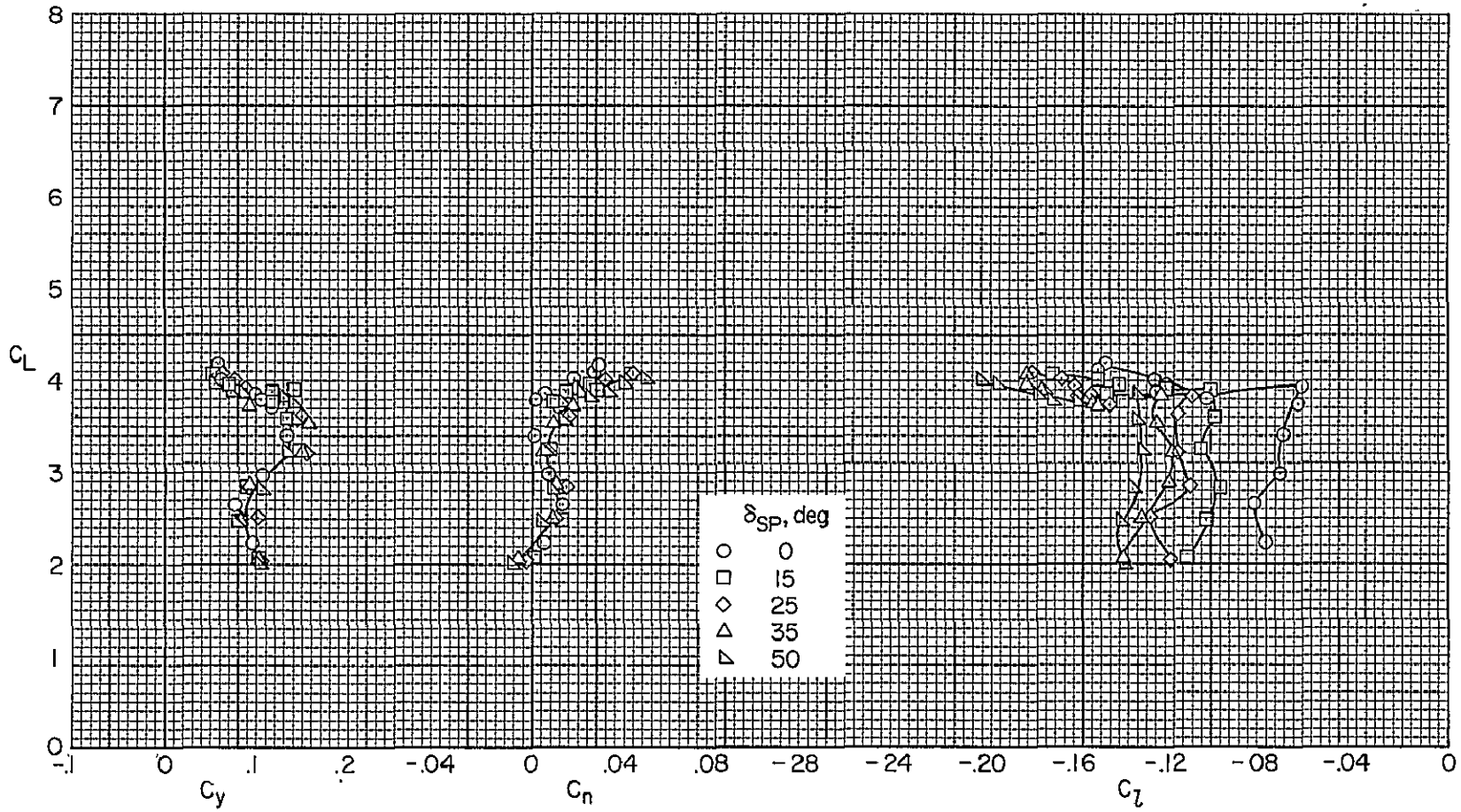

(i) C_{J_I} = 0.35, Δd = 75%.

Figure 12.- Continued.

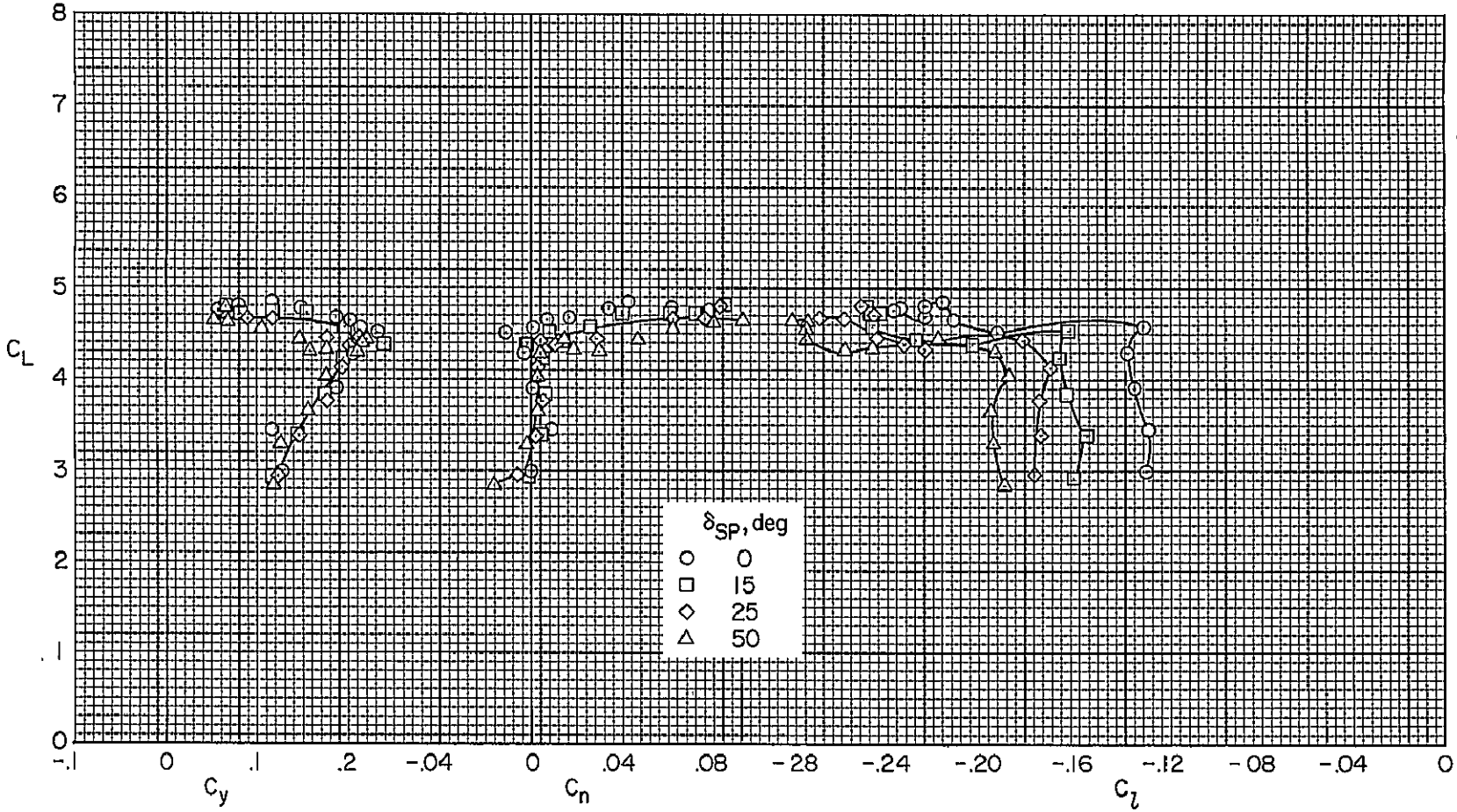

(j) C_{J_I} = 0.62, Δd = 75%.

Figure 12.- Continued.

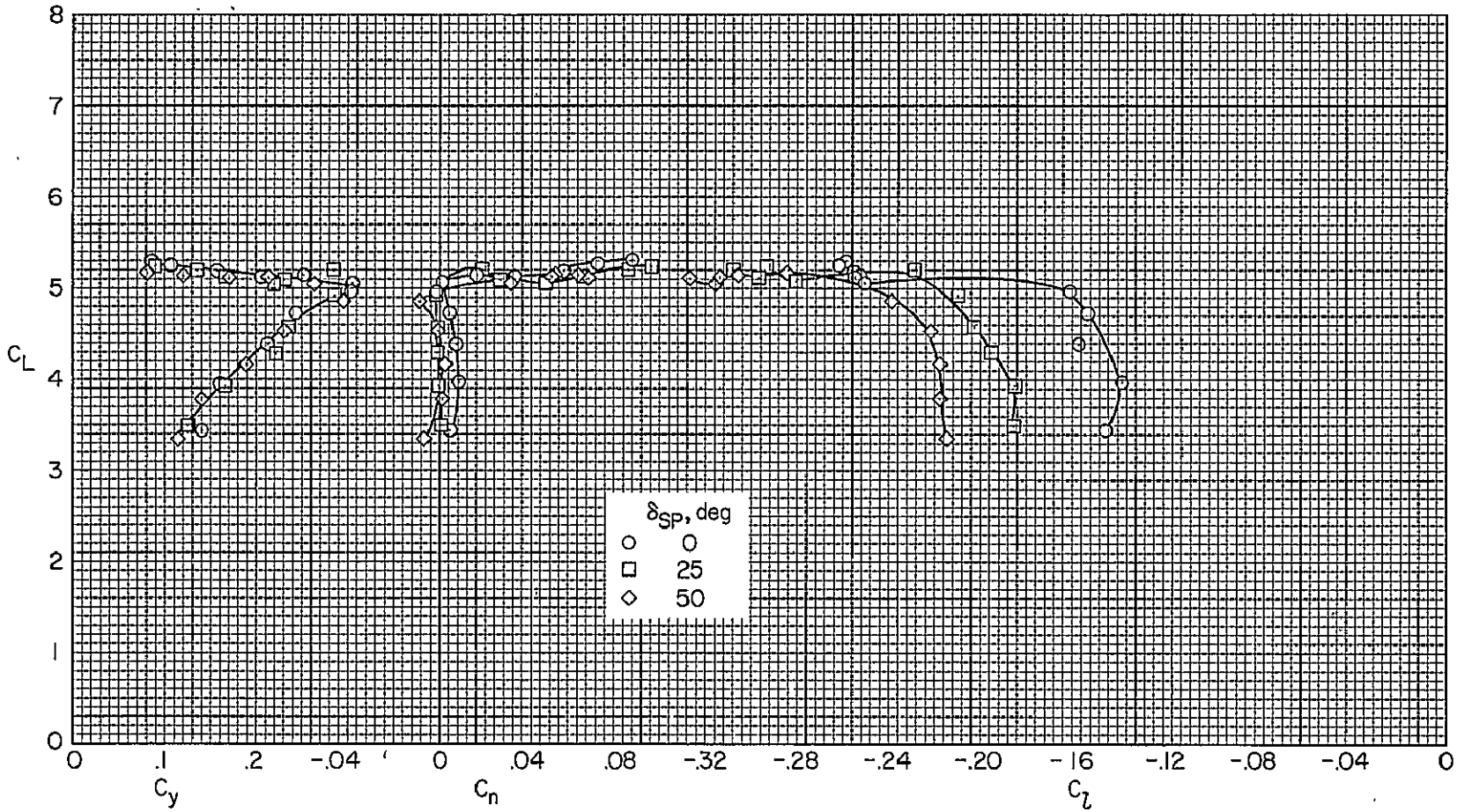

(k) C_{J_I} = 0.86, Δd = 75%.

Figure 12.- Concluded.

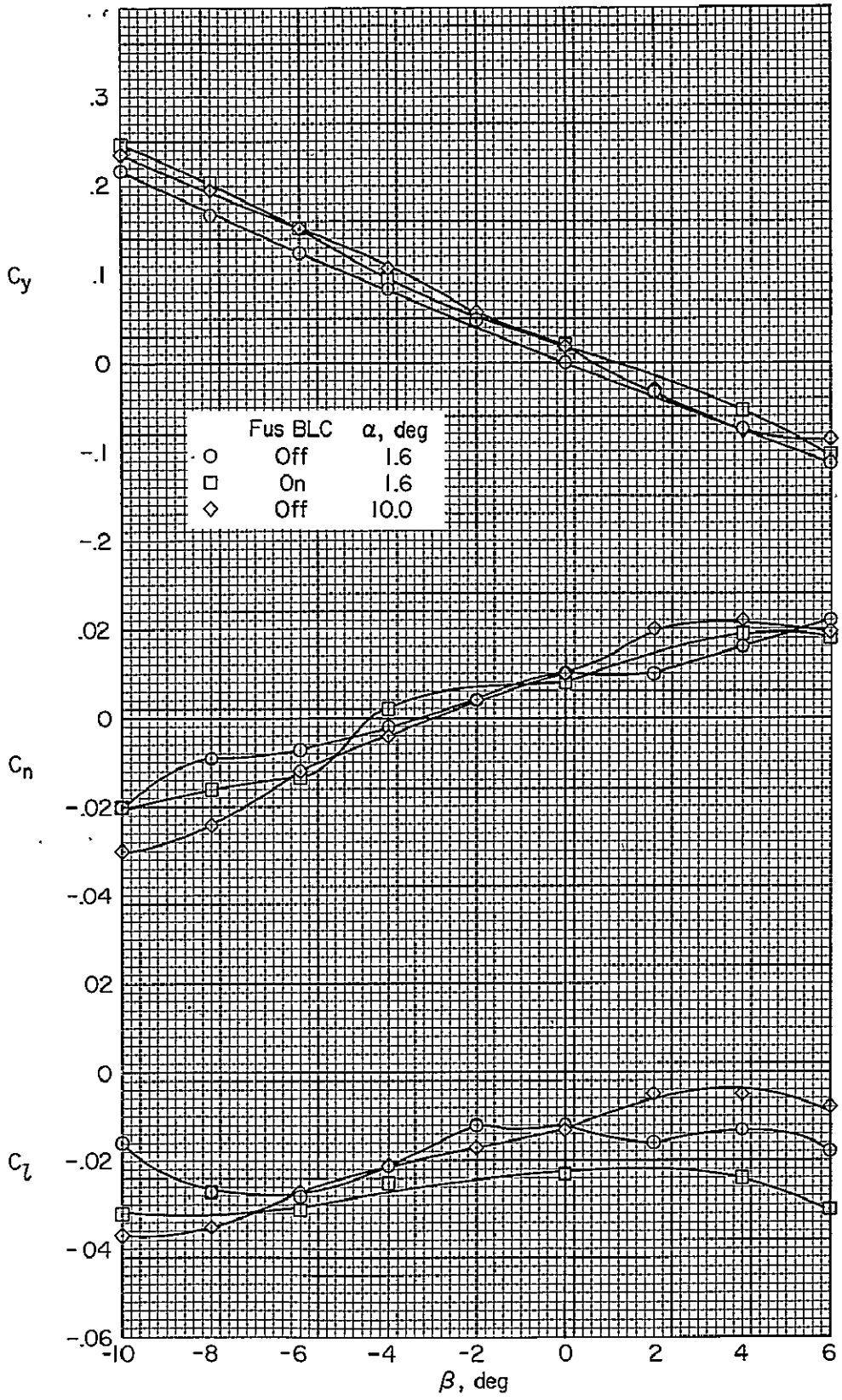

(a) Effect of fuselage BLC; $C_{J_I} = 0.82$, $\delta_a = 45/45$.

Figure 13.- Lateral-directional characteristics of the model with $\delta_f = 75^\circ$; $C_{T_{th}} = 0.81$, $\delta_{th} = 85^\circ$, $i_t = -4^\circ$, $\delta_e = 0^\circ$.

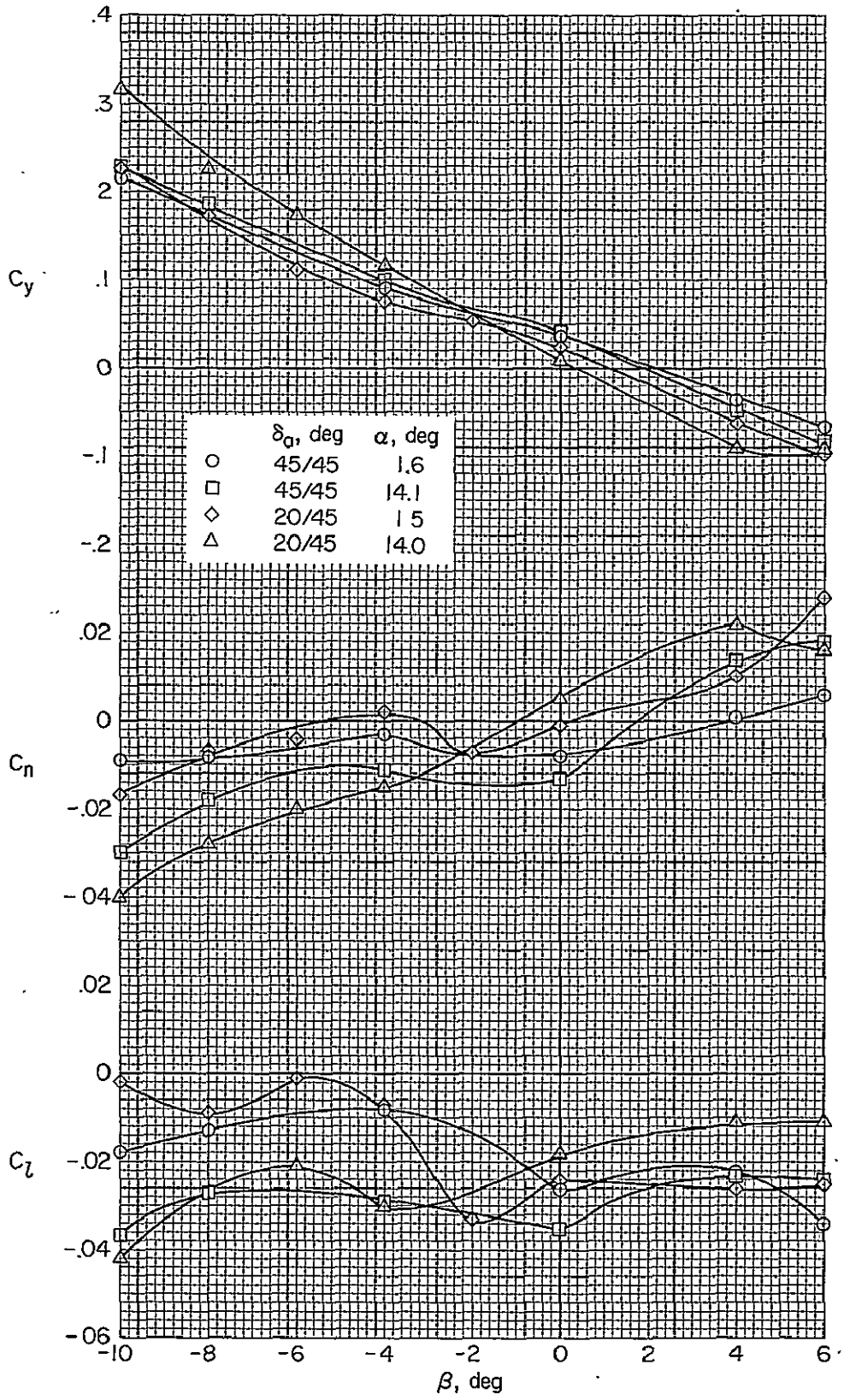

(b) Effect of symmetrical aileron deflection; C_{J_I} = 0.87, BLC on.

Figure 13.- Concluded.

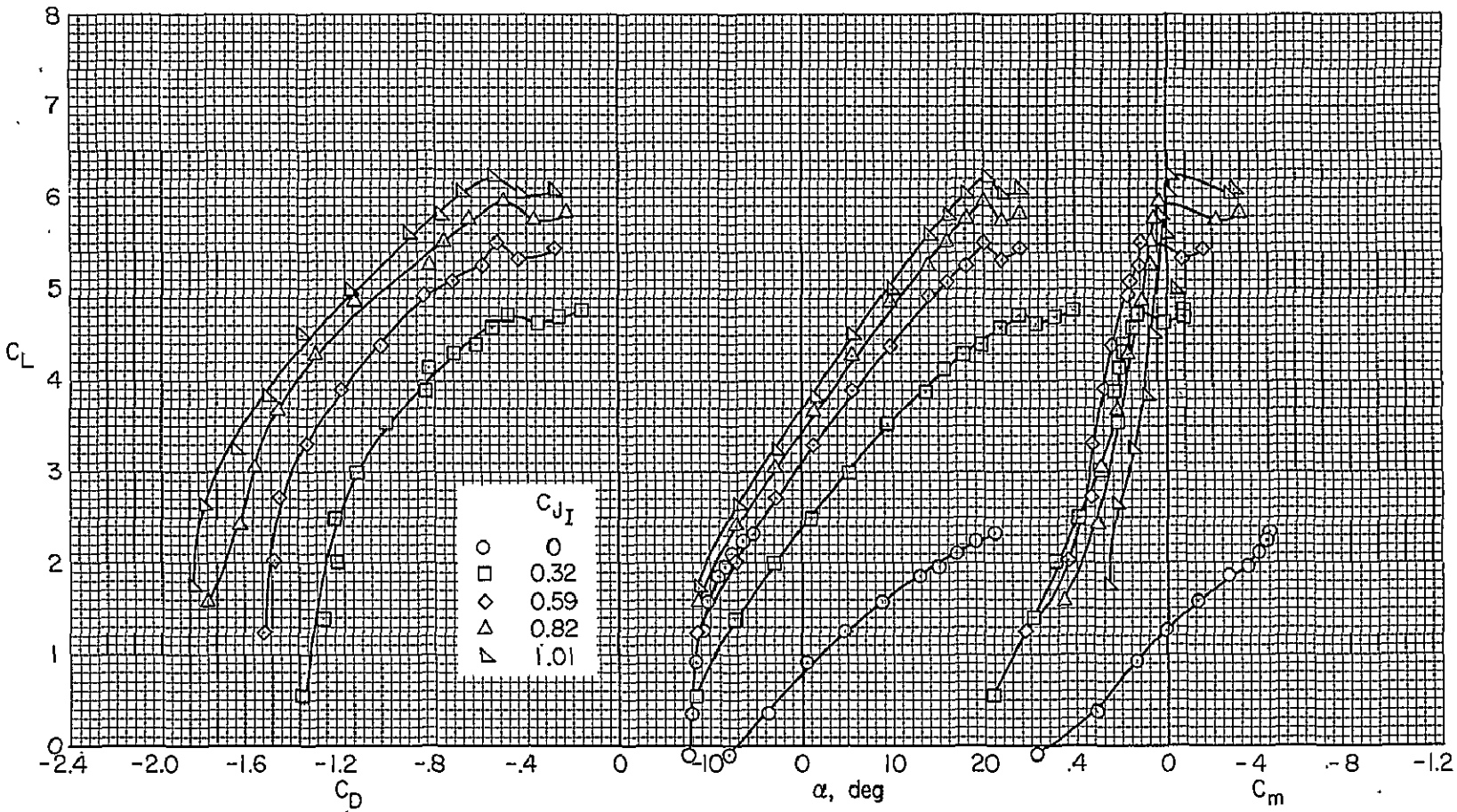

Figure 14.- Effect of C_{J_I} on the longitudinal characteristics of the model with $\delta_f = 50^\circ$; $\delta_a = 45/45$, $C_{T_{th}} = 1.46$, $\delta_{th} = 0^\circ$, BLC off, $i_t = -4^\circ$, $\delta_e = 0^\circ$.

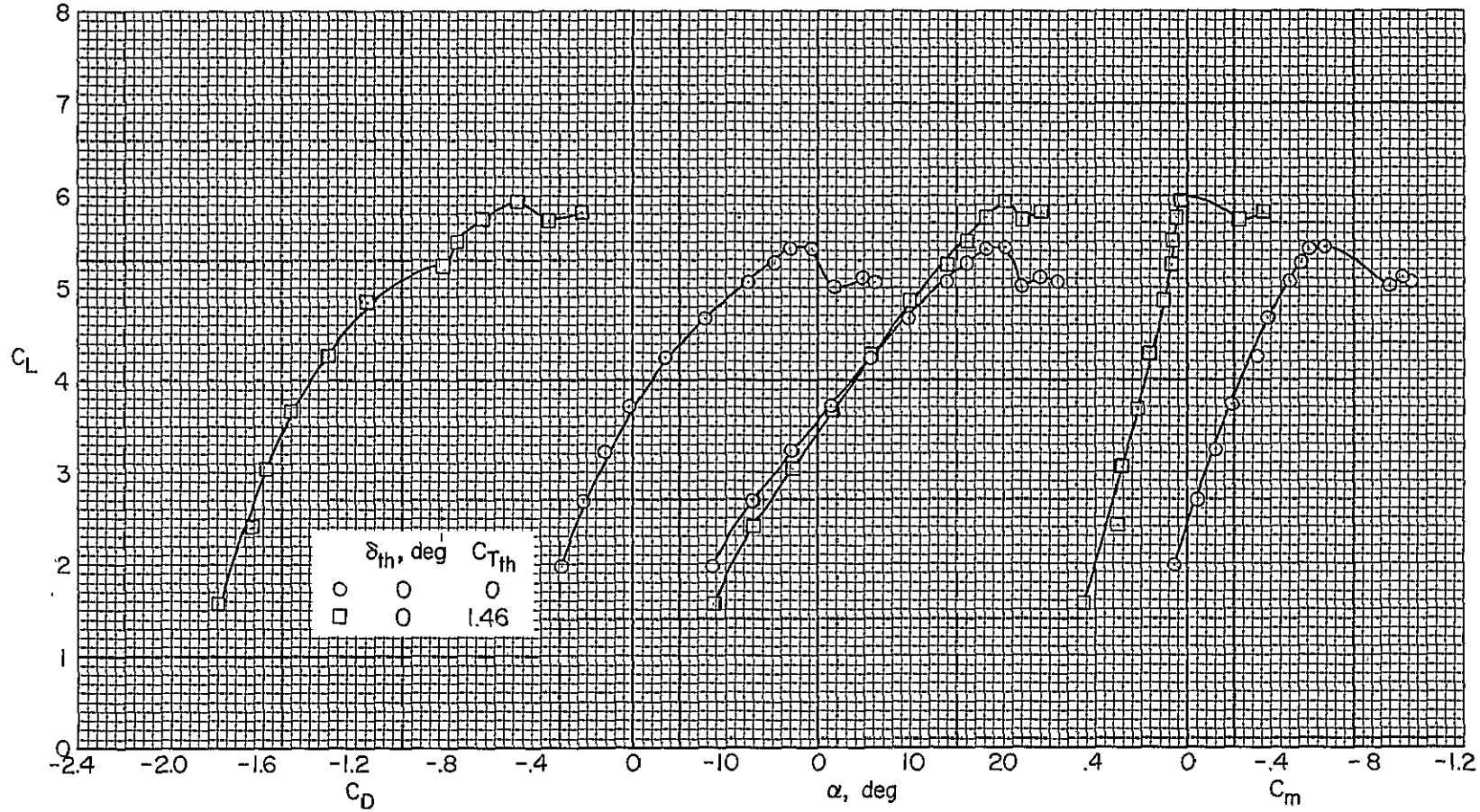

(a) $C_{J_I} = 0.82$.

Figure 15.- The effect of $C_{T_{th}}$ on the longitudinal characteristics of the model with $\delta_f = 50^o$; $\delta_a = 45/45$, BLC off, $i_t = -4^o$, $\delta_e = 0^o$.

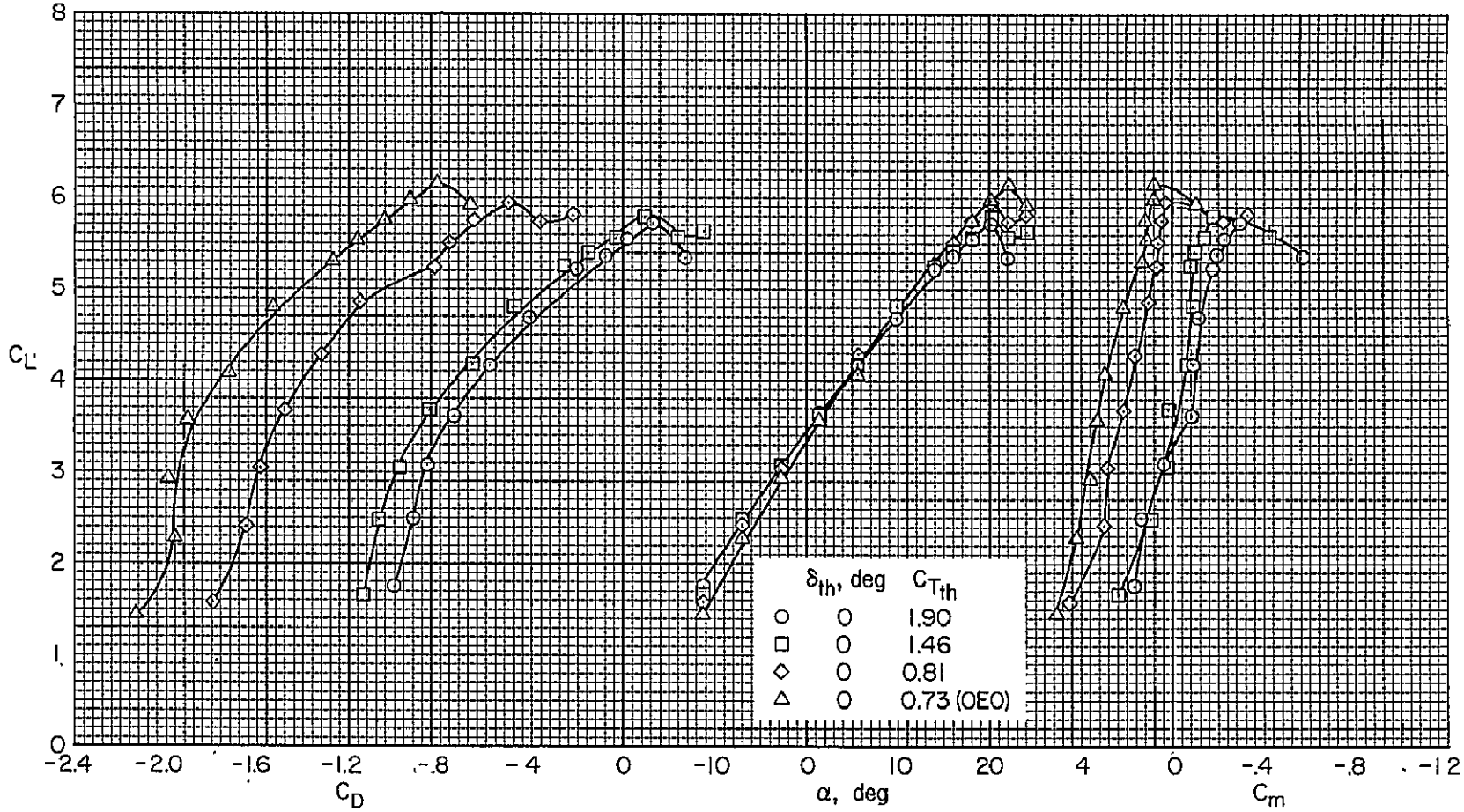

(b) $C_{J_I} = 0.82$.

Figure 15.- Continued.

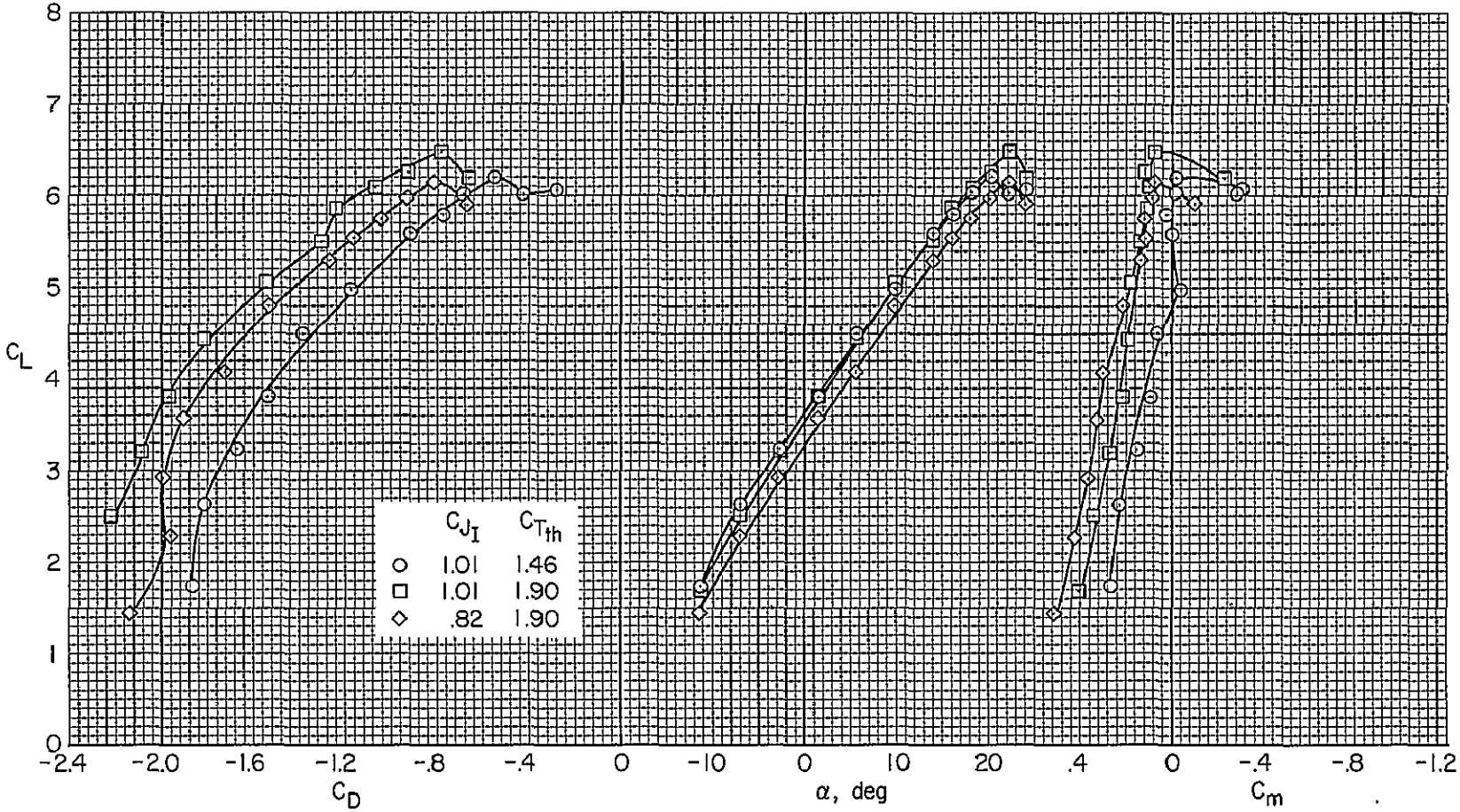

(c) Variable C_{J_I}.

Figure 15:- Concluded.

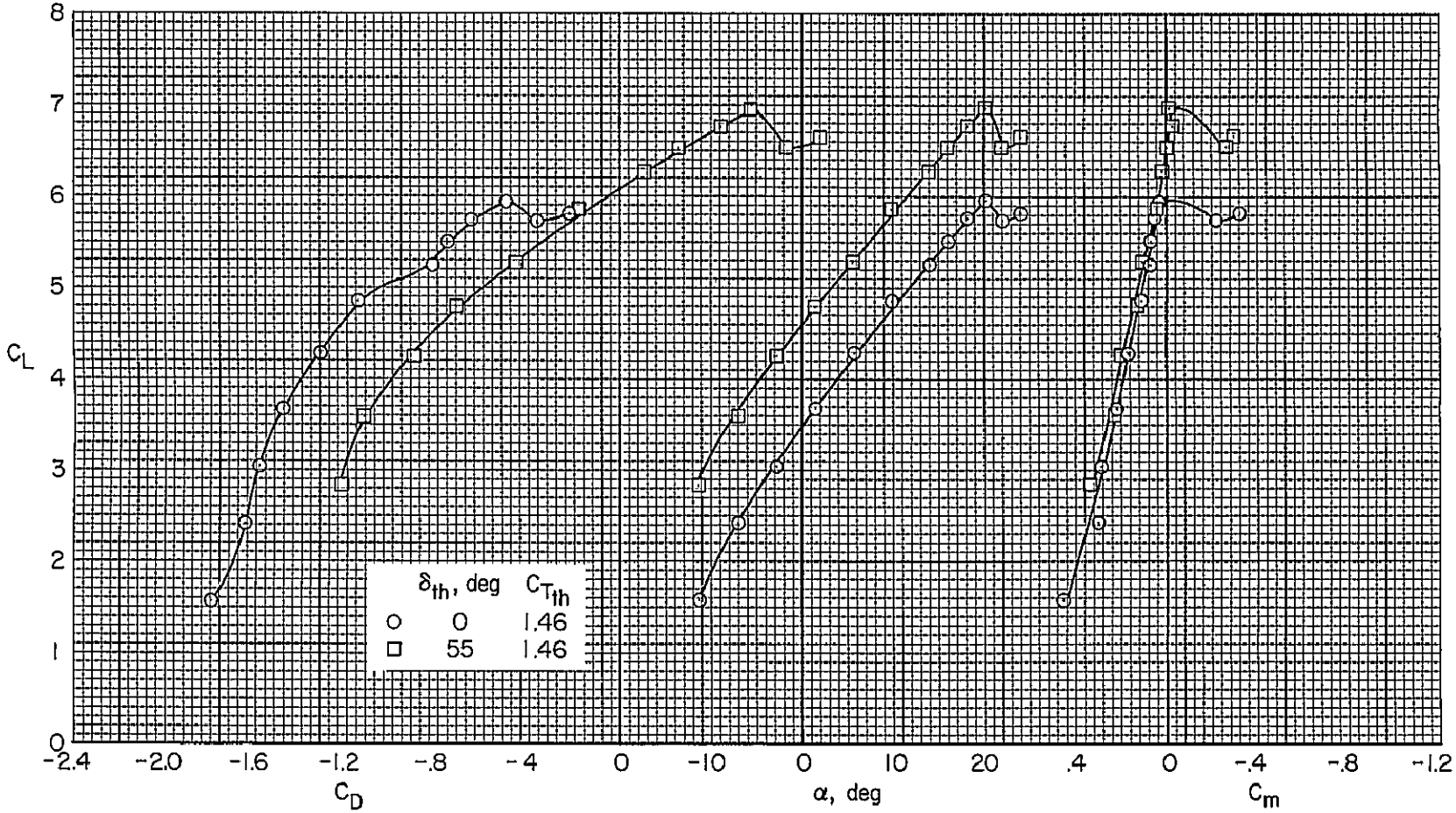

(a) $C_{J_I} = 0.82$.

Figure 16.- The effect of δ_{th} and C_{J_I} on the longitudinal characteristics of the model with $\delta_f = 50^o$; BLC off, $\delta_a = 45/45$, $i_t = -4^o$, $\delta_e = 0^o$.

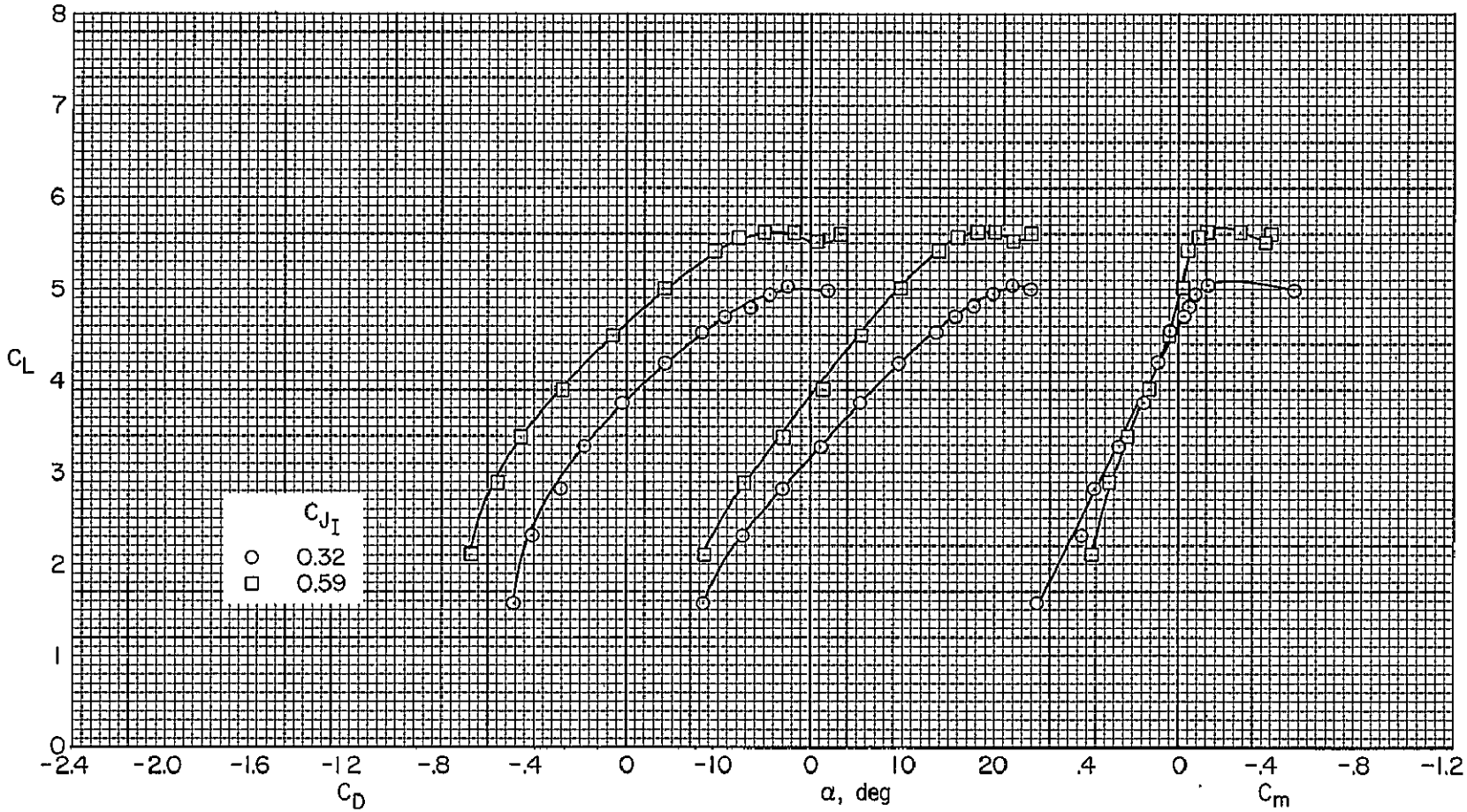

(b) $\delta_{th} = 55^{\circ}$, $C_{T_{th}} = 0.81$.

Figure 16.- Concluded.

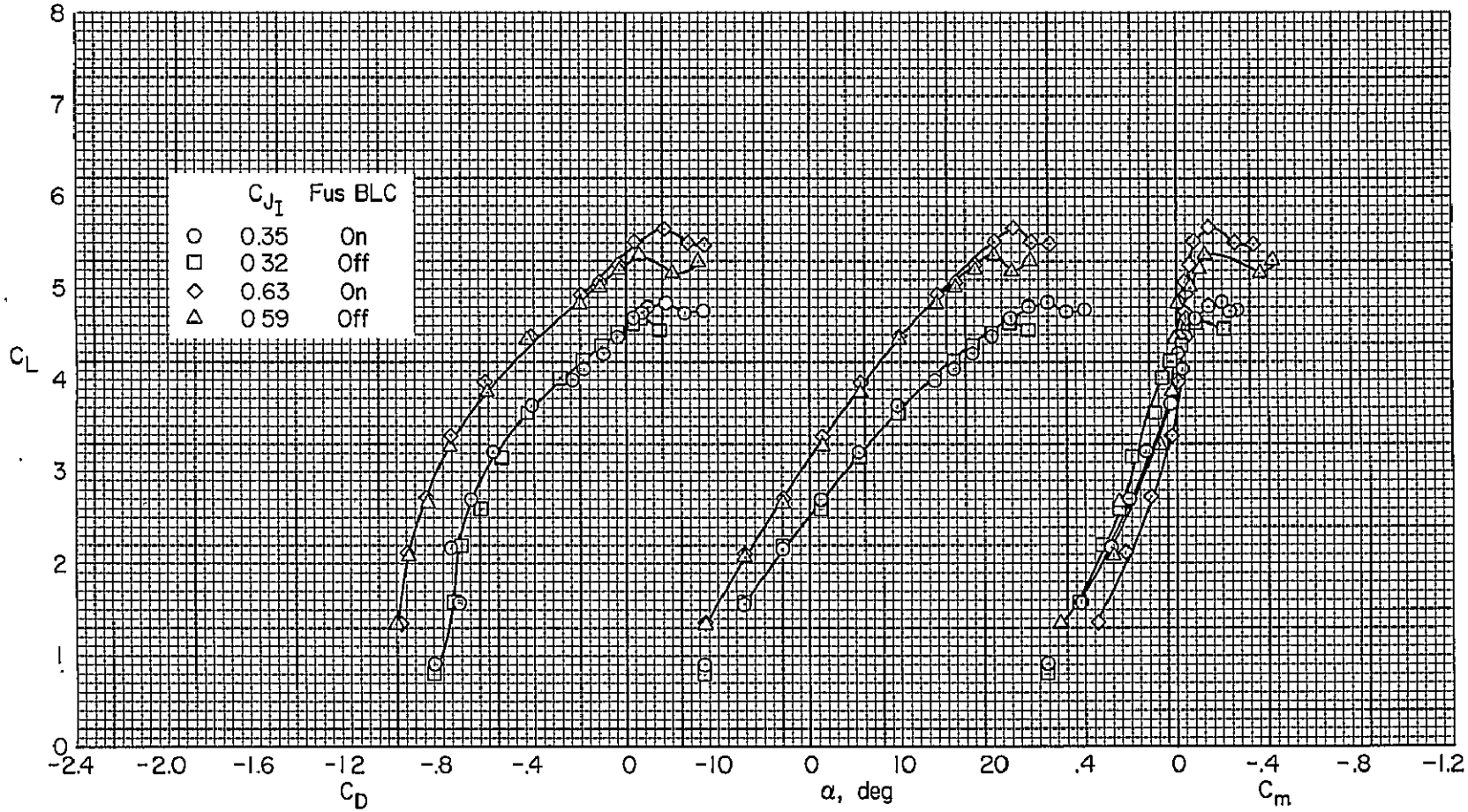

Figure 17.- The effect of C_{J_I} and fuselage BLC on the longitudinal characteristics of the model with $\delta_f = 50^\circ$; $C_{T_{th}} = 0.81$, $\delta_{th} = 0^\circ$, $\delta_a = 45/45$, $i_t = -4^\circ$, $\delta_e = 0^\circ$.

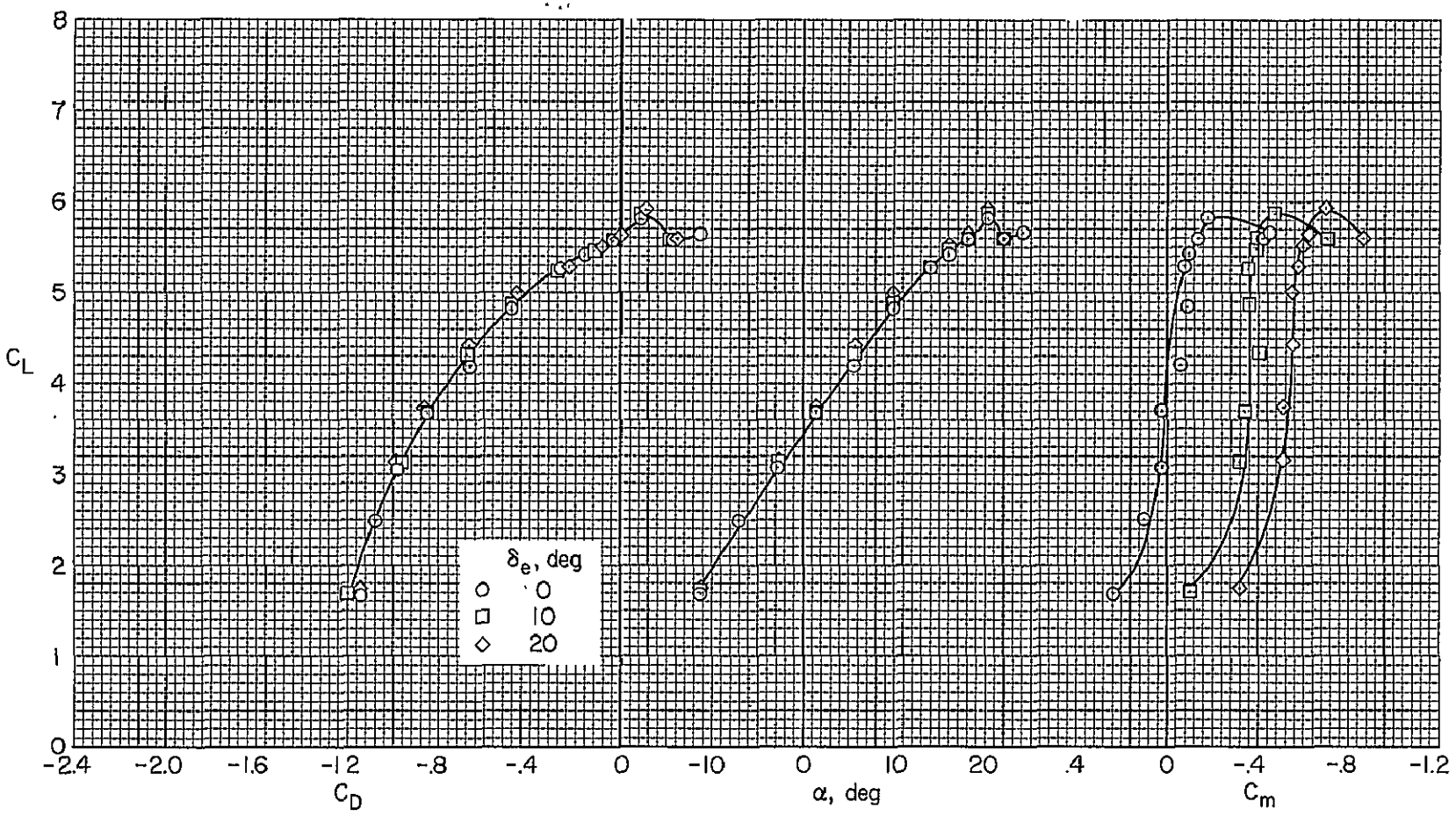

Figure 18.- The effect of elevator deflection on the longitudinal characteristics of the model with $\delta_f = 50^o$; $C_{J_I} = 0.82$, $\delta_{th} = 0^o$, $C_{T_{th}} = 0.81$, BLC off, $i_t = -4^o$.

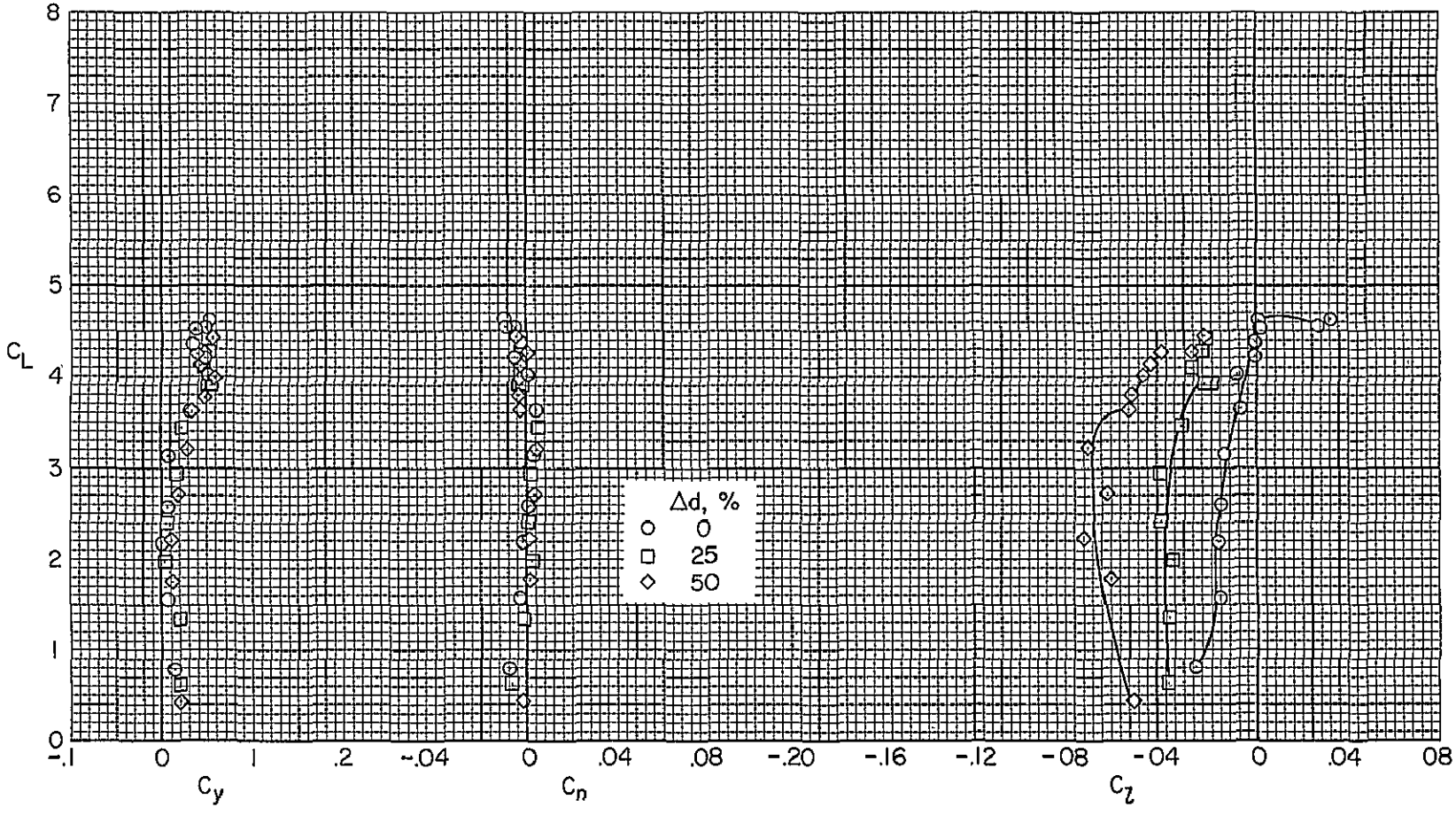

(a) $C_{J_I} = 0.30$.

Figure 19.- The effect of augmentor throttling of the outboard 50% of the flap semispan on the lateral-directional characteristics of the model with $\delta_f = 50^\circ$; $C_{T_{th}} = 0.81$, $\delta_{th} = 0^\circ$, BLC off, $\delta_a = 45/45$, $i_t = -4^\circ$, $\delta_e = 0^\circ$.

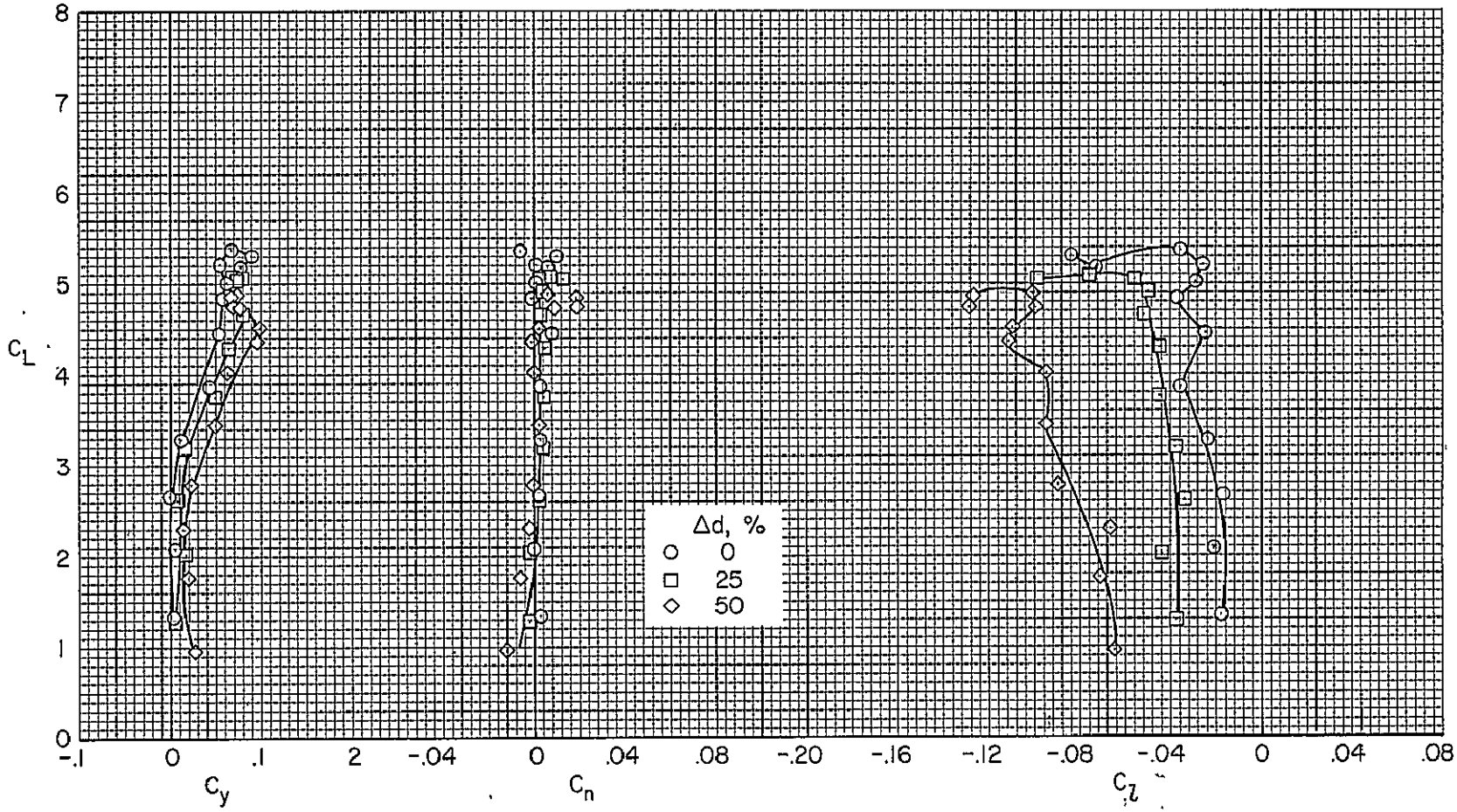

(b) $C_{J_I} = 0.55$.

Figure 19.- Concluded.

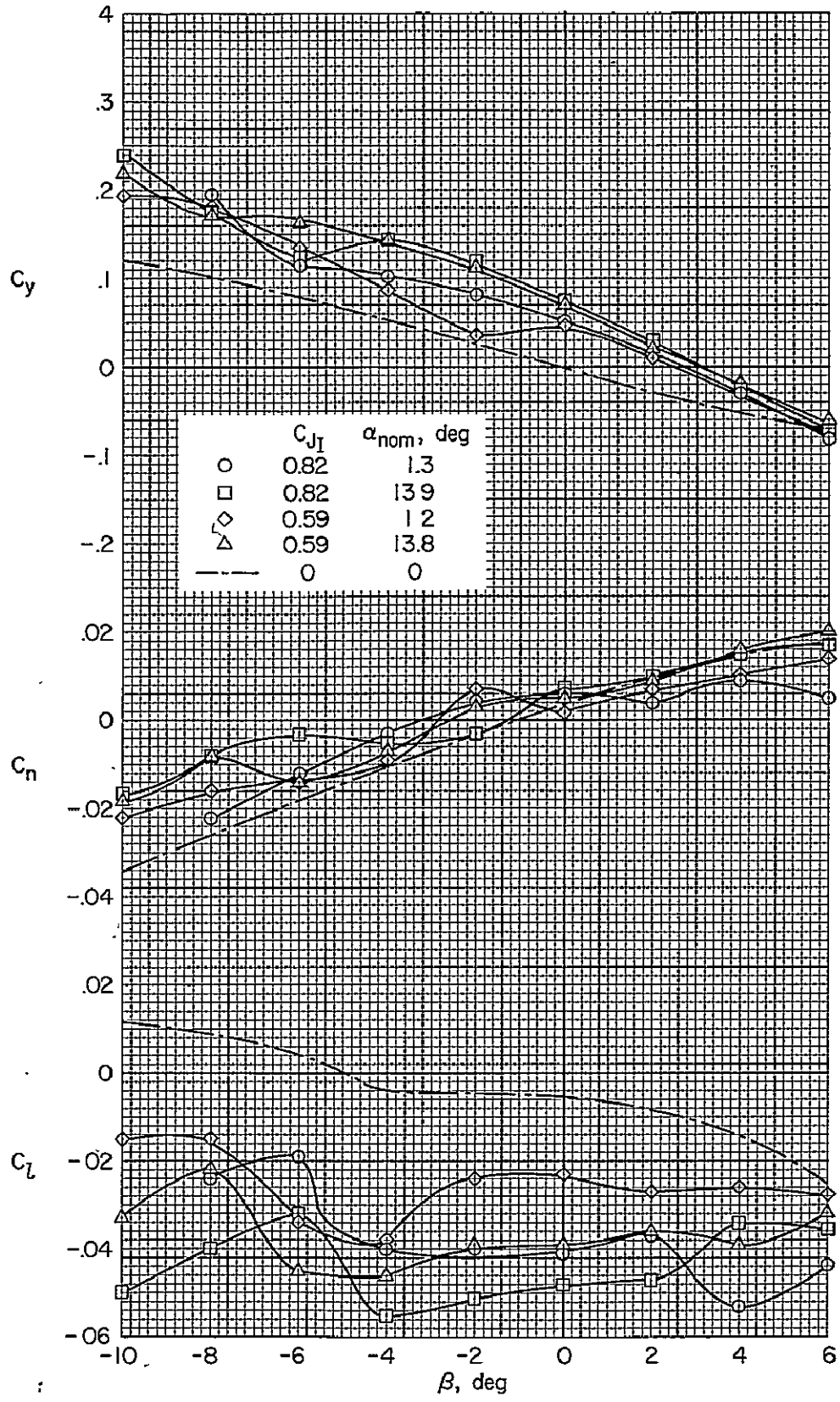

Figure 20.- The effect of C_{J_I} and α on the lateral-directional characteristics of the model at sideslip with $\delta_f = 50^o$; $C_{T_{th}} = 1.46$, $\delta_{th} = 0^o$, BLC off, $\delta_a = 45/45$, $i_t = -4^o$, $\delta_e = 0^o$.